INFRARED SURFACE BRIGHTNESS DISTRIBUTIONS OF GALAXIES

A Thesis Presented for the Degree of

Doctor of Philosophy

by

ANDREW J. ADAMSON

Department of Astronomy, University

of Leicester.

1983.

SUMMARY

Near-infrared (1.2-2.2 micron) surface brightness measurements across the faces of a sample of nearby galaxies are presented, employing a variety of instrumental techniques.

NGC 2683, 4565, and 5907 are seen almost edge-on, and for two of these, optical (V) data were obtained simultaneously with the infrared, using a widethrow-chop two channel photometer developed at Leicester by Dr.D.J.Adams. The results of these observations are presented in a single Chapter (3), in which the infrared measurements are used to define obscuration-free scale sizes for the disks, and the optical-infrared colours place constraints on possible mechanisms for the production of colour-index gradients.

The remaining observational chapters (2 & 4) are a chronological record of use of the infrared system of the Anglo-Australian Telescope, documenting steps toward DC-mapping of extended objects, begun in 1980 with semi-DC observations of NGC 5128 at 2.2 microns (Chapter 2). Significant data were obtained in the course of these experiments, and in the final chapter we present J, H and K maps of M83, a large face-on spiral, which were obtained with the intention both of resolving the controversy over the Freeman Type I- Type II surface brightness profiles, and of detecting the density wave in the "old disk", suspected to drive the optical spiral star formation pattern. Our discussion of these observations also contains a number of warnings about the pitfalls which lurk in the DC-measurement process, most of which are concerned with the knowledge (or lack of it) of the sky background level when observing very extended objects.

The first chapter gives a short introduction to some of the outstanding problems of extragalactic astronomy, and the uses to which infrared measurements can be put in tackling these problems.

The overall objective of the Thesis is to illustrate, through observational results, the wide range of applications which near-infrared imaging finds in studies of galaxies. The contrast between the three observational chapters highlights this point.

CONTENTS

Page no.

NOMENCLATURE

The following terms have been adopted as standard throughout this Thesis.

TERM	MEANING
SB	Surface brightness in logarithmic units, mag.arcsecond^{-2}.
F	Spectral flux density in units of W. m^{-2}. Hz^{-1}. arcsecond^{-2}. Fluxes in wavelength units are not used in this Thesis.
σ	Surface brightness: exactly as SB. This version is used in diagrams only. Also occasionally used to denote rms noise amplitude; the distinction should be obvious from the context.
R_g	Galactocentric radius: measured in kpc. or arcseconds from the infrared centre of the object. Sometimes referred to as r, especially in equations.
Scalelength	Applied to a galactic disk, the galactocentric radius at which the disk brightness in linear units is e^{-1} times the central disk brightness, the latter deriving from a fit to measurements exterior to the nuclear bulge.
h	Scalelength. Used in equations.
Metallicity	Fractional abundance of elements heavier than ^{4}He.

Z	Metallicity.
"	Arcsecond(s).
p.a.	Position angle, measured from north through east.
R_e	In de Vaucouleurs' surface brightness distribution law for elliptical galaxies, the "effective radius".
z	In a disk galaxy: distance above the plane.

CHAPTER 1.

INTRODUCTION.

CHAPTER 1. INTRODUCTION

In the Chapters which follow, we present detailed optical and near-infrared mapping data and surface brightness profiles of galaxies over a wide range of morphological type. While a complete review of surface photometry would be out of place in this introduction, as would coverage of the mainly statistical multiaperture observations by Frogel, Persson and Aaronson (1975-1978; various permutations of authors - hereafter FPA), we will try here to demonstrate the need for infrared mapping, and to define the possible interpretations of the resulting data. The reader requiring a more complete review of the subject is referred to Rieke and Lebofsky (1979) for some relevant facts on past infrared galaxy work, to de Vaucouleurs (1959) for a (still valid) discussion of the gross properties of galaxian light distributions, and to Strom and Strom (1978) for an excellent short review of the disk galaxies, which group will be the main subject of this thesis. We begin with a brief look at (i) the properties of galaxies in the wavebands we will be considering, and (ii) the surface brightness profile of a "classical" composite disk-and-spheroid galaxy.

1.1 (a). Basic properties of galaxies in the near infrared.

Table 1.1 gives the characteristics of the filters relevant to the observations presented in this thesis. We have included there the temperature of the black body whose spectral flux output peaks in each of the wavebands. This column is one of the bases for the importance of infrared measurements to studies of galactic light distributions, as will become clear shortly.

The table provides the framework for discussion of the broadband colours of galaxies: the important point is that the near infrared bands are sensitive to much cooler sources, although the temperature is still within the bounds of what can reasonably be expected from stellar

Table 1.1. Wavebands and Black Body Temperatures.

BAND NAME	λ_0	$\Delta\lambda$	T_{BB}
B	0.44 μ	0.098 μ	11600
V	0.55	0.089	9310
J	1.25	0.3	4100
H	1.65	0.3	3100
K	2.20	0.4	2300

effective temperatures (see Johnson 1966a). This sensitivity to cool objects is reflected in the near infrared colours of galaxies: the pioneering work of Johnson (1966b), which has since been amply corroborated, revealed that the 1.2-3.5 micron colours are dominated by stars cooler than prevail in the optical. We will see shortly that the V-K colour index is an extremely useful tool for the study of many of the properties of galaxies. On the gross level, the value of roughly 3 for this index in galaxies places a limit of about K4 on the earliest possible stellar type responsible for the near-infrared radiation, assuming the giant star-domination which has recently been shown to be the case through more subtle use of the infrared colours (Frogel et al. 1978).

The value of V-K = 3.0 is not, of course, unique for all galaxies: the large sample of objects observed by Aaronson (1977) shows significant variation as a function of position in the Hubble sequence of galaxy types, from 3.3 for the ellipticals, down to 2.8 for late type (Sc-Scd) spirals. The behaviour of the near infrared indices is less definite: across the same range of morphological type, J-H remains effectively constant around 0.74, and H-K ranges from 0.18 at either end of the sequence to 0.23 at Sb-Sbc. These colours all imply a cool, late-type stellar origin for the infrared fluxes.

(b) The classical surface brightness profile.

Although a number of exceptions have been reported, which will be discussed later, a spiral galaxy can generally be shown to comprise two or three distinct, functionally simple components, the sum of which gives the normal profile shown in Fig.1.1. Central to all but the latest type spirals is a nuclear "bulge", or spheroid, probably formed at a single epoch early in the life of the galaxy. The light distribution of this component is generally found to follow the de Vaucouleurs' law for elliptical galaxies (see, eg., de Vaucouleurs 1959; de Vaucouleurs and Capaccioli 1979, Freeman 1978):

$$\log(I/I_e) = -3.33 ((r/r_e)^{1/4} - 1) ;$$

$$SB = 8.325 ((r/r_e)^{1/4} - 1) + SB_e ,$$

where I_e and SB_e are respectively the light intensity and the surface brightness measured at the "effective radius", within which one half of the total light from the galaxy (or in our case the spheroid) originates. ("Surface brightness", as used throughout this thesis, is a logarithmic measure of the light falling in the aperture: its units are magnitudes per square arcsecond, or mag.arcsec.$^{-2}$ for short. Note that it is not a flux unit, which is possibly, in Physics, the more usual interpretation of "brightness". Fluxes will be referred to as such, or as "surface flux", in units of W.m.$^{-2}$Hz^{-1}arcsec.$^{-2}$).

Exterior to the bulge, the light distribution is dominated over many kiloparsecs by a flattened component obeying an "exponential" surface brightness law (de Vaucouleurs 1959; Burstein 1979) :

$$I = I_0 e^{-r/h};$$

$$SB= SB_0 + 1.0857 (r/h) ,$$

where I_0 and SB_0 are the light intensity and the surface brightness extrapolated to r=0, and h is the exponential scale parameter (hereafter referred to as the "disk scalelength"). Most of the blue

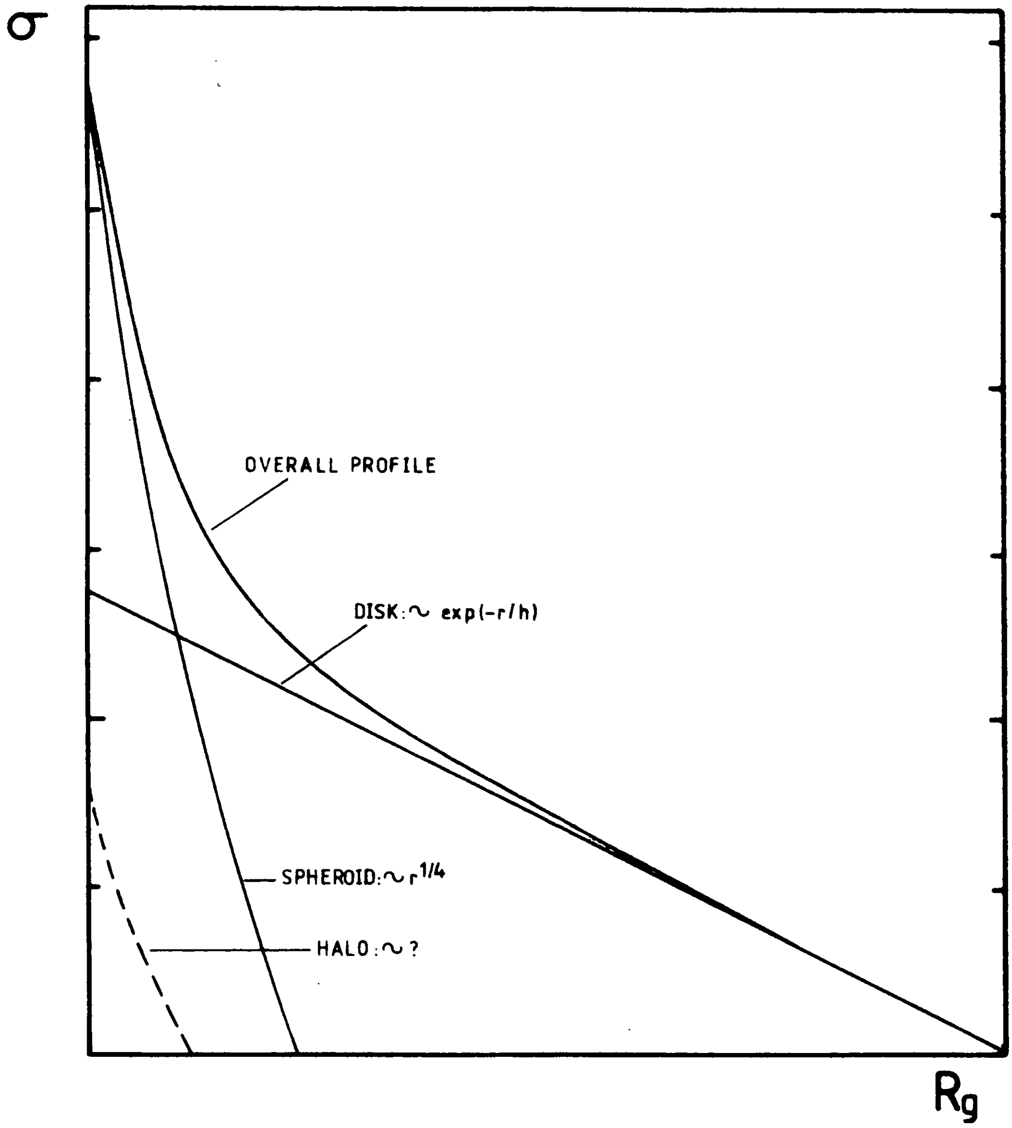

FIGURE 1.1

Classical composite disk-and-spheroid galactic brightness profile.

The surface brightness is in logarithmic units.

light, in which the majority of previous observations of these disks have been made, is contributed by a bright population of young stars in the immediate vicinity of the spiral arms: the exponential behaviour therefore becomes apparent only when the light is averaged in some way over areas of the disk. De Vaucouleurs(1963) achieved this averaging by plotting brightness levels as a function of another "effective radius" ($A^{1/2}/\pi$), where A is the total area of the isophote at a given SB; other publications have employed annular integrations in the plane of the disk (see, eg., Talbot et al. 1979).

The exponential disk has been modelled by van der Kruit and Searle (1981), using a modified isothermal sheet: their model disk is everywhere isothermal, follows an exponential distribution in the radial direction in the plane, and a more exotic law perpendicular to the plane : $SB(z) \propto \mathrm{sech}^2 (z/z_0)$ (cylindrical polars are used to describe disk systems), where z_0 is the scale<u>height</u>. This class of model has been compared, with some success, to the z-distributions of the light in systems seen approximately edge-on (van der Kruit and Searle 1981 a,b , 1982 a,b).

The third component shown in Figure 1.1 (dotted, to emphasise its unverified nature) is the "halo". Elusive to observation, such a component has been invoked in attempts to explain (i) the stability of kinematically "cold" disks against the rapid barlike distortions which plague numerical simulations, and (ii) the apparent flatness of the observed rotation curves of galaxies out to very large radii, requiring more mass than is inferred from optical observations of the luminosity of the disks. There is no reason, however,to demand that the halo consist of stars; for example, a halo made entirely of <u>massive</u> neutrinos would satisfy the two criteria above whilst remaining undetected in the surface brightness profile.

The classical surface brightness profile for disk galaxies as presented above is, by its nature, an average and an approximation. There do exist documented cases of galaxies whose disk profiles deviate markedly from the pure exponential form (eg., Boroson 1981; Kormendy 1977); the latter author suggested that a central "hole" in the disk was consistent with some of his observations.

1.2 THE INADEQUACIES OF OPTICAL OBSERVATIONS

While it is accepted that observations in blue and visible light have been fundamental to our present understanding of the structure, composition and history of galaxies, they suffer a number of drawbacks which compromise their usefulness to a certain extent. There are a number of areas in which infrared measurements, although at present more time consuming, offer the best way forward. These are described below.

(a) Density distribution in the "old disk"

As previously noted, the blue light distribution of spirals is heavily affected by bright young stars in and near the spiral arms. Good age discrimination is vital in any attempt to define the distribution of older stars in the underlying disk (Schweizer 1976). We reproduce in Fig.1.2 Schweizer's analysis of the relative contribution to the fluxes in each of the Johnson wavebands of (i) a 100 square-parsec patch of the galactic disk (components from Oort 1958) and (ii) a typical OB association of the same area. The near-IR fluxes are clearly substantially less affected by emission from young stars; surface photometry at these wavelengths is therefore observation of an almost completely different stellar subsystem to that seen in blue light, where most previous detailed photometry has been carried out. The poorer age discrimination available from optical observations was reflected in the convoluted analysis employed by Schweizer (1976) to show that his "broad azimuthal brightness variations" were a property of the <u>old</u> disk.

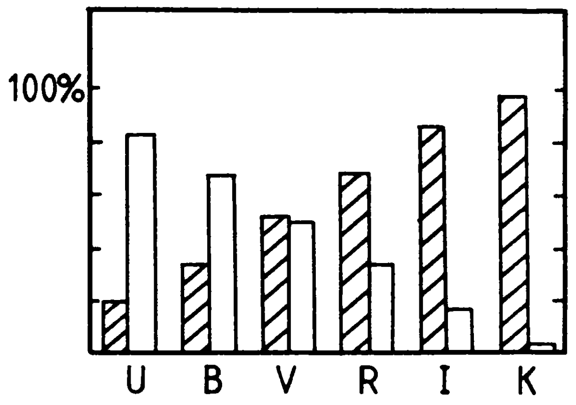

FIGURE 1.2

Relative contributions to the Johnson wavebands of an OB-association and (shaded) a patch of the disk of our Galaxy in the Solar neighbourhood. After Schweizer, 1976.

(b) De-reddened surface brightness profiles

The series of papers by Heidmann et al. (1971 a,b,c) is the most complete study of the variation of the observed parameters of galactic disks with inclination. The maximum theoretical effect of a thin, well ordered dust layer on the surface brightness of a disk galaxy is 0.752 magnitudes (a factor of 2; corresponding to complete absorption of all the visible light originating behind the layer). Heidmann et al. show in their Paper III (1971 c) that the amount by which the actual extinction falls short of this limit is a strong function of (i) the geometry of the absorbing layer and (ii) the inclination to the line of sight. Previous observational results required the inclusion in their discussion of models involving dust distributed in disks of limited angular extent and (worse) in annular formations which could easily affect the properties of the luminosity distribution inferred from optical observations.

Observations of systems seen edge-on are potentially disastrously affected by reddening; derivation of the parameters of the disk can become very complicated. We illustrate this point by reference to van der Kruit and Searle (1981a), who presented photographic photometry of the highly inclined ($i=88^{\circ}.5$) late-type spiral NGC 5907. The need to avoid extinction effects in the equatorial plane forced their fit of an isothermal disk model to be made to the measured surface brightness about 2 kpc. above the plane, where the signal was much less than would have been available on the major axis.

Appendix A describes the wavelength dependence of interstellar extinction assumed throughout this Thesis; the relevant point here is that the extinction in magnitudes at 2.2 microns, A_K, is less than 10% of the corresponding visual extinction, A_V, substantially reducing the reddening problems discussed above. (As an example, observation of the disk in NGC 5128, presented in Chapter 2, is impossible in visible light, where the extinction due to the dust lane reaches 7 mag. in places).

1.3 INTERPRETATION OF NEAR-INFRARED AND COMBINED OPTICAL-IR DATA.

(a) Near-infrared data alone

The programme of observations which led to this Thesis began with the capability of measuring only the near infrared (JHK) brightness of galaxies; the acquisition of a simultaneous optical system (details of which appear in Chapter 3) significantly broadened the scientific potential of our observations. However, the measurements originally envisaged (near IR off-nucleus surface photometry) provide, by themselves, useful data on the distribution of stars in the old disk. The observations carried out at Tenerife (Chapter 3) were intended to use the low extinction at 2.2 microns to permit measurements of the disk in highly inclined systems, combining the two infrared advantages in a single programme. Fluxes in at least two wavebands were to be measured; this allows a check on contamination of the K band flux by thermal emission from HII-regions, the relative numbers of which are suspected to be a function of position in the disk (eg. Schweizer 1976: the ratio of arm-to-disk intensity increases with distance from the nucleus).

The responsiveness of the JHK fluxes to properties of old stellar populations creates an opportunity to study localised variations in the surface number density of old stars in galactic disks, which are believed to drive the star formation responsible for the optically-prominent spiral features (this is the basis of the density-wave theory). This method - the measurement of IR surface brightness variations - is in principle more direct than is possible via observations at shorter wavelengths. In Chapter 4, it is applied to a nearby, almost face-on spiral, M83 (NGC 5236), and a value for the amplitude of the density wave is determined.

(b) Combined IR and optical data

The addition of visible light profiles to our data significantly expands the possibilities for relating the observations to quantities relevant to the formation and evolution of the galaxies. In particular, the V-K colour index has been proposed as a probe for at least three independent galactic properties. In the following paragraphs, we will briefly scan the literature, and try to place limits on the observational precision required for the production of useful results.

(i) metallicity gradients

The effectiveness of V-K as an indicator of metallicity has been amply demonstrated elsewhere (Aaronson et al. 1978 ; Strom et al. 1976). We will assume throughout this Thesis that the simple empirical calibration given by the latter authors holds for stars dominant in the 2.2 micron bandpass:

$\triangle(V-K) \sim 0.85 \triangle \log(Z)$, where Z is the metal-to-hydrogen ratio.

Spatial variations in Z, in the sense of decreasing metallicity with increasing galactocentric radius, are a definite prediction of gas-dynamical models of galaxy formation (eg. Larson 1976). Such gradients occur as a result of the increased time scale for star formation in regions of low density far from the galactic nucleus. Ten thousand million years post-formation, the metallicity of Larson's model 9 galactic disk (with an exponential scalelength between 5 and 6 kpc.- typical of the spirals considered in this Thesis) changes by $\Delta \log(Z) = -0.6$ between 5 and 30 kpc., or $d \log(Z)/dR_g = -0.024$ per kpc.

Temporarily disregarding the effects of reddening and contamination of the visual flux by emission from recently formed stars (the above calibration of V-K in terms of metal content is strictly safe only in application to E and S0 systems), the Larson model therefore predicts a change of about 0.5 mag in V-K between the inner and outer disk, a variation which should be detectable through the scanning techniques employed by us. Multiaperture observations such as those presented by FPA only divulge radial colour information upon differentiation; whilst the measurements are themselves of high internal accuracy, they are dominated by nuclear emission and are not always sufficiently precise to demonstrate the presence or absence of radial colour gradients across a single object. We note in passing that the near-infrared colour indices also correlate on their own with metallicity (eg. Aaronson et al 1978); however, the change in J-K for a given metallicity variation is much smaller than that induced in V-K, simply because the latter index, having a longer baseline, is more affected by the change in the effective temperature of the giant branch, which is responsible for the near-infrared variations. We do not expect the near-infrared colours presented in the following Chapters to be able to compete with V-K as a metallicity indicator, although the fact that J,H and K are less affected by reddening may argue in their favour.

(ii) haloes

A large amount of observing time in the late 1970's was spent on searches for optical haloes surrounding spiral galaxies (eg., Spinrad et al 1978; Kormendy and Bruzual 1978; Hegyi and Gerber 1977). Ostriker and Peebles (1973) had implemented numerical simulations of galactic disks which could only be stabilised against the rapid development of barlike modes by the inclusion of a kinematically "hot" halo component with mass comparable to that of the disk. Furthermore, various observations of the flat rotation curves of spiral galaxies (eg. Rubin 1979; Rubin et al. 1980) seemed to imply the presence of large amounts of material not directly observed in the distribution of visible light. Prime suspects for the inhabitants of the proposed "haloes" are late (M8) dwarf stars; the presence of such a cool red population on a large scale might be detectable via its effect on the (V-K) colour at large radii where the disk and spheroid are relatively faint.

In this respect we note that previous observers have produced conflicting results. With some simplifying assumptions about the stellar populations involved, the V-I gradient found in NGC 4565 by Hegyi and Gerber (1977) implies a V-K trend of $\Delta(V-K)/\ \Delta(R_g)$ greater than + 0.05 mag. per kpc between 13 and 35 kpc. On the other hand, interpolation between the smoothed isophotes presented by Spinrad et al.(1978) for NGC 253, a late Sc spiral, gives a believable, but barely statistically significant $\Delta(R-I)/\ \Delta R_g = -0.04$ mag/kpc., in the sense of bluer colour with increasing radius.

These two studies specifically set out to measure the halo population, covered larger radial ranges than are considered in our Chapter on edge-on spirals, and resulted in small, statistically uncertain trends in the colour indices. It seems unlikely that red haloes will prove detectable in the optical and infrared work presented in Chapter 3, which is restricted to the relatively bright disk components.

In this respect, it is important to realise that the near-infrared colours in themselves are insensitive to the type of population changes supposed to take place as the halo takes over from the main body of the galaxy. The J-K colour of M dwarf stars is very similar to that of the giant stars, later than K5, known to dominate the near infrared emission from the centres of E galaxies (sources: Johnson 1966b, Frogel et al. 1975). A long baseline in wavelength is needed to take advantage of the extremely red colours of the predicted halo population.

(iii) thermal emission from HII-regions

As pointed out earlier, the fractional contribution from the spiral arms to the total light of a spiral disk increases with distance from the nucleus. The tendency for the broadband optical colours to become bluer with increasing radius may be explained this way, although there is clearly competition between this effect and the metallicity driven changes discussed above. Its importance to the V-K index is less easy to assess: the expected brightening in the V band may be quenched by an increase in the relative dust content, while the 2.2 micron fluxes may well be enhanced by transition and dust radiation from HII regions (eg., Willner, Becklin and Visvanathan 1972). The V-K colour could conceivably, therefore, become redder with increasing galactocentric radius. Thermal contamination of the infrared fluxes is expected to set in first at 2.2 microns; the J-K and H-K colour indices may be of use in estimating its importance.

The results presented by Aaronson (1977) of J,H and K observations of a large sample of disk galaxies distributed along the Hubble sequence, show no variation in the H-K index as a function of Hubble type to a limiting value of 0.02 mag., and no evidence of a trend in the near-infrared colours with increasing aperture size, to the same order of precision. Taken together, these two facts imply that the effect on the V-K colour of thermal contamination of the 2.2 micron flux may be minimal (but see NGC 5907, Chapter 3 of this Thesis).

(iv) stellar ages

Struck-Marcell and Tinsley (1978) have demonstrated that the V-K colour index is about three times more sensitive to stellar ages and star-forming bursts than are the UBV colours. Models of galaxy formation such as those presented by Larson can lead, via stellar age gradients across the disks, to appreciable trends in V-K, in the sense of bluer colour with increasing radius. The size of the trend calculated by Struck-Marcell and Tinsley is on a par with the variations expected from the metallicity gradients discussed earlier, but the application of this result to observed colour gradients is not easy in the case of galaxies with current star formation: for example, the unusually blue V-K colour predicted for a recent star-forming burst is not a property for which active galaxies (such as M82) are renowned.

1.4 OUTLINE OF THE FOLLOWING CHAPTERS

Chapter 2 presents a 2.2 micron map of the peculiar elliptical galaxy NGC 5128, associated with the giant double radio source Cen A. This observation represents the end of a previous programme of infrared mapping of active galaxies undertaken in the late 1970s at Leicester (Abolins et al.1979; Abolins 1980). The low extinction at 2.2 microns is used to map a star-forming disk in the optically-obscured "dark lane" of this unusual object.

Chapter 3 presents optical and infrared surface brightness profiles along the major axes of three bright edge-on spirals (NGC 2683, 4565 and 5907). The observations were obtained with a widethrow-chopping twin channel photometer at the Tenerife flux collector. There is evidence for colour gradients along the major axis of one of the objects (NGC 5907).

Chapter 4 gives maps and surface brightness profiles at J,H and K of the nearby spiral galaxy M83 (NGC 5236). Spiral structure is detected at all three wavelengths. A value for the amplitude of the density wave in the old disk is directly obtained.

REFERENCES

Aaronson,M. 1977, Ph.D. Thesis, Harvard University.

Aaronson,M., Cohen,J.G., Mould,J., & Malkan,M. 1978, Astrophys.J., 223,824.

Aaronson,M., Frogel,J.A., & Persson,S.E. 1978, Astrophys.J., 220,442.

Abolins,J.A., Adams,D.J., Jameson,R.F., Hough,J.H., & Axon,D.J. 1979, Mon.Not.R.astr.Soc., 186,23p.

Boroson,T. 1981, Astrophys.J.Suppl.Ser., 46,177.

Burstein,D. 1979, Astrophys.J., 234,435.

de Vaucouleurs,G. 1959, Handbuch der Physik, Springer-Verlag,53,275.

de Vaucouleurs,G. 1963, Astrophys.J., 137,720.

de Vaucouleurs,G., and Capaccioli,M. 1979, Astrophys.J.Suppl.Ser., 40,699.

Freeman,K.C. 1978, in "Structure and Evolution of Nearby Galaxies", IAU Symposium 77, D.Reidel , page 3.

Frogel,J.A., Persson,S.E., Aaronson,M., Becklin,E.E., Matthews,K., & Neugebauer,G. 1975, Astrophys.J., 200,L123.

Frogel,J.A., Persson,S.E., Aaronson,M., & Matthews,K. 1978, Astrophys.J., 220,75.

Hegyi,D.J., & Gerber,G.L. 1977, Astrophys.J., 218,L7.

Heidmann,J., Heidmann,N., & de Vaucouleurs,G. 1971, Mem.R.astr.Soc, 75,85.

Heidmann,J., Heidmann,N., & de Vaucouleurs,G. 1971, ibid., p.105.

Heidmann,J., Heidmann,N., & de Vaucouleurs,G. 1971, ibid., p.121.

Johnson,H.L. 1966a, Ann.Rev.Astron.Astrophys., 4,193.

Johnson,H.L. 1966b, Astrophys.J., 143,187.

Kormendy,J. 1977, Astrophys.J., 217,406.

Kormendy,J., & Bruzual,G. 1978, Astrophys.J., 223,L63.

Larson,R.B. 1976, Mon.Not.R.astr.Soc., 176,31.

Oort,J.H. 1958, Ricerche Astr. Specola Vaticana, 5,145 (= Stellar Populations, ed. D.J.K. O'Connell, S.J.).

Ostriker,J.P., & Peebles,P.J.E. 1973, Astrophys.J., 186,467.

Persson,S.E., Frogel,J.A., & Aaronson,M. 1979, Astrophys.J.Suppl.Ser., 39,61.

Rieke,G.H., & Lebofsky,M. 1979, Ann.Rev.Astron.Astrophys. 17,477.

Rubin,V.C. 1979, Comm.Astrophys., 8,79.

Rubin,V.C., Ford,W.K., & Thonnard,N. 1980, Astrophys.J., 238,471.

Schweizer,F. 1976, Astrophys.J.Suppl.Ser., 31,313.

Spinrad,H., Ostriker,J.P., Stone,R.P.S., Chiu,L-T.G., & Bruzual,G. 1978, Astrophys.J., 225,56.

Strom,S.E., & Strom,K.M. 1978, in "Structure and Properties of Nearby Galaxies", IAU Symposium 77, D.Reidel, page 69.

Strom,S.E., Strom,K.M., Goad,J.W., Vrba,F.J., & Rice,W. 1976, Astrophys.J., 204,684.

Struck-Marcell,C., & Tinsley,B.M. 1978, Astrophys.J., 221,562.

Talbot,R.J., Jensen,E.B., & Dufour,R.J. 1979, Astrophys.J., 229,91.

van der Kruit,P.C., & Searle,L. 1981a, Astron.Astrophys., 95,105.

van der Kruit,P.C., & Searle,L. 1981b, Astron.Astrophys., 95,116.

van der Kruit,P.C., & Searle,L. 1982a, Astron.Astrophys., 110,61.

van der Kruit,P.C., & Searle,L. 1982b, Astron.Astrophys., 110,79.

Willner,S.P., Becklin,E.E., & Visvanathan,N. 1972, Astrophys.J., 175,699.

CHAPTER 2.

A 2.2 MICRON MAP OF NGC 5128.

CHAPTER 2

A 2.2 MICRON MAP OF NGC 5128

2.1. INTRODUCTION

In the late 1970s, infrared galactic research at Leicester concentrated mainly on "active" galaxies (Abolins et al. 1979; Abolins 1980). We report here observations which form the concluding phase of this programme: a near infrared map of the dust lane in NGC 5128, the parent galaxy of the giant double radio source, Cen A. When this work was published (in condensed form: Adams et al. 1983), it represented the first reported results of an innovative use of the infrared photometry system at the Anglo-Australian Telescope, observing the object in DC-coupled mode, no use being made of the normal infrared "chopping" procedure. While the above paper was in press, two sets of infrared data were published by other groups: however, both used lower spatial resolution than our study, and the basic conclusions of our paper remain intact.

2.2. THE OBJECT

NGC 5128, which plays host to the giant double-lobed radio source Cen A, is in many respects one of the most unusual objects in the night sky. The galaxy itself, optically many times smaller than the radio source, has an extremely active nucleus which has been observed at radio, infrared and X-ray wavelengths, but never in visible light. The galaxy is classed as an E0 pec., because of a dense dust lane which bisects its optical image, completely obscuring the nucleus. The most common interpretation of the geometry is that the dust lane encircles the galaxy, and lies in a plane approximately containing the line of sight.

Detailed studies of this object have recently been made by observers working at visible wavelengths from large southern hemisphere telescopes (NGC 5128 lies at δ =-43°). High resolution measurements of optical colour indices across the face of the galaxy by van den Bergh (1976) and by Dufour et al (1979) revealed extensive evidence for the presence of blue stars and HII-regions at the edges of, and in some cases within, the dust lane. The presence of these young tracers indicates that star formation has occurred in the dust lane within the last 25 million years. The surface brightness profile and stellar bands of the unobscured main body of the galaxy rank it with normal elliptical galaxies, although its integrated colour is slightly bluer. The physical distinction between the E component and the dust lane was clarified by Graham's (1979) spectroscopic observations, which demonstrated that the young component, defined in this case by HII-regions, rotates rapidly in its plane, whereas the elliptical component rotates only slowly, if at all.

How this apparently Elliptical-type galaxy acquired its rapidly rotating dust lane is as yet unclear, but one of the more popular explanations involves the capture and disruption of a spiral galaxy. Another unanswered question is why NGC 5128 should have developed its active nucleus and radio lobes, but it seems likely that the origin of the galaxy's activity could have been related to the onset of star formation in the dust lane some 10^7 years ago. The solution to these questions in NGC 5128 should shed light on the evolution of more distant double-lobed radio galaxies (Cen A is the nearest of the class), which are also centred on apparently elliptical galaxies. Our contribution is a high resolution look, through the dust, at the flattened component beneath.

Previous infrared observations of NGC 5128 (eg.,Becklin et al. 1971, Kleinmann and Wright 1974, Grasdalen and Joyce 1976) have concentrated on the optically obscured nuclear region, which contains an intense and highly self-obscured point source. Prompted by unpublished 60 micron observations by Harvey, Telesco (1978) detected strong 10 micron emission from the dust lane, at projected distances of up to 2 kpc. from the nucleus. Galactic 10 micron fluxes are normally dominated by emission from warm (100 K) dust in HII-regions: the dust lane is therefore independently identified as a region of star formation. Optical study of the distribution of the stars is ruled out by the large extinction in the dust lane; near-infrared observations, much less affected by reddening (Appendix A), were called for. An unpublished 2.2 micron map of the object, made with a 22 arcsecond aperture by Adams and Giles (1978), suggested the presence of the expected dust lane emission, but the morphology was confused by the field stars which are apparent in the higher resolution work presented here. Lack of spatial resolution also adversely affected the results of Harding et al.(1981), who employed a 30-arcsecond aperture at J, H and K, and failed to detect any small-scale structure.

2.3. OBSERVATIONS

(a) Scan patterns.

NGC 5128 was scanned in 1980 April with the 3.8 metre Anglo-Australian Telescope on Siding Spring Mountain, NSW, Australia. The projected aperture was 7 arcsec., and a standard K (2.0-2.4 micron) filter was used. Two sets of declination scans were made, each scan separated from the nearest neighbours in its set by 6 arcseconds, the second set (hereafter called the "interlaced" set), being displaced from the first by 3 arcseconds, to provide complete sampling of the object. Weather conditions impaired the signal-to-noise ratio of the interlaced set, requiring correction at the data analysis stage, to be discussed later. Guiding errors were checked by "peaking up" the infrared signal on the nucleus, and were in all cases less than 2 seconds of arc. Each scan contained 76 half-second integrations.

(b) DC measurement of extended objects.

Infrared astronomical measurements are traditionally made using a "chopping" technique, in which the difference in flux from two adjacent patches of sky is repeatedly measured (these patches are referred to as the "signal" and "reference" beams respectively). Whilst for point sources the instantaneous background subtraction and AC signal provided by this technique have resulted in its widespread popularity, it is clear that a narrow chopper throw can lead to problems when observing extended objects such as galaxies. There are two ways round the problem of reference beam "contamination": one, to be discussed in Chapter 3, is to employ a chopper throw large enough to place the reference beam well beyond any detectable emission from the galaxy; in practice this requires a throw of more than 8-10 arcminutes on the sky, and careful photometer design to ensure that equal amounts of thermal emission from the telescope are "seen" by the detector at either extreme of the chop cycle. A more elegant way of measuring infrared emission from extended objects would obviously be to do away with the chopping technique altogether. A decision was taken to attempt this second alternative in observing NGC 5128.

The AAO infrared system is conventional in using an Indium Antimonide detector and a focal plane vibrating-mirror chopper. The amplification system is novel, however, and has good DC stability (Barton and Allen 1980). The speed of the electronics allows the counts in the "sky" and "object" beams to be summed independently, such that the DC measurement of extended objects becomes feasible. With the novelty of this concept in mind, our observations were made with the chopper running, so that it would be possible to resort to more traditional analysis methods involving correction for reference beam flux, if the DC measurements were unsatisfactory (the feasibility of fully-DC mapping is demonstrated in Chapter 4). The chopper was set to throw 12 arcseconds E-W on the sky.

The surface brightness response of the system was calibrated by measurement of the count rates from standard stars, and by scanning a star through the beam to determine the projected aperture size.

It will become clear later that the object is by no means faint even at the north and south extremes of the area mapped. In other words, the off-galaxy background level was not reached at the ends of the scans, or at least those passing through the centre of the galaxy. This posed a number of problems at the analysis stage, which will be discussed in the next section. An observational procedure to remove this difficulty was devised and applied with moderate success in the mapping of M83 (Chapter 4): in the meantime, the methods applied to this object appear to provide a reasonable estimate of what the measured background level would have been.

2.4. DATA REDUCTION

(a) Basic strategy.

The basic requirement was the production of a rectangular array representing the spatial distribution of fluxes across the galaxy's surface. Scans were therefore taken from the two sets (original and interlaced), in order of decreasing right ascension, and stored on computer file with measurements in order of increasing declination. This particular format was dictated by the contouring routines available.

As noted previously, it was decided to observe with the chopper running normally, although it was suspected that fully DC mapping was possible. Two independent measurements were therefore available at each point of each scan, corresponding to the counts in the "signal" and "reference" beams (hereafter in this Chapter, beams "A" and "B"). As a concession to standard IR photometry, the values contained in the AAO computer output were "A", and "B"-"A" counts. The counts in beam A were isolated at each point of the array.

Drifts in the IR signal level due to the changing sky background flux, were apparent in the raw data, but were in all cases small and on a long enough timescale to be assumed linear within the space of one pass over the object: linear fitting to the levels at the ends of individual scans was therefore applicable. Centre-weighted smoothing was used in reducing the data to the map shown later, in which the four nearest neighbours to each point were given quarter weight. As mentioned earlier, a deterioration of the seeing impaired the signal-to-noise ratio of some scans in the interlaced set: in these cases, the smoothing was modified such that nearest neighbours in declination were completely suppressed, and the nearest points in the two adjacent (non-interlaced) scans were accorded equal weight with the central measurement.

The main difficulty encountered at this stage was the fact that the "sky" level was reached at neither end of the scans near the nucleus, disqualifying the normal technique which refers the count levels within a given scan to zero at its ends, with suitable linear fitting to background drifts. Under the assumption that scans at the east and west extremes of the area covered were far enough away from the galaxy that their north and south ends were effectively measuring the sky level, we determined the flux levels at the ends of the rest of the scans in the following manner (Fig. 1).

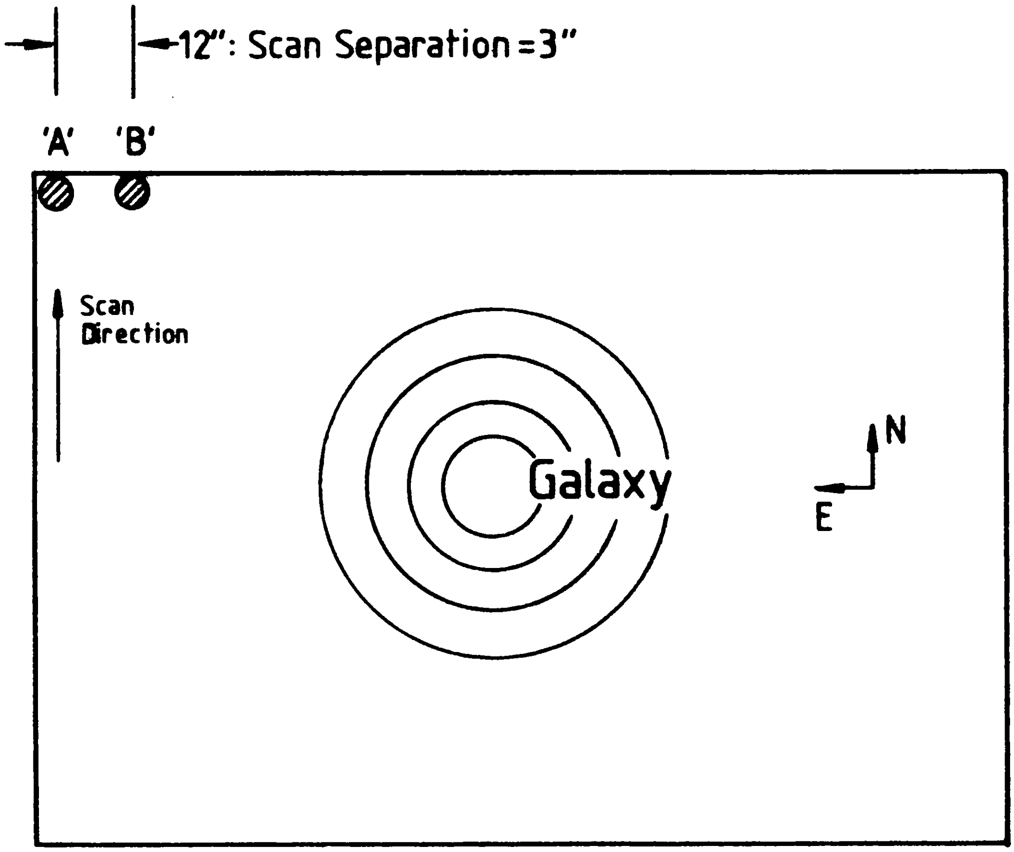

FIGURE 2.1

Scan pattern and background level estimation.

Referring specifically to the northeast corner of the map, with beam A measuring the sky level (ie. 0 galaxy counts), we can use the available A-B count to calculate the flux from the galaxy one chopper throw to the west; this is exactly the way one would proceed in the absence of either the fast AAO electronics or a widethrow chopper. Now the chopper throw employed was an integral number of scan separations, so beam "B" in Fig. 1 also corresponds to beam "A" of the fourth scan from the east. A running summation along the edge of the map therefore divulges the run of the flux levels: this was carried out at both the north and south edges, and checked by repeating the procedure starting with beam "B" at the western end, and working east.

The map presented later contains the information from beam A only: this means that only half the available information was used, but combining the counts from both beams into a single map proved to pose more problems than expected, and in the end the beam B data were retained as a check on the general morphology of the beam A map. The agreement was satisfactory.

(b) Surface brightness profiles.

While the two-dimensional mapping representation is necessary for an understanding of the dust-lane morphology, the physics of the elliptical component are best represented in the form of a one-dimensional profile, giving surface brightness as a function of galactocentric radius. The detailed behaviour of the individual pixels was investigated by plotting a regular selection of one quarter of the measurements against the fourth root of the radius, in order to test for adherence to de Vaucouleurs' law (see Chapter 1). This type of plot, however, was prone to the effects of the dust lane, and consequently did not permit an accurate assessment of the $R^{1/4}$ law parameters. The E component was therefore isolated from the rest of the galaxy by annular integrations to the SW of the dust lane: for values of R_g separated by 4 arcseconds, the measured fluxes were averaged over a 90° annular segment of 4 arcsec. radial extent, whose centre lay on a line perpendicular to the dust lane, in p.a. 209°. The SW sector was chosen because the nucleus is asymmetrically placed in the dust lane, permitting measurement of the unobscured E component to small radii (about 20 arcsec.) This analysis was performed by hand-selection of pixels, allowing the images of foreground stars to be excluded from the averaging. A least squares fit was made to the surface brightness distribution as a function of $R^{1/4}$, excluding points within the dust lane, which were affected by obscuration, as will be shown explicitly later.

2.5. RESULTS

(a) Features of the infrared map.

Fig. 2.2 is the 2.2 micron map of NGC 5128. Even brief comparison with a visible-wavelength photograph (eg., Sandage 1961; Grindlay et al. 1975) illustrates the effective transparency of the dust lane in the near-infrared. The nucleus of the galaxy, which is completely inaccessible to visible observations, dominates the 2.2 micron emission, and the gross circular symmetry of the E component is apparent. Absorption features are present, however, at the edges of the dust lane (marked by dotted lines in the diagram): the deepest of these, in the region around $\Delta\alpha$ =+30", $\Delta\delta$ =-25" relative to the nucleus, is about 0.7 mag. deep at this wavelength, assuming both circular symmetry of the underlying galaxy, and the absence of emission from the dust lane.

The signal from the nucleus is K = 8.3 $\pm$ 0.1 mag. in our 7 arcsec. aperture, consistent with the results of Grasdalen and Joyce (1976), who obtained K = 8.59 $\pm$ 0.03 and K = 7.92 $\pm$ 0.03 in 5.2 and 12.2 arcsecond apertures respectively. Our aperture was too large to place limits on the variability of the K = 9.2 mag. point source discussed by Grasdalen and Joyce.

(b) The elliptical component.

The V and B-band observations of van den Bergh (1976) and Dufour et al. (1979) demonstrated that the optical flux distribution in the main body of NGC 5128 obeys the de Vaucouleurs law for normal elliptical galaxies (see Chapter 1 for the form of this law). The near-

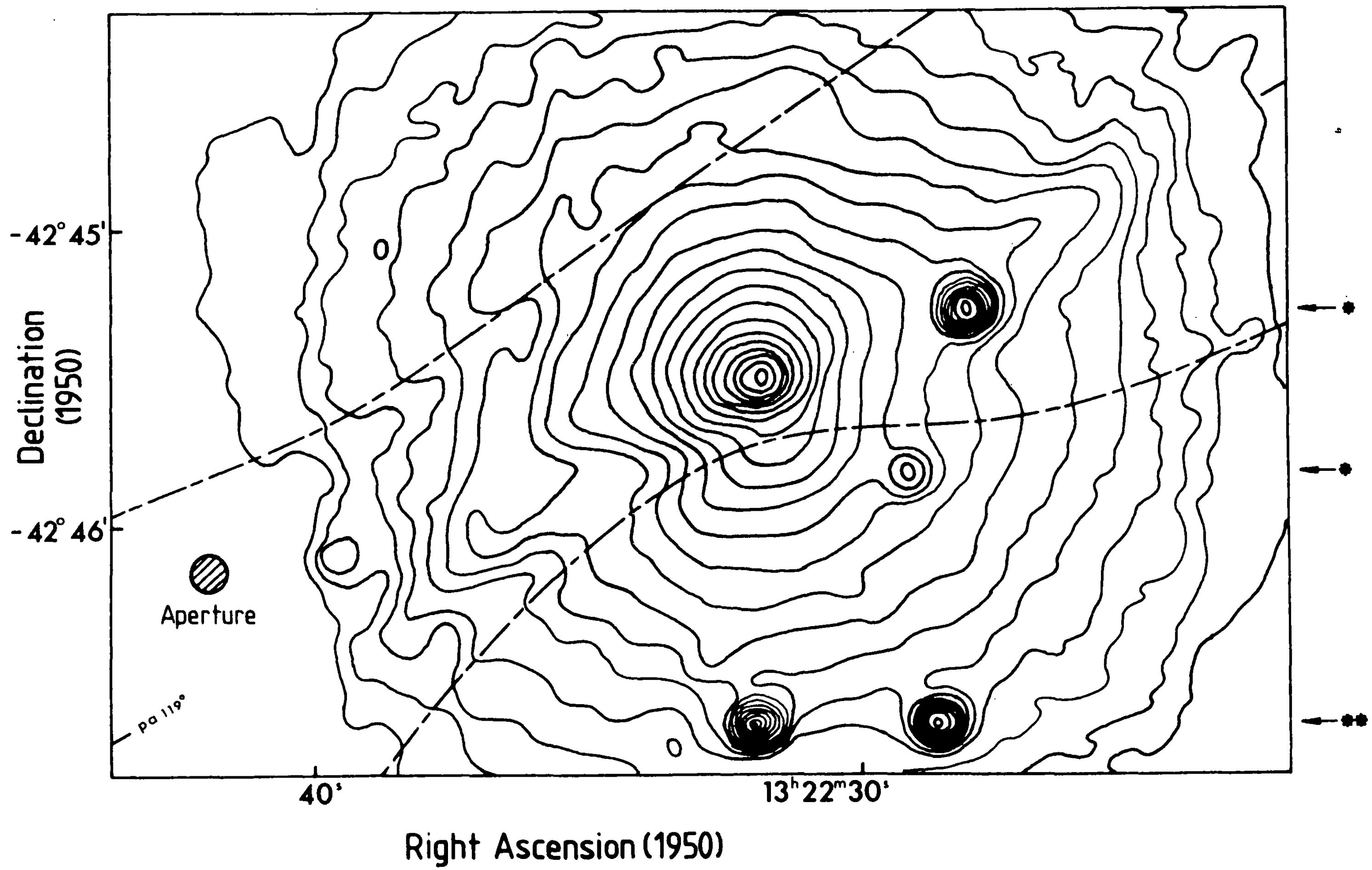

FIGURE 2.2

NGC 5128 at 2.2 microns. The edges of the absorption lane, and four field stars are indicated. Lowest contour is at 17.5 mag/sq.arcsec.; interval is -0.25 mag.

infrared surface brightness, if also primarily due to stellar continuum emission, should follow the same distribution. The annular averages in the SW sector, described in a previous section, resulted in an excellent fit of the surface brightness, SB_K, to $R_g^{1/4}$:

$SB_K = (2.54 \pm 0.02)R_g^{1/4} + (9.33 \pm 0.06)$. Rewriting this as

$SB_K = 8.325 \ ((R_g/(116 \pm 5))^{1/4} - 1) + (17.65 \pm 0.06)$, the data are seen to follow de Vaucouleurs' law with effective radius, $R_e = 116 \pm 5$. The infrared fluxes exterior to the dust lane are thereby identified with continuum emission from stars in an essentially normal elliptical galaxy, as previously noted by Harding et al. (1981).

Figure 2.3 shows the surface brightness, SB_K, as a function of $R_g^{1/4}$, for one quarter of the measurements used to produce the map of Figure 2.2. The least squares fit line described above is included for comparison, and it is clear that the scatter about the integrated relation is relatively small. Also included in the diagram are lines describing the optical surface brightness distribution according to Dufour et al., and a clear difference between the two sets of measurements is apparent. The infrared fit excludes points within the dust lane ($R_g^{1/4}$ less than about 2): these measurements fall systematically below the best fit line in Figure 2.3. It was suspected that the background level difficulties described before, mostly affecting infrared points at large radii where the signal is faintest, could have been responsible for the discrepancy between the optical and infrared fits. However, inspection of a single scan across the dust lane reveals that a constant correction of 0.48 mag. to obscured points was sufficient for continuity at the edge of the lane, as demonstrated in Figure 2.4. Application of this correction to measurements with R_g less than 2.0 in Figure 2.3 reinforces the slope adopted for the best fit in the infrared, and the discrepancy between the optical and infrared slopes (and hence effective radii) persists.

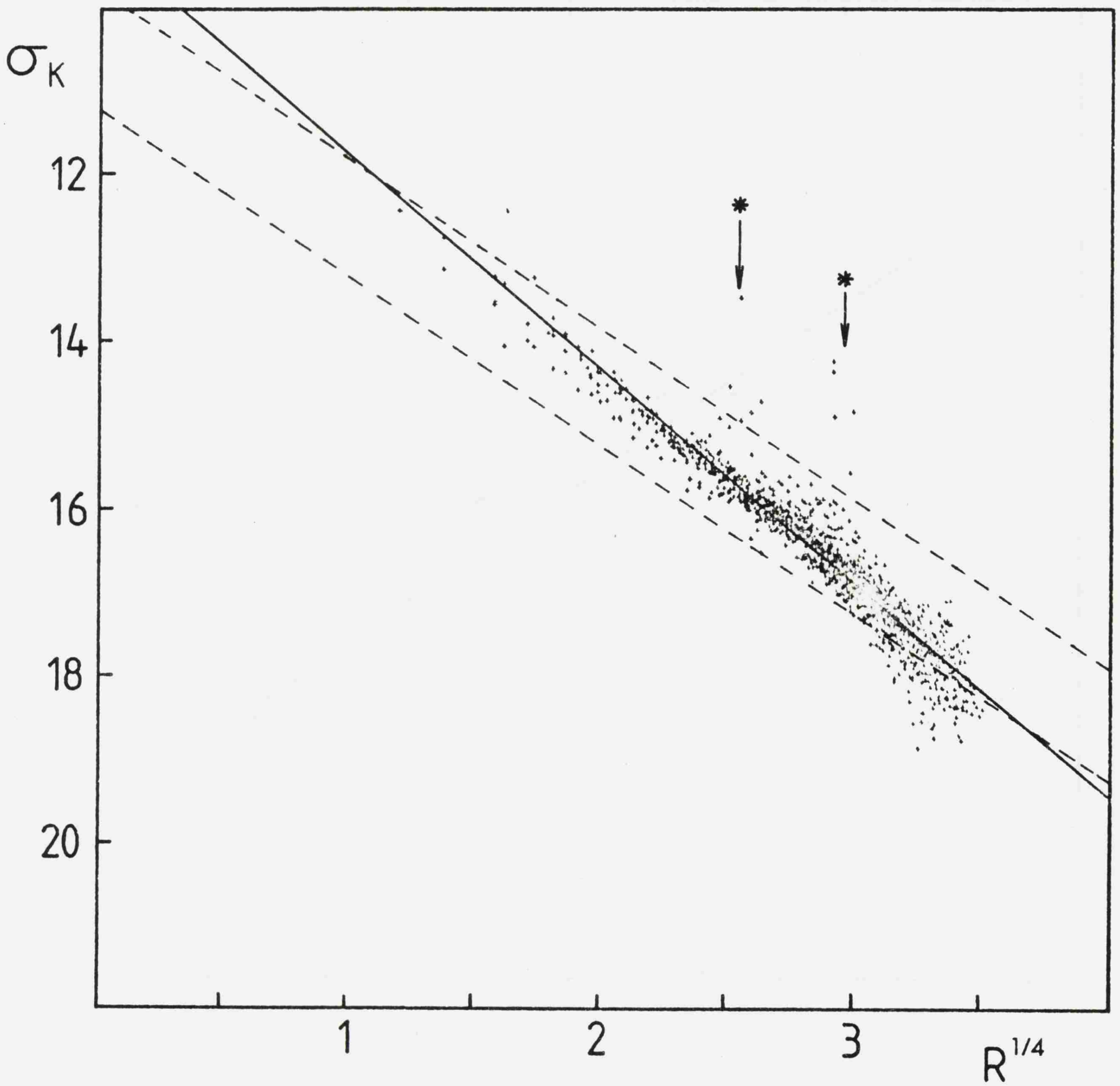

FIGURE 2.3

2.2 micron surface brightnesses as a function of $R_g^{1/4}$. The solid line indicates least-squares fit to the annular integrations described in the text. Points affected by field stars are indicated. For clarity, only one quarter of the measurements have been plotted. The dotted lines have the slope inferred from optical studies of the E component.

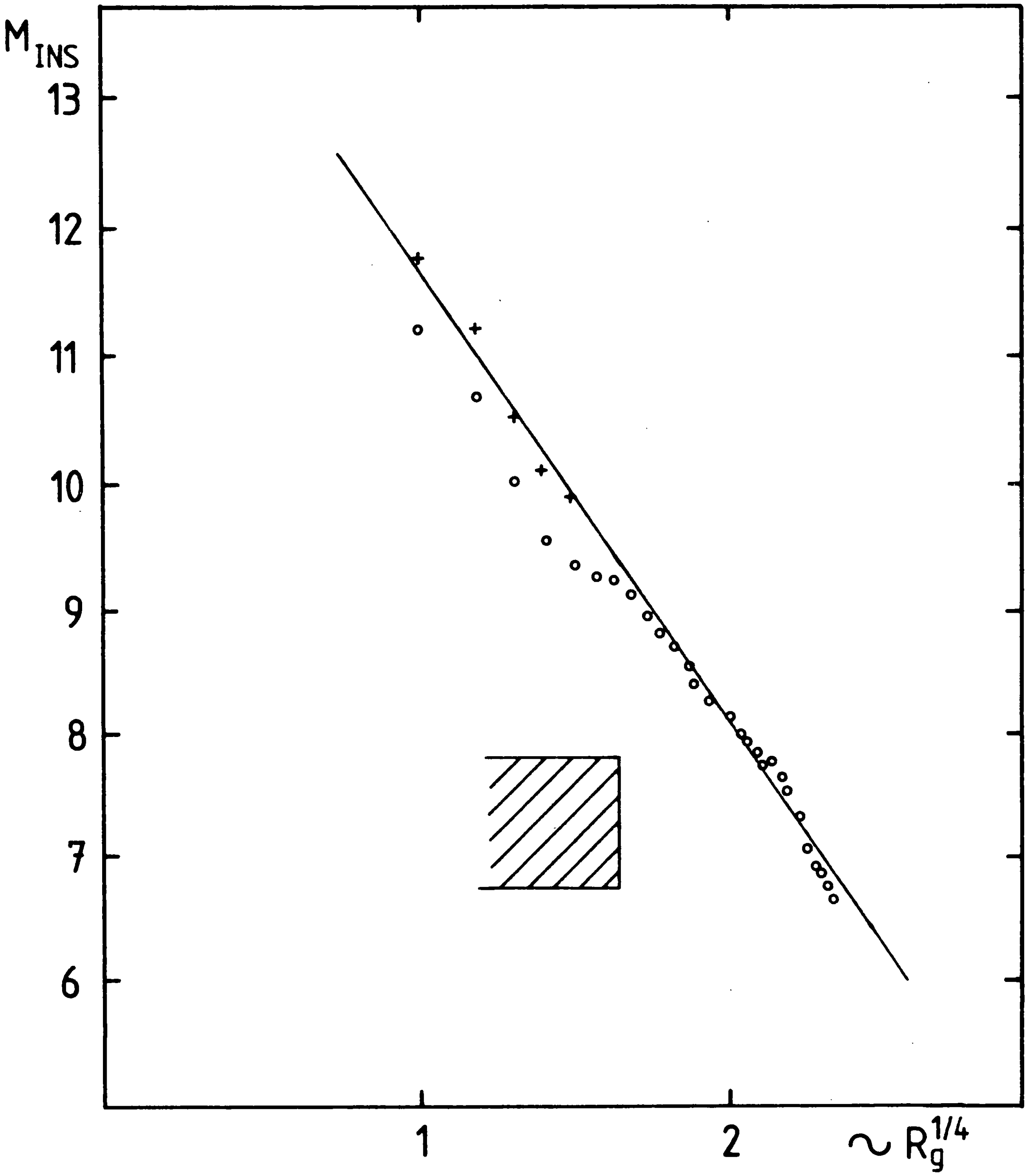

FIGURE 2.4

The effect of the dust lane on a cut across the galaxy from the nucleus south. Crosses indicate measurements within the dust lane after correction for 0.48 K mag. of extinction. Vertical axis is 2.5log(count).

The 2.2 micron profile presented by Harding et al.(1981) was in substantial agreement with the optically determined effective radius, and also showed no evidence for the absorption feature apparent in Fig.2.4. However, their beam diameter (30 arcsec) allowed at most only two resolution elements within the span of the dust lane, and the detection of such features was therefore unlikely. For the same reason, any of their measurements within 30 arcseconds of the nucleus are probably affected by beam convolution. We note that only four of their measurements lie further from the nucleus than the edge of the dust lane.

Comparison of the infrared effective radius with the value of 300" obtained from blue-light surface photometry by Dufour et al. (1979) implies the presence of an (optical-infrared) colour gradient across the face of NGC 5128. Such a result is in qualitative agreement with the work of Strom et al.(1976), who showed that the outer regions of elliptical galaxies are bluer in V-K than their nuclei. At distances of 50-100 arcseconds from the NGC 5128 nucleus, we obtain a V-K index of 2.8 ± 0.3 by comparison with the data given by van den Bergh, or an intrinsic index of 2.5 ± 0.3 after correction for foreground visible extinction of $A_V = 0.3$ mag. This is unusually blue for an early type galaxy: we note, however, that Strom et al.(1978) found changes of up to -0.4 mag in V-K along the minor axes of two early type galaxies, which would permit the central regions of NGC 5128 to be more normal in V-K, with a value around 3 mag.

(c) The dust lane sources.

Inspection of the isophotes approximately 60 arcsec. NW of the nucleus (in p.a. 299°) shows that the flux from this region, in spite of the dust extinction, is in excess of the elliptical component flux measured at the same galactocentric radius outside the dust lane. This excess emission, which is also apparent on the other side of the nucleus, is resolved in declination by individual scans, having a full width (perpendicular to the dust lane) of 15 arcseconds, considerably less than the 60 arcsec. total width of the dust lane itself. The feature can be traced to within 50" of the nucleus, before it becomes lost in the strong E component flux. Spatial resolution is critical for success in observing this feature: the 30 arcsecond aperture employed by Harding et al. was large enough that the emission was (i) unresolved and (ii) compensated for by the deep extinction at the north and south edges of the dust lane. A subtle distortion of the 2.2 micron contours presented by Walsh and White (1982) is apparent, but their 12" beam was again slightly too large for a detailed assessment of the morphology.

Fig. 2.5 shows the excess dust lane fluxes measured within an 18" wide strip along p.a. 119°. Measurements were averaged over annular segments of 4 arcseconds radial extent. As noted above, the excess emission becomes diluted in the E component as the nucleus is approached: in order to study the dust lane in detail, therefore, it is necessary to first remove the contribution from the main body of the galaxy. This was achieved by subtracting, from each radial bin in the dust lane strip, the elliptical component flux averaged over the appropriate SW-sector annulus. Points within 20" of the nucleus were not treated in this way, because of uncertainties caused by the steepness of the E component at small radii. Two 2.2 micron emission peaks are seen in Fig. 2.5, equally spaced at about 65", or 1.625(D/5) kpc. (where D Mpc. is the distance to NGC 5128) on either side of the

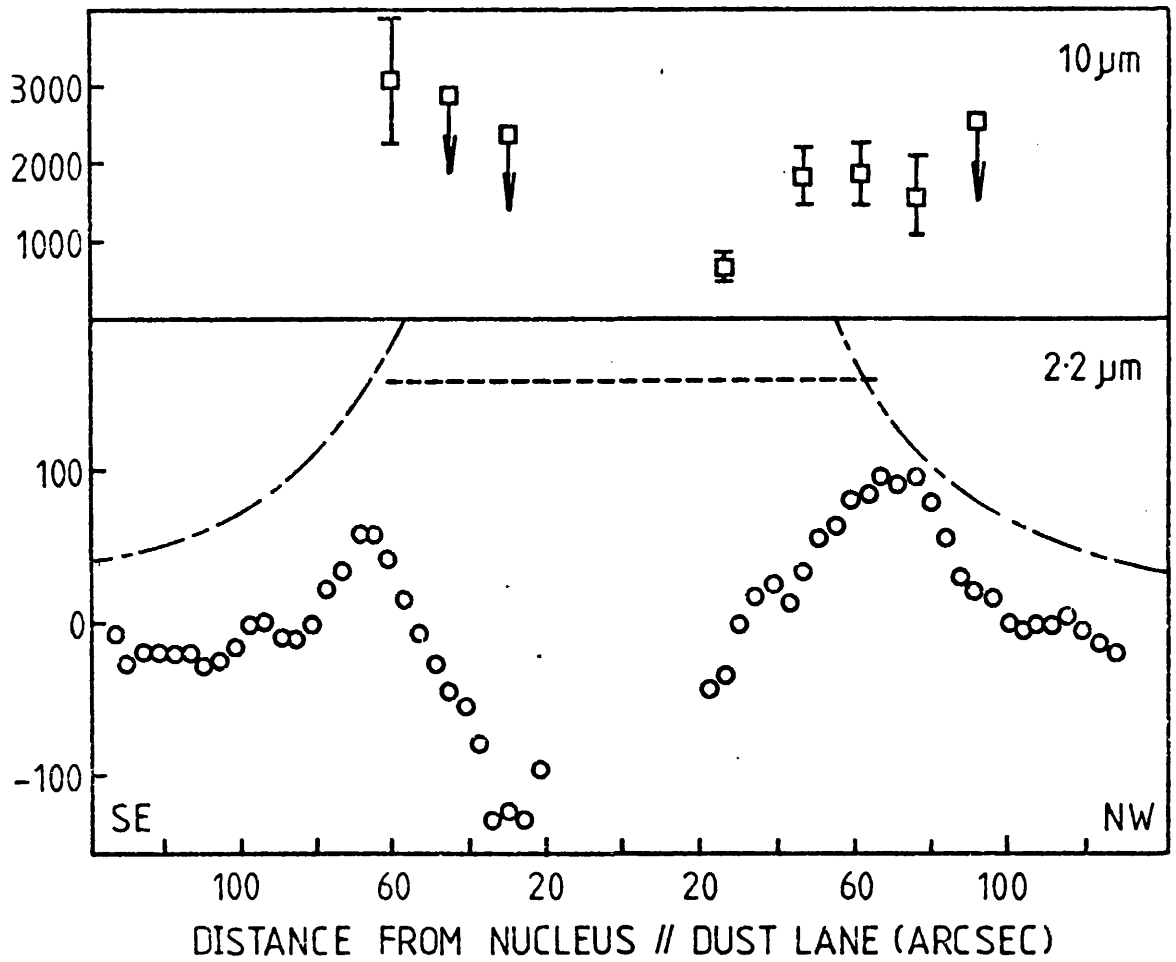

FIGURE 2.5

(lower) 2.2-micron fluxes from the dust-lane after subtraction of the E component (shown by the chain-dot line). The dashed line shows the flux level assumed in calculating the total excess. (upper) 10-micron data from Telesco (1978). All fluxes in units of 10^{-32} W. m^{-2}. Hz^{-1}. $arcsec^{-2}$.

nucleus. The northwestern peak is approximately 1.5 times brighter than its southeastern counterpart, probably because of the difference in character between the dust lane extinctions of these two regions, a difference apparent on optical prints of the galaxy.

The upper half of Figure 2.5 represents the 10 micron fluxes measured along the dust lane by Telesco (1978). A degree of correlation between 2- and 10-micron distributions is apparent. At the northwestern peak, 65" from the nucleus, the 2.2 micron surface flux, averaged over the 18" strip, is 9.7×10^{-31} $W.m.^{-2}Hz.^{-1}arcsec.^{-2}$. Interpolating between Telesco's sources 7 and 8 to locate the same area of the dust lane, the corresponding 10 micron flux is 1.7×10^{-29} $W.m.^{-2}Hz.^{-1}arcsec.^{-2}$ of a 14 arcsecond aperture. The ratio of flux densities is therefore of order 20, and will not change by more than a factor of two if averaged over a larger area of the dust lane. (The area discussed here was observed at 3.5 microns by the author and Ian Gatley at the UKIRT in July 1980. A 3 sigma upper limit of $3.83 \times 10^{-30} W.m.^{-2}Hz.^{-1}arcsec.^{-2}$ was recorded in a 10.8 arcsecond beam, and comparison of alternate beamswitch pairs showed that contamination from the gradient of the E component was negligible).

The basic infrared colour information is listed in Table 1, where we have included for comparison the 10/2 micron flux ratios for galactic HII-regions, normal dwarf stars, and the star forming region at the centre of another active galaxy, M82. The 2.2-10 micron colour of the excess emission from the dust lane is consistent with the source region containing a mixture of HII-regions and normal stars. The flux ratio is similar to that observed in the (much brighter) central region of M82, and the identification of the dust lane as an area of star formation seems secure.

TABLE 2.1

OBJECT	10/2 micron Flux Ratio	REFERENCE
HII-region	300	Wynn-Williams and Becklin (1974)
NGC 5128	20	This Thesis
		Adams et al. (1983)
M82: 5.8"	20	Rieke et al. (1980)
		Abolins et al. (1979)
M82: 35.0"	10	Kleinmann and Low (1970)
MOV star	0.05	Bopp et al. (1974)

Any discussion of the morphology of the region containing the source of the excess 2.2 micron flux must necessarily include an assessment of the effects of extinction. In the following analysis we will assume that the emission source lies largely behind dust clouds which contribute the bulk of the reddening; we note that the conclusions we shall reach would be invalidated if the true geometry involved mixing of the emitting and absorbing material.

We aim to investigate the plausibility of the simple disk-like structure proposed by Telesco (1978), in the light of the 2.2 micron measurements. Following Telesco, we postulate the underlying morphology to be one of constant excess surface brightness from $R_g = -65$ to $+65$ arcseconds along the dust lane. The 2.2 micron deficits seen within 50" of the nucleus are then a natural consequence of the dominance of the elliptical component at all radii: that the "excess" as calculated above is negative at small radii merely reflects the difference between the unobscured and dust-lane reddened E component fluxes.

For the value of the constant excess surface flux in the simple model above, we will assume the peak value in Fig.2.5, corrected for 0.56 mag. of extinction, obtained from van den Bergh's visible extinction E_{B-V} = 1.85, via the van de Hulst reddening law. The plausibility of the model can then be demonstrated by calculating the differential extinction between the dust lane and the elliptical component required to produce the observed differences in Fig. 2.5. The resulting values of extinction range from 0.22-0.36 mag between 20 and 70 arcsec. NW of the nucleus, and from 0.38-0.68 mag over the same radial range in the southeast. These 2.2 micron extinctions imply obscuration in the visible up to 7 mag.; such values were inferred by van den Bergh(1976) from the optical colours of the dust lane.

The 2.2 micron emission is thus consistent with a constant surface brightness "disk", centred on the nucleus of the galaxy. We note here that Walsh and White (1982) interpreted the continued steep decline of the 2.2 micron surface brightness over the 10 micron-bright region in terms of a radially varying 2-10 micron colour temperature. Our analysis demonstrates that since emission from the E component dominates the contribution from the dust lane, any attempt to assign colour temperatures must first involve isolation of the dust lane from the main body of the galaxy.

We have insufficient information to determine whether the disk brightness shows a maximum or a minimum at the nucleus; either situation could be adequately fitted with realistic extinction values. At radii greater than 70" in Figure 2.2 the excess emission is clearly seen against the elliptical background: the decrease in the surface flux at large radii seen in Figure 2.5 is therefore probably an intrinsic property of the disk, and not an artifact of extinction. The radius of the feature is 2.0(D/5) kpc., placing it well inside the "ring" of HII-regions discovered by Graham (1979), which has a radius of 4.1kpc.

As a comparison with the flat and spheroidal components of spiral galaxies, we have estimated the total unobscured 2.2 micron flux from the dust lane sources on the basis of the simple model structure described above. From -80 to +80 arcseconds along p.a. 119^{o}, the excess flux in the 18" wide strip is 4.5 x 10^{-27}W.m.$^{-2}$Hz.$^{-1}$, corresponding to an integrated apparent magnitude of K = 7.2 . The total 2 micron magnitude of the elliptical component is K = 3.75, obtained by integrating de Vaucouleurs' law (van den Bergh 1976), with the parameters determined earlier. In the abscence of obscuration, therefore, the feature observed in the dust lane would contribute about 2% of the 2.2 micron luminosity of NGC 5128.

2.6 CONCLUSIONS

Near-infrared observations with good spatial resolution demonstrate the presence of a flattened emission feature in the dust lane of NGC 5128, with a thickness of less than 0.36 (D/5) kpc. Comparison with the 10 micron observations of Telesco shows the 2-10 micron colour to be similar to that of the star forming central regions of M82.

REFERENCES

Abolins,A.J. 1980, Ph.D. Thesis, Leicester, University of Leicester.

Abolins,J.A., Adams,D.J., Jameson,R.F., Hough,J.H., & Axon,D.J. 1979, Mon.Not.R.astr.Soc., 186,23p.

Adams,D.J., & Giles,A.B. 1978, private communication.

Adams,D.J., Adamson,A.J., & Giles,A.B. 1983, Mon.Not.R.astr.Soc., 202,241.

Barton,J.R., & Allen,D.A. 1980 Publ.Astr.Soc.Pacific,92,368.

CHAPTER 3.

INFRARED AND OPTICAL PROFILES OF EDGE-ON SPIRALS.

3.1 INTRODUCTION

Observations are presented of highly inclined spiral galaxies in the J, H, and K Johnson wavebands. Optical (V-band) measurements are presented for a subset of the objects. The two main objectives of this study were:

(i) the use of the near-infrared data to circumvent the problems caused by dust obscuration at shorter wavelengths (the objects are all inclined at greater than 80° to the plane of the sky;

(ii) to combine near-infrared and optical measurements in a search for metallicity-driven colour changes as a function of position in the galactic disks.

Time constraints result in the inclusion of somewhat less than the full quota of information available from these observations; a single parameter was chosen from the data set (the brightness distribution along the major-axis) which was considered to minimise the effort required to arrive at scientifically significant results.

All initial reduction of the raw data into radial count variations was performed by hand, as the data were sufficiently irregular to obviate the use of any but the most ad hoc. computer techniques. This proved to be a most aggravating and time-consuming procedure, in the end requiring on the order of one month's work before any processing into magnitudes or fluxes could be contemplated. Some idea of the size of the data set involved will be gained later from Figure 3.3, where we show one of the four sets of scans of NGC 2683, this particular set being the 1.2 micron measurements. Each individual scan required assessment of the background level, a search for foreground stars, and

TABLE 3.1

Observed edge-on spiral galaxies.

OBSERVING RUN	NGC	WAVEBANDS OBSERVED	DISTANCE + SOURCE	TYPE	INCLINATION + SOURCE	
Feb.1981	4565	J,K	18.4 (1)	Sb	86	(3)
Jul.1981	5907	H,K,V	13.0 (2)	Sc	88.5	(1)
	7814	H,K,V	20.8 (2)	Sab	----	
Feb.1982	2683	J,K,V	4.03 (2)	Sb	80.5	(1)
	4594	K,V	18.2 (1)	Sab	84.0	(2)

Inclinations are quoted from the following sources:

1. Heidmann et al. (1971) Mem. Roy. astr. Soc. 75,121.
2. Sandage (1961) Hubble Atlas.
3. de Vaucouleurs (1958).

Morphological types are quoted from:

Sandage (1961)

Heidmann et al. (1971)

or estimated from Palomar sky survey plates.

Distances are from:

1. Faber and Gallagher (1979)
2. de Vaucouleurs et al. (1975), assuming a Hubble constant of 60 km./sec./Mpc.

estimation of the signal counts from the galaxy. The group of scans shown in the Figure is itself a combination of the data from two separate nights, each with its own calibration measurements. Approximately 10 such sets, some subdivided to a greater extent, comprise the raw data analysed in this Chapter.

All observations were made at the 60-inch flux collector of the Observatorio del Teide, Tenerife, Spain, during the following three observing seasons:

Jan - Feb 1981

July 1981

Feb - Mar 1982 .

Table 3.1 summarises the galaxy observations made during these runs. We attempted to cover as wide a range of morphological type (ie. of bulge-to-disk ratio) as possible within a relatively small sample, from NGC 5907, almost a pure disk, to the bulge-dominated NGC 4594. The data set on NGC 7814 will not be presented here, as bad weather limited the available radial coverage: this is a significant shortcoming for observations of an early type system whose bulge and disk components inherently resist separation. The data on NGC 4594 are yet to be analysed.

3.2 INSTRUMENTATION

All observations in this Chapter employed the Leicester widethrow photometer designed by D.J.Adams. This instrument is built around a rotating sector-wheel chopper, which is standard in most respects except that the spacing between the fixed and rotating mirrors is of the order of two inches, which, when translated into 8 arcminutes at the Cassegrain focus of the Tenerife flux-collector, is sufficient to place the sky reference "beam" well away from detectable regions of all but the largest nearby galaxies. The scanning described in the next section can therefore be carried out without the reference-beam contamination which affects narrow-throw work on extended objects.

The infrared flux is detected with a liquid N_2 - cooled Santa Barbara In Sb cell operated in the Johnson-noise limited manner described by Hall et al. (1975); filters used give the standard Johnson 1.2 micron (J), 1.65 micron (H), and 2.2 micron (K) passbands.

From July 1981 onwards, the photometer included an optical channel, giving the Johnson V passband, behind a gold dichroic reflecting the chopped infrared light into the In Sb cryostat. The photomultiplier employed was an EMI 9789B 52-mm. tube, and the V filter was Chance OY 4 glass. With the optical detector connected directly to pulse-counting electronics without gating or phase-sensitive detection, the photometer was capable of measuring (object-sky) in the infrared, and 1/2 (object+sky) in V. In order to minimise data reduction problems, observations of the galaxies were performed in such a way that the off-galaxy background was always measured (see next section).

3.3 SCANNING TECHNIQUES

The 60-inch flux collector provides for offsetting in both axes and at a variety of rates. Whilst normally used for object acquisition, this facility also permits the observer to scan an aperture across extended objects with reasonable precision (about 5 arcsec): the observations reported here made exclusive use of this method.

Scanning a square patch of sky around an object seen effectively edgewise would entail the loss of a prohibitive amount of observing time spent integrating on the blank sky background. We attempted to minimise such wastage by adopting the type of scan pattern shown schematically in Figure 3.1. Scans were performed in blocks of (typically) three, each block being staggered relative to its neighbours in the in-scan direction (generally RA), the amount of

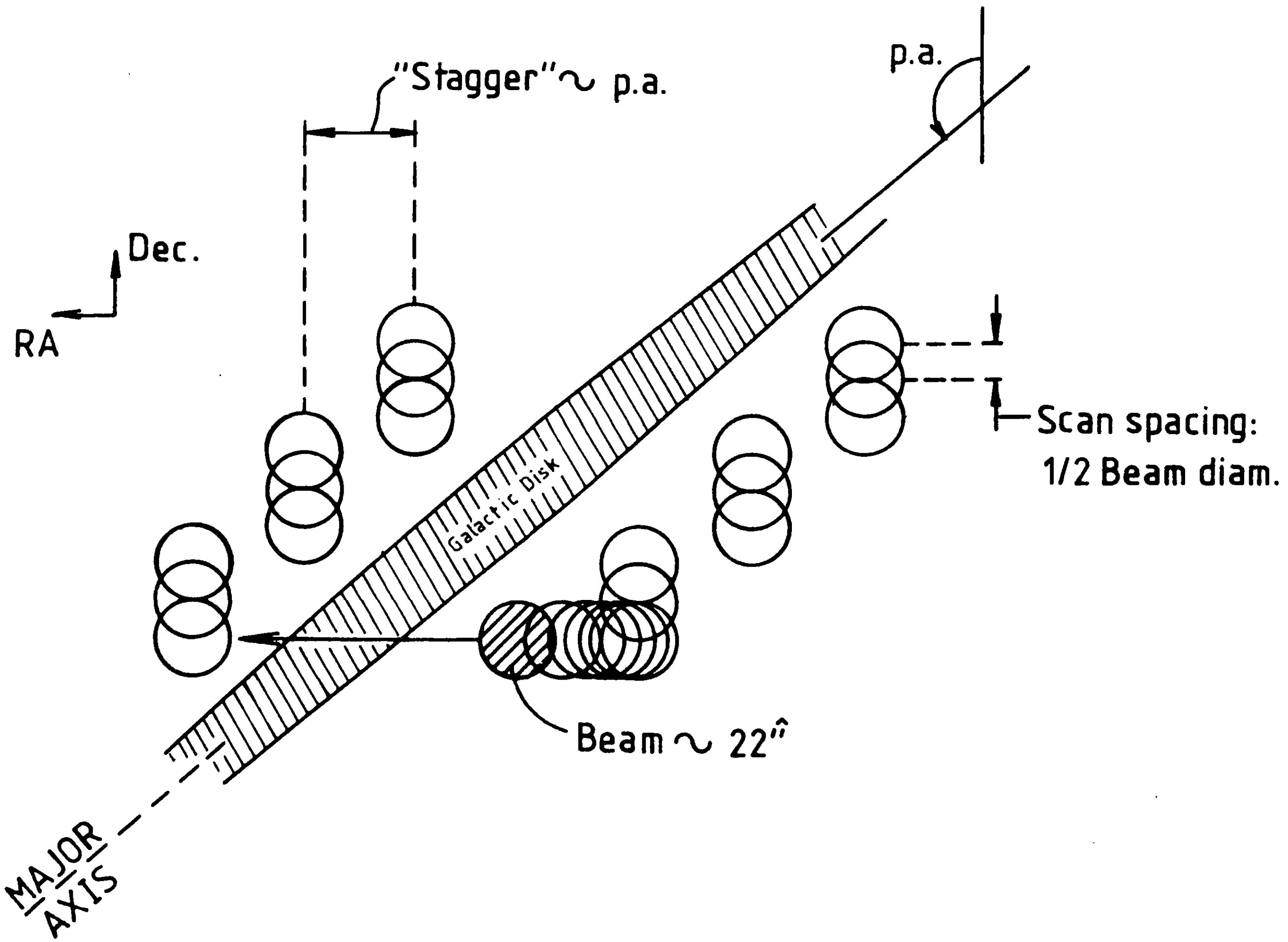

FIGURE 3.1

Schematic scan pattern.

stagger being proportional both to the position angle of the galaxy's major axis, and to the inclination of the galaxy to the plane of the sky. The nominal aperture in all cases was 22 arcseconds, and scans, normally performed in RA (for reasons of tracking accuracy), were separated in declination by half this amount, to provide complete sampling and the possibility of consistency checks between scans.

The minimum resolution element in a completely sampled map is one half of the beam diameter used. With a view to picking out foreground star contamination at the data reduction stage, integration times were chosen such that several integrations were performed per spatial resolution element scanned by the telescope aperture. Scan lengths were chosen which ensured that the start and end positions were clear of the optical extent of the object, thus ensuring accurate assessment of the "sky level" and of background drifts.

Apart from the obvious detector noise, the precision of the data are limited by the pointing accuracy of the telescope, which was seen to depend heavily on hour angle and (less) on declination. The second part of the observational procedure outlined below describes our efforts to reduce the effects of poor pointing and to permit identification of scans with unacceptable positioning errors (in what follows, capitals, eg., "OFFSET", denote functions provided by the telescope drive system):

(a) acquisition

- (i) find an SAO star close to the galaxy
- (ii) "peak up" infrared signal in the smallest aperture
- (iii) align optical aperture for maximum counts
- (iv) OFFSET telescope to the galaxy
- (v) "peak up" infrared signal on the nucleus
- (vi) centre an offset guide star in offset guider eyepiece

(b) scanning

(i) remove backlash in the declination drive wheels using offset guide star and drive handset

(ii) OFFSET to the required declination channel

(iii) OFFSET to the RA of the start point of the scan

(iv) perform slow OFFSET back across the object at the required scan rate

(v) RETURN to the declination of the nucleus

(vi) RETURN to the RA of the nucleus

(vii) check position of the offset guide star relative to the eyepiece centre mark to provide a measure of the positional error accumulated during the scan

(viii) redo the scan if this error is excessive.

In an attempt to build up signal to noise ratio and as a check on consistency and telescope positioning, each scan of NGC 2683 in January 1982 consisted of two passes over the object, the slow OFFSET ((iv) above) being RETURNed immediately the end of the scan path was reached.

Every attempt was made at the telescope to ensure a "top hat" beam profile, although we would emphasize that pristine top hat profiles are less important to scanning work than to multiaperture observations (eg., Frogel et al. 1975; Aaronson 1977), where small irregularities at the top of the profile can, in combination with miscentering of the beam, lead to excessive errors in the behaviour of magnitude growth-curves at large apertures (Frogel et al. required a beam profile flat-topped to about 2% for their observations of E and S0 galaxies).

3.4 DATA REDUCTION

(a) Binning

The oversampled scanning data were binned into resolution elements according to the following formula:

$N = {}^{D}/_{2Rt}$, where N is the number of integrations averaged to produce each map element, D is the beam diameter in arcseconds, R is the scan rate in arcsec./sec., and t is the integration time in seconds. This procedure produced sets of numbers representing the closest possible approach to complete sampling, with typical over- or under-sampling (the fractional amount by which the size of the final map element exceeds or falls short of the half-beam resolution element) less than 10%.

(b) Count Estimation

The data for each galaxy consist of a series of scans which cut across the major axis at various distances from the nucleus. The time constraints mentioned above meant the omission from this thesis of all but the measurements on the major axis; there will therefore be no discussion of, for instance, the variation of scale height with galactocentric radius. However, this omission reduced the data reduction task to the step of estimating the major-axis count rate at each radial position. The data were typically of the form shown in Fig.3.2.

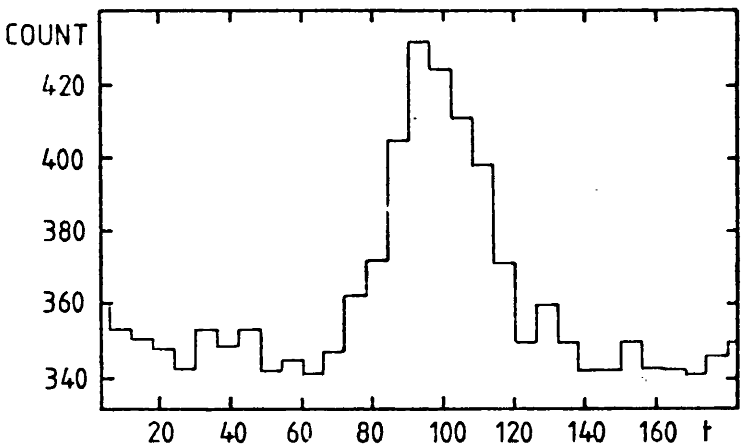

FIGURE 3.2

A typical binned scan across NGC 4565, at 2.2 microns.

The major-axis count rate, assumed to be the maximum of the scan (but see (ii) below), was evaluated as follows:

(i) the peak count was read from computer printout of the binned data;

(ii) a plot of the raw (unbinned) data was searched for evidence of a stellar image near the peak; if one was found, it was removed by interploation (if possible) and the binning was performed again;

(iii) the background level at the time of crossing the major axis was estimated from an eye-fit to the count levels at either end of the scan;

(iv) the signal count then followed by subtraction.

Step (ii) above is illustrated in Figure 3.3, where we show a complete 1.2 micron run on NGC 2683, before binning. Stellar contamination of the signal and reference beams is indicated.

In observing NGC 5907, the criterion that the start and end positions of the scans should be clear of detectable emission from the galaxy was not wholly satisfied: Fig.3.4 shows a typical scan across the object in binned and unbinned form, and the background level is clearly not attained in the binned data (a photograph given later, in Figure 3.8, shows the area scanned). The background level for each scan was therefore estimated from the asymptotic behaviour of the unbinned data. The run of the background levels thus calculated was a smoothly varying function of the time of observation, increasing our confidence in the method.

(c) Reduction to surface brightness

The counts obtained as described above were transformed into magnitudes via the count rates obtained from standard stars listed by Johnson (1966). These stars were observed typically both before and

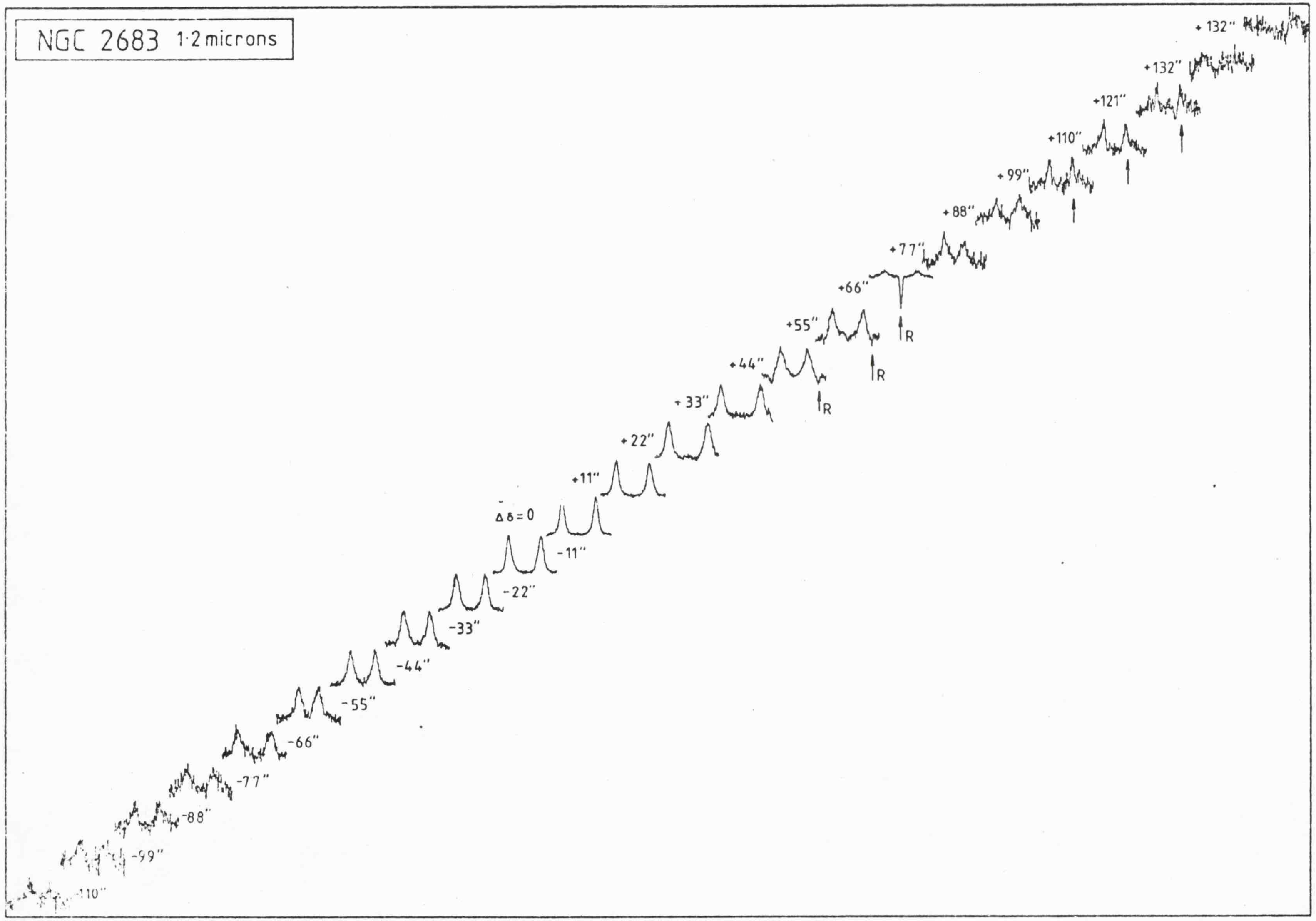

FIGURE 3.3

A complete 1.2 micron run on NGC 2683. Reference beam and signal beam contamination are indicated.

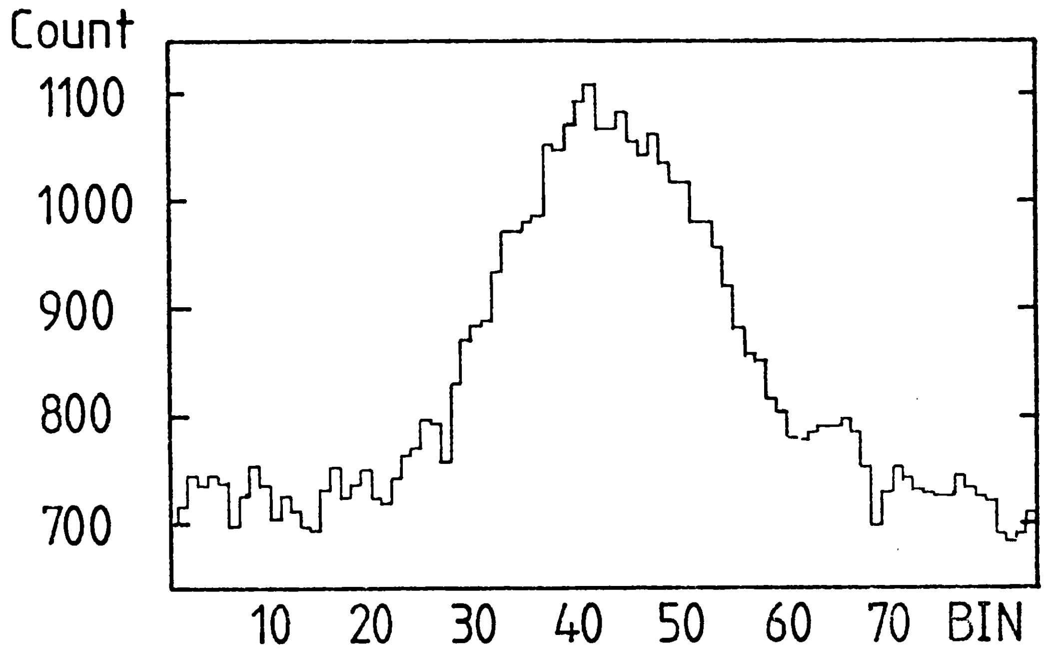

FIGURE 3.4

Detection of NGC 5907 at the extremes of the scans. The background level was eventually estimated from the asymptotic behaviour of the unbinned data (upper plot). Detection at significant distances above the plane is implied (3.6 b iii).

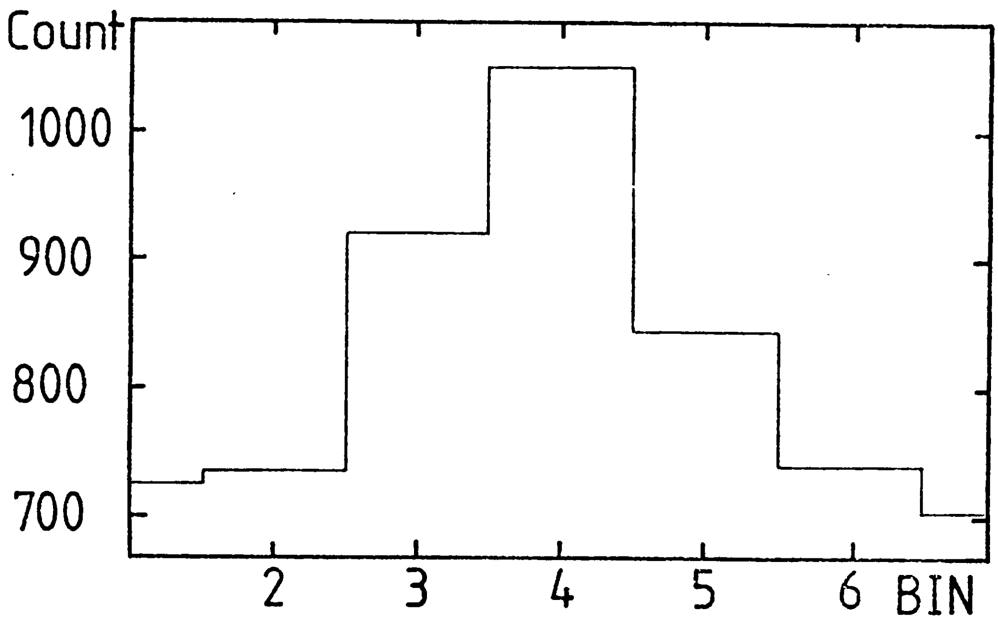

after the galaxy observations were made, and always after the infrared cryostat was refilled with LN_2. No galaxy was observed at an airmass greater than 1.5, and the observational errors at the faint edges of the galaxies were generally larger than the airmass corrections inferred from the standard measurements. Airmass corrections were therefore not applied to the data, the standard star measurements corresponding to each set of galaxy scans being simply averaged.

The optical standard measurements made in January 1982 are probably affected by dead time errors: the cathode-to-anode voltage had been increased to 1300V from the 950V employed in the observations of NGC 5907, with a consequent increase in pulse rate as more photons were detected. No facility was available for measuring the optically bright Johnson standards (for example by the use of neutral-density filters). The resulting dead-time losses, as yet uninvestigated, probably give rise to a systematic 10% error in the surface brightness scale. Our discussion of the galactic brightness profiles, restricted to the presence or absence of colour index gradients, is not seriously affected by this uncertainty.

The final step of the reduction to surface brightness, in magnitudes per square arcsecond, was achieved using the half-power beam diameter to estimate the area of the projected aperture. The 22" nominal diameter was checked by scanning faint stars. The beam diameters inferred from these "star scans" were uncertain by up to 2 arcseconds, resulting in a non-random uncertainty in the final surface brightness scale of approximately $\pm$ 0.18 mag.

The internal consistency of the optical data is improved by the availability of two sets of scans for each galaxy; one for each infrared waveband observed. The visible magnitudes presented in later diagrams result from weighted averages of the fluxes derived from these two sets. One particular night's data in the V band on NGC 2683 were seen to be systematically fainter than expected from previous scans; in this case the standard measurement was assumed to be at fault, and the calibration was instead performed with respect to the nucleus of the galaxy, which was measured in all sets of scans. The two data sets were then averaged in the manner described above.

(d) Disk parameters

The two most immediately interesting parameters available from these data are (i) the disk scalelength and (ii) the disk surface brightness extrapolated to $R_g = 0$. For surface brightness distributions following the exponential disk law described in Chapter 1, the observed logarithmic surface brightness is a linear function of radius: $SB = SB_0 + (\text{const})R_g$. SB_0 is then directly the second required parameter, and the disk scalelength is given by 1.086/(const). It will be seen later that the linear surface brightness distribution adequately describes all of the disks observed.

(e) Colour information

As noted in Chapter 1, the variation of optical-infrared colour indices across the face of a galaxy can provide useful information on a number of properties of the stellar mix. Whilst the situation in spiral galaxies is confused somewhat by the presence of visible obscuration, the sense, and to a lesser extent the size of colour index gradients, if any, still permit the identification by elimination of the dominant mechanism.

Colour indices (SB_V-SB_K, etc.) were formed at each measured radial position in all three of the objects. Variations were then investigated by calculating the unweighted linear regression of colour index on radius. In cases where the galaxy showed a prominent nuclear bulge, the radial range over which this fitting was performed was restricted to regions exterior to the bulge, such that any gross change due to the transition from the spheroid to the disk population was avoided. The linear fitting was chosen simply because there is no a priori reason to assume any particular form for the variation of the colour index; the trends are in any case so subtle that a number of plausible functions would fit the data within the errors. Our purpose was only to determine whether such variations exist. The formulae employed for the linear regression slope, intercept and errors are standard, and may be found in (for example) Barford (1967).

(f) Folding data about R=0

In an attempt to boost signal-to-noise in the faint disks, some of the data sets were "folded" about $R_g = 0$, and the least squares treatment repeated. The results of this processing will be presented alongside the more normal fitting later. It was not attempted where there were obvious differences between the exponential slopes on the negative-R and positive-R sides of the nucleus (cf the J brightness profile for $R_g < 0$ in NGC 2683; Fig.3.12).

3.5 RESULTS AND DISCUSSION

(a) NGC 4565

The observed area of this galaxy is shown by the box in the photograph, Figure 3.5.

(i) Brightness profiles and comparison with previous results

The radial variation of surface brightness at 1.2 and 2.2 microns is presented in Fig. 3.6(a). In this and all subsequent surface brightness and colour-index plots, negative values of R_g correspond to measurements south of the nucleus. A two-component brightness distribution is clearly indicated, with a central excess over an exponential disk at large radii. Table 3.2(a) gives the parameters of the least-squares exponential fits to the outer points: agreement between the north- and south-side distributions was good enough to

FIGURE 3.5

NGC 4565. The area covered by our observations is shown enclosed.

Aperture diameter was 22 arcsec.

warrant application of the folding procedure (3.4 f), and the resulting fits are shown in Figure 3.6(b), and given numerically in Table 3.2(b).

Table 3.2.

NGC 4565 DISK PARAMETERS

(a) UNFOLDED

Johnson Band	Radial Range (kpc)	A $(\mathrm{mag.arcsec^{-2}kpc^{-1}})$ $(SB = SB_0 + A\ R_g)$	SB_0 $(\mathrm{mag.arcsec^{-2}})$	h (kpc) $(I=I_0e^{-R/h})$
J	> 4	0.08 ± 0.01	17.3 ± 0.1	13.1(+2.5,-1.8)
J	<-6	0.066 ± 0.01	17.55 ± 0.02	-16.3(+3.4,-5.8)
K	> 7	0.07 ± 0.01	16.2 ± 0.16	15.2(+2.9,-2.1)
K	<-7	0.07 ± 0.02	16.24 ± 0.25	-15.0(+3.2,-5.6)

(b) FOLDED

J	> 7	0.07 ± 0.01	17.45 ± 0.1	14.9(+2.3,-1.8)
K	> 7	0.07 ± 0.01	16.23 ± 0.1	15.3(+2.5,-1.9)

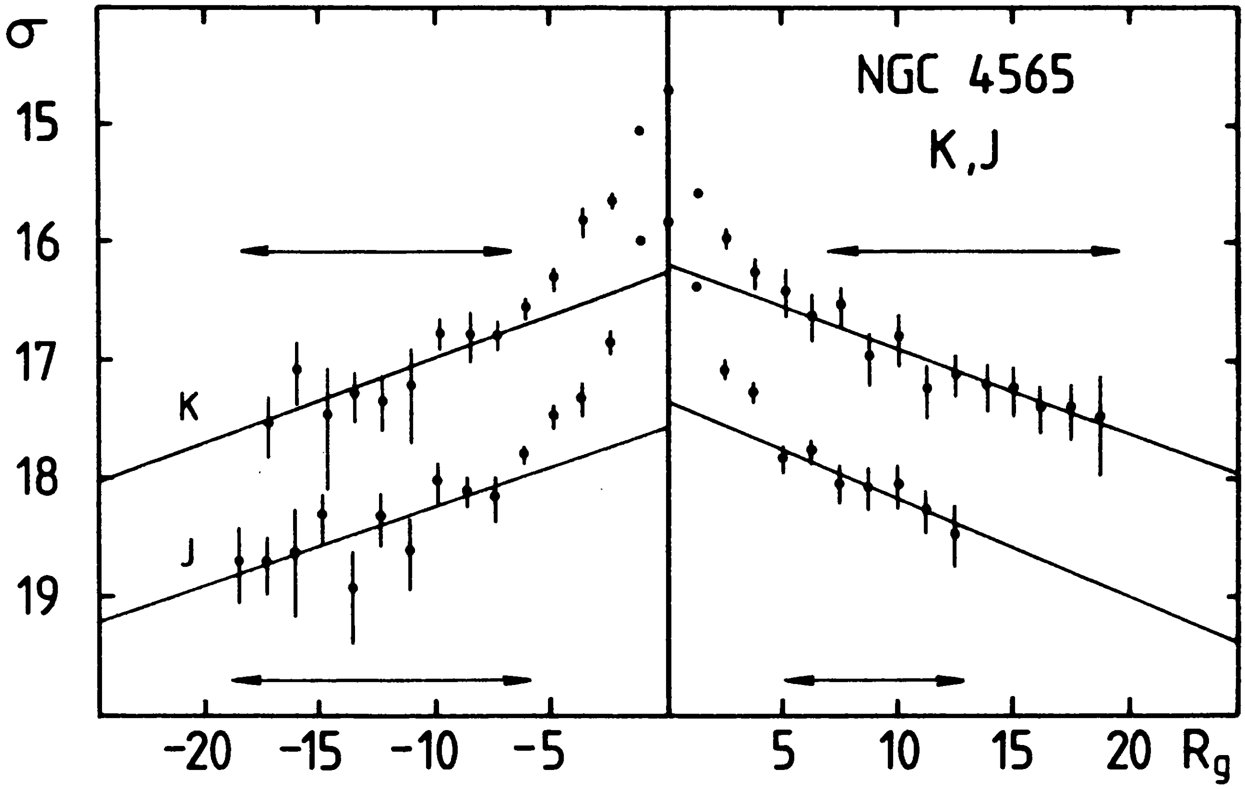

FIGURE 3.6

(a-upper) J & K surface brightness against radius (kpc) for NGC 4565.

The best-fit lines are described in the text.

(b-lower) J & K profiles, showing folded fits. Open squares indicate measurements by Hohlfeld & Krumm (1981).

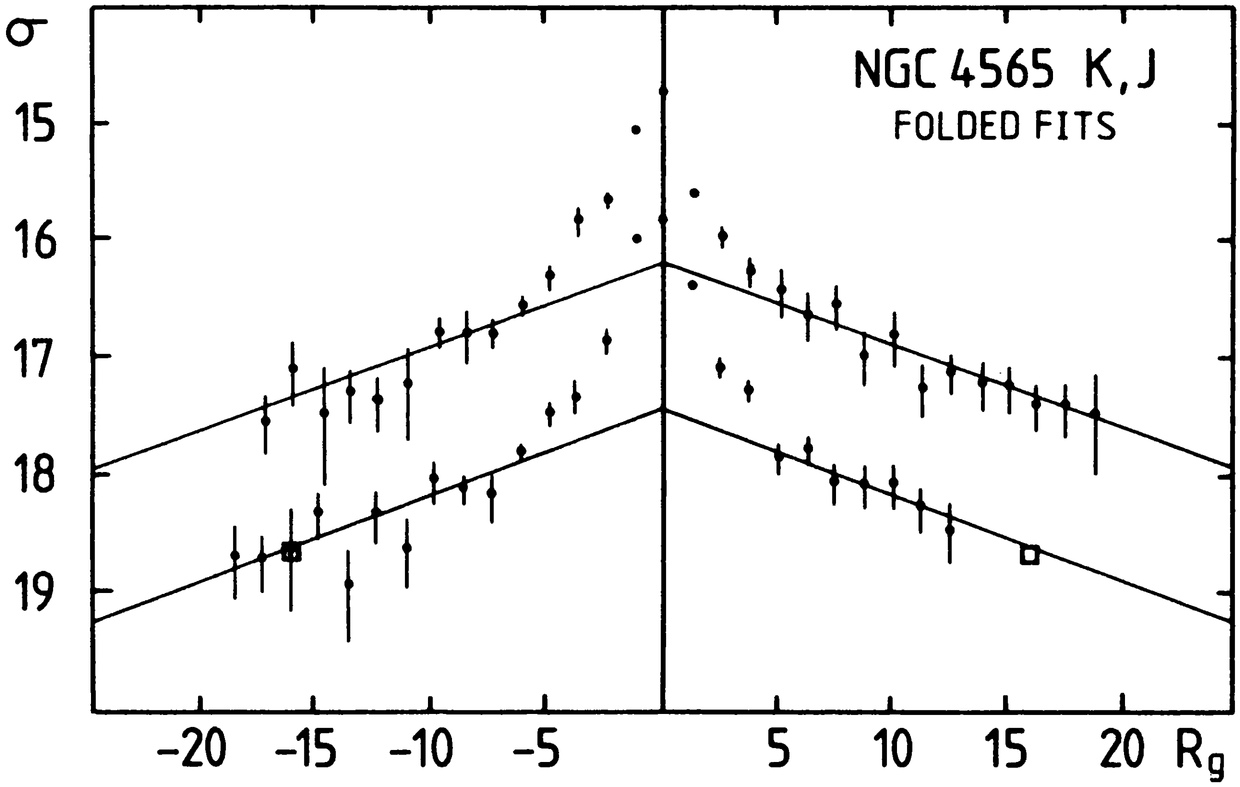

Previous observations of this object have concentrated on the possibility of detecting an optical halo (eg Hegyi and Gerber 1977), and on the debate as to whether such a halo would prove photometrically separable from the faint outer reaches of the known nuclear spheroid (eg Spinrad et al.1978, Kormendy and Bruzual 1978). The distribution of light in the disk has recieved less attention than it deserves, especially as the angular size and brightness of NGC 4565 make it a potentially rewarding object for study. We now summarise the available data relevant to our observations.

Frankston and Schild (1976) made optical and infrared (I;1 micron) observations with a solid-state array detector, but analysis of the resulting maps reveals that their sky-background subtraction was inadequate; they accept that flux levels beyond 30" from the nucleus cannot be trusted. Their discussion was limited to the shape of cuts taken perpendicular to the disk, as these are less affected by poor background corrections than are the absolute flux distributions on the major-axis. Spinrad et al.(1978) present smoothed optical isophotes; unfortunately, only one of these falls within the radial range covered here. For our purposes, the most useful optical data are those derived from photographic photometry by van der Kruit and Searle (1981). They fit a truncated isothermal disk model to high resolution photographic measurements and derive a scale length of 5.5 kpc. at 10Mpc, which translates to 10.1 kpc at our assumed distance of 18.4 Mpc (Table 3.1). They do not give a figure for the expected error in this determination. Their value lies twice our quoted error below the mean of about 15 kpc. (folded fits: Table 3.2 b); the discrepancy might therefore disappear if we extended our radial coverage.

For the present, therefore, we will limit our discussion to the near-infrared colours, with confidence in the magnitude scale enhanced by the single measurement within our radial range made by Hohlfeld and

Krumm (1981; see our Fig. 3.6 b). The latter authors also present two points at radii up to 540 arcseconds (48 kpc) along the major axis; in Table 3.3 we compare these measurements with an extrapolation of the best-fit to our data, folded about R_g=0. The agreement at 300" is encouraging for our estimation of the scalelength. At 540" the Hohlfeld and Krumm measurement is substantially below the disk extrapolated from smaller radii; this "cut off" is also apparent in the optical observations of van der Kruit and Searle, who speculate that it may be due to critical instability in the gaseous disk from which the galaxy formed.

Table 3.3

1.2 Micron disk extrapolation and comparison with data from Hohlfeld and Krumm (1981).

R_g (arcsec)	R_g (kpc)	SB_J (mag/arcsec^2) (Hohlfeld+Krumm)	(this thesis)	Comment
180	16.03	18.7$\pm$0.1	18.6$\pm$0.1	measured
300	26.7	19.1$\pm$0.2	19.3$\pm$0.3	extrapolated
540	48.0	22.8$\pm$0.9	20.8$\pm$0.5	extrapolated

(ii) Central surface brightness of disk component

From Table 3.2(b), the disk surface brightness extrapolated to R_g=0 from larger radii is:

$SB_J(0) = 17.45\pm0.1$;

$SB_K(0) = 16.23\pm0.1$. The implied J-K colour of the flattened component is therefore $(J-K)_0 = 1.2\pm0.1$. The discrepancy between this figure and the value resulting from the least-squares fit to the colour-index data (Table 3.4: $(J-K)_0 = 1.5\pm0.3$; see next

Table 3.4

Linear Fits to Colour Index Across NGC 4565

Colour Index (mag.)	Radial Range (kpc.)	($CI=CI_0+BR_g$) B (mag/kpc)	CI_0 (mag)
J - K	> 7.0	-0.03 ± 0.05	1.58 ± 0.5
J - K	<-7.0	-0.009 ± 0.03	1.4 ± 0.4

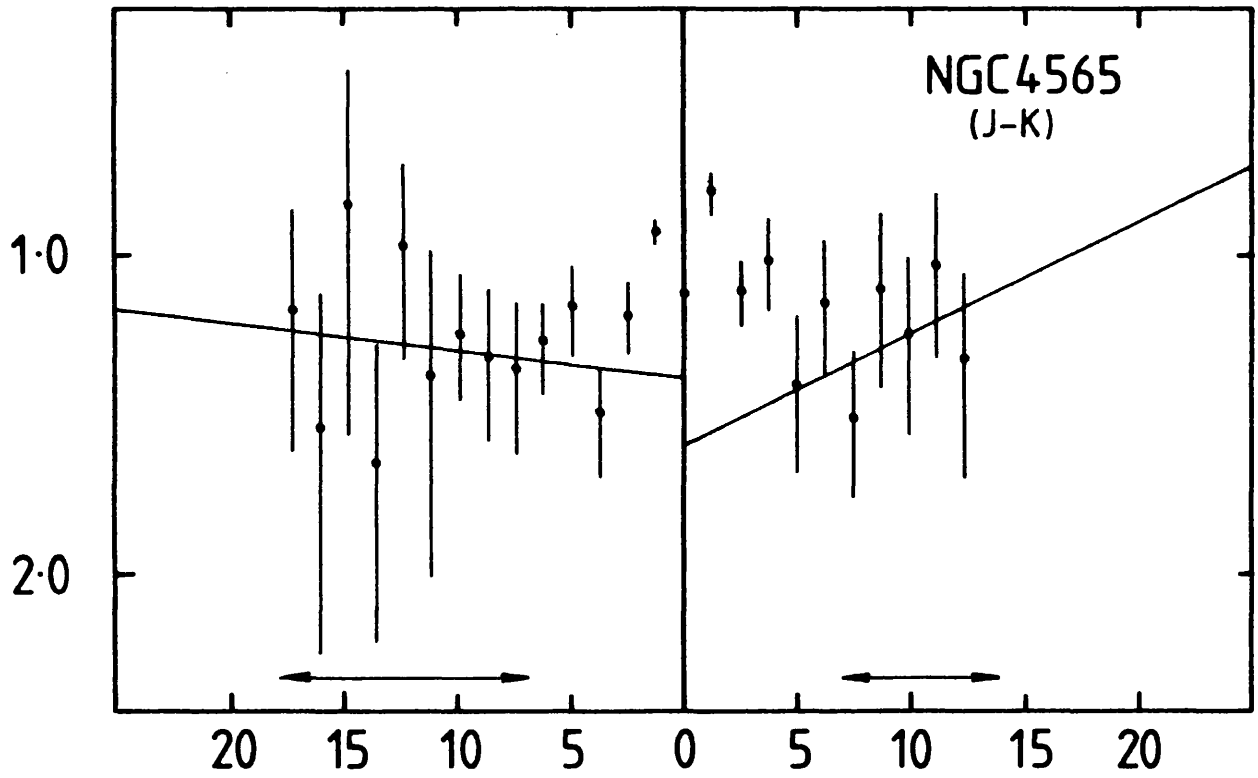

FIGURE 3.7

NGC 4565 Observed J-K colour indices, showing least-squares fits.

section) results from the more limited radial range for which both J and K magnitudes were available for the formation of the colour index.

(iii) Disk colours as a function of radius

Figure 3.7 shows the observed J-K colour for those positions of the disk at which both J and K fluxes were measured. In this and all subsequent colour index plots, positive values of the slope parameter, B, imply increasing index with increasing radius on either side of the nucleus. In order to avoid contamination from the nuclear bulge, the linear regressions shown, and given in Table 3.4, were restricted to galactocentric radii greater than 7 kpc. The Table shows that the J-K colour remains constant to within 0.05 mag.kpc^{-1} over a range of 10kpc in radius. The plot of the J-K index implies that the nuclear bulge, prominent in the surface brightness profiles within 5 kpc. of the centre, may be systematically about 0.2 mag. bluer than the immediately surrounding disk. The average J-K colour of the innermost five points of Fig. 3.7 is $\langle J-K \rangle = 1.03 \pm 0.02$, in reasonable agreement with the value of 1.12 (38 arcsecond aperture) found by Aaronson (1977), given that our equipment is not ideally suited to spot photometry, and that Aaronson expressed difficulty with his beam profile at 1.2 microns.

(b) NGC 5907

The photograph overleaf (Fig. 3.8) shows the area observed, and goes some way to explaining the difficulties encountered in estimating the background level.

(i) Surface brightness profiles

The basic data at V, H and K are given in Figure 3.9 (a). For clarity, the 1.65 micron points have been shifted down in surface brightness by 1 magnitude. Once again, the profiles suggest the

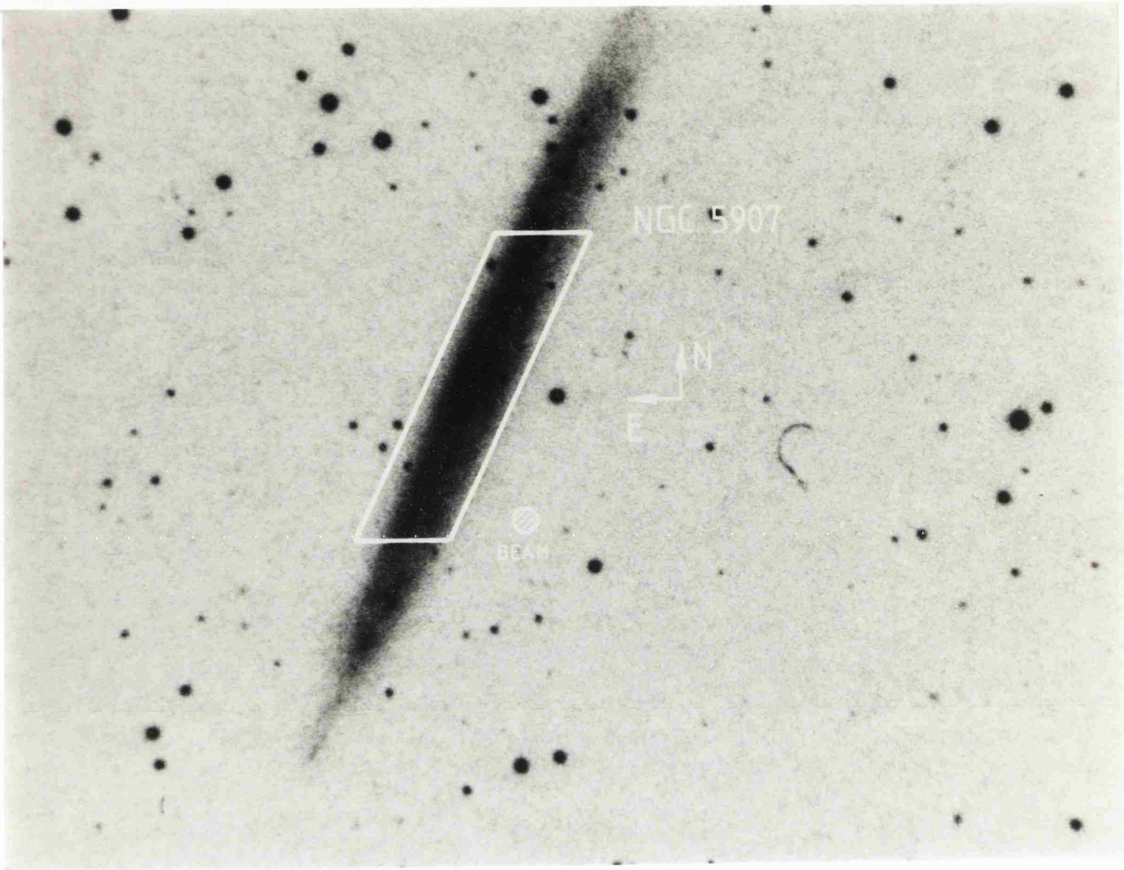

FIGURE 3.8

NGC 5907 from the Palomar sky survey, showing the area scanned.

Indicated beam size is 22 arcsec.

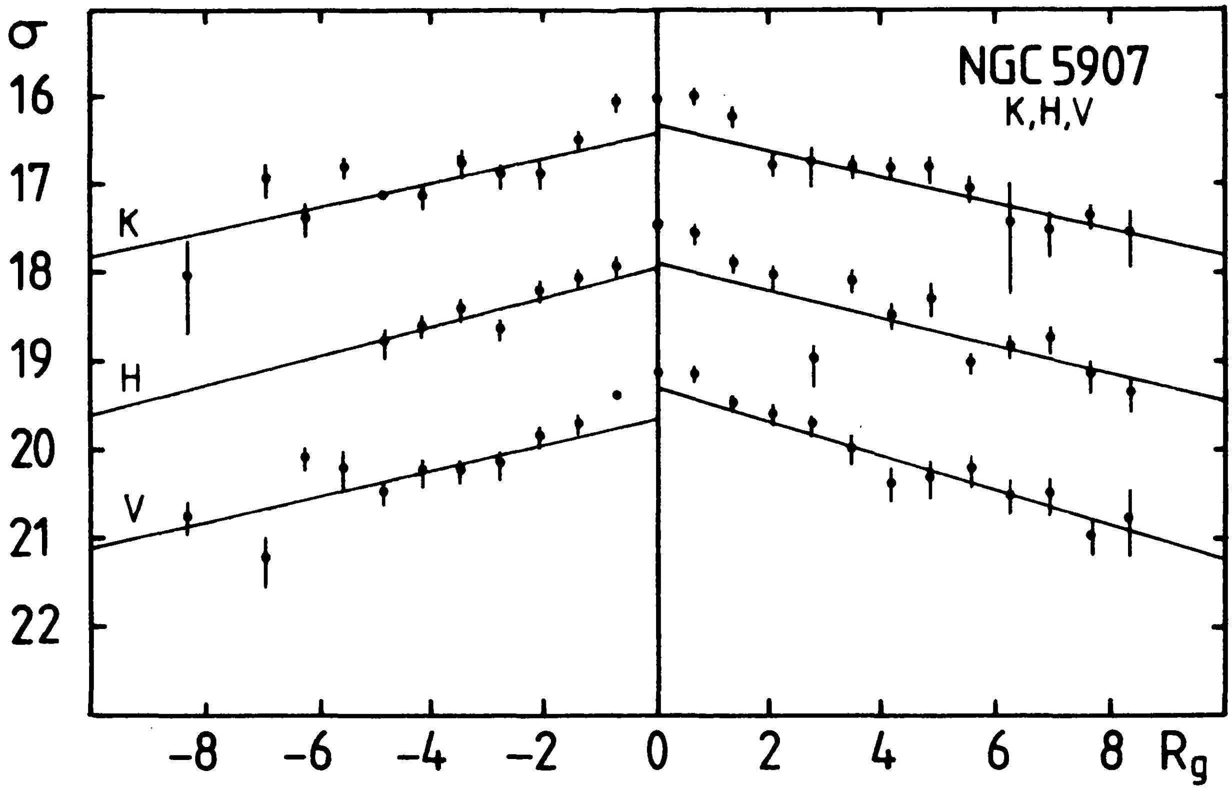

FIGURE 3.9

(a-upper) V,H and K surface brightness of NGC 5907, in a 22" aperture. The 1.65 micron measurements have been shifted down by 1 mag. for clarity.

(b-lower) as (a), but linear regressions performed on data folded about $R_g=0$.

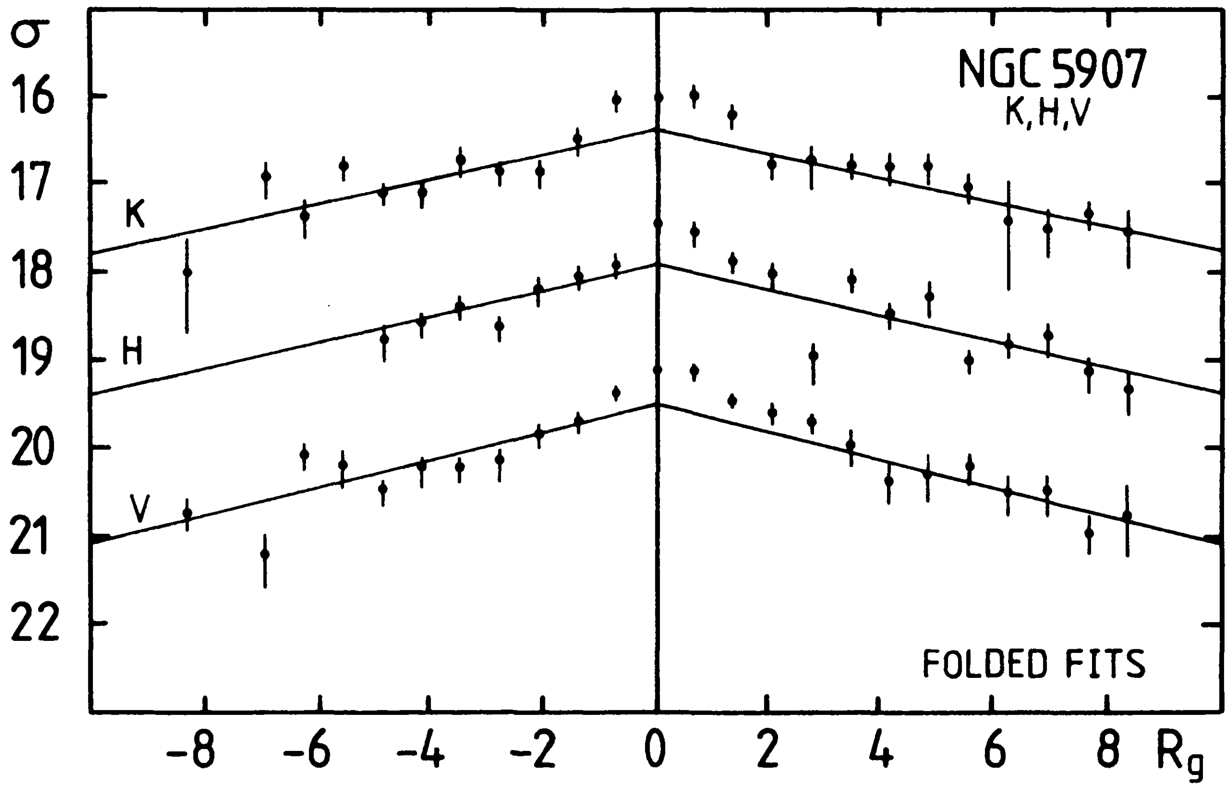

Table 3.5

NGC 5907 DISK PARAMETERS

(a) UNFOLDED

Johnson Band	Radial Range (kpc)	A (mag.arcsec^{-2}kpc^{-1})	SB_0 (mag.arcsec^{-2})	h (kpc)
		($SB = SB_0 + A\ R_g$)		($I=I_0e^{-R/h}$)
V	> 2.0	0.2 ± 0.03	19.2 ± 0.1	5.5(+0.8,-0.6)
V	<-2.0	0.14 ± 0.05	19.6 ± 0.3	-7.5(+2.0,-4.2)
H	> 1.5	0.16 ± 0.05	16.9 ± 0.3	6.9(+3.4,-1.7)
H	<-1.5	0.16 ± 0.08	16.9 ± 0.3	-6.6(+2.1,-5.6)
K	> 1.5	0.15 ± 0.02	16.3 ± 0.1	7.3(+1.4,-1.0)
K	<-1.5	0.14 ± 0.05	16.4 ± 0.3	-7.9(+2.1,-4.8)

(b) FOLDED

V	> 2.0	0.16 ± 0.03	19.5 ± 0.15	6.6(+1.5,-1.0)
H	> 1.5	0.15 ± 0.04	16.9 ± 0.2	7.3(+2.6,-1.6)
K	> 1.5	0.14 ± 0.03	16.4 ± 0.14	7.76(+2.1,-1.4)

presence of a central component, on a scale of order 1 kpc., possibly becoming more prominent towards the near-infrared. For this reason, the linear regressions shown in the Figure and given in Table 3.5(a), and the folded fits (Fig. 3.9 b; Table 3.5 b) were made under the exclusion of points near the centre of the galaxy. The large-radius behaviour in all cases is seen to be reasonably approximated by the exponential function.

The linearity of the optical detector at faint light levels is confirmed by the agreement between our value for the V scalelength, 6.6 ± 1 kpc. (from the folded data, Table 3.5 b), and the model fit given by van der Kruit and Searle (1981), with a scalelength of 6.74 kpc. when adjusted to our assumed distance of 13 Mpc. for NGC 5907.

(ii) Colour index variations

Although the absolute levels of the three profiles may be compromised by the beam-size and calibration uncertainties discussed previously, the presence or absence of gradients in the colour indices and the relative slopes of the profiles at different wavelengths are still of interest. In this respect, NGC 5907 may well be the most interesting object studied here. The radial dependence of the three available colour indices is shown in Figure 3.10. The straight line fits are given in Table 3.6: in view of the subtlety of the nuclear bulge, and its apparent lack of effect on the colour indices, the nuclear measurements were included in the fitting procedure.

Whilst it is accepted that the results are at most only at the 1-sigma level, and that the trend in V-K can only be stated to be less than 0.03 $mag.kpc^{-1}$ over this radial range, inspection of Fig. 3.10 reveals the mean colour trend in every case (all three indices, both north and south of the nucleus) to be positive with increasing radius, an unlikely result in the purely random case. Erring on the side of

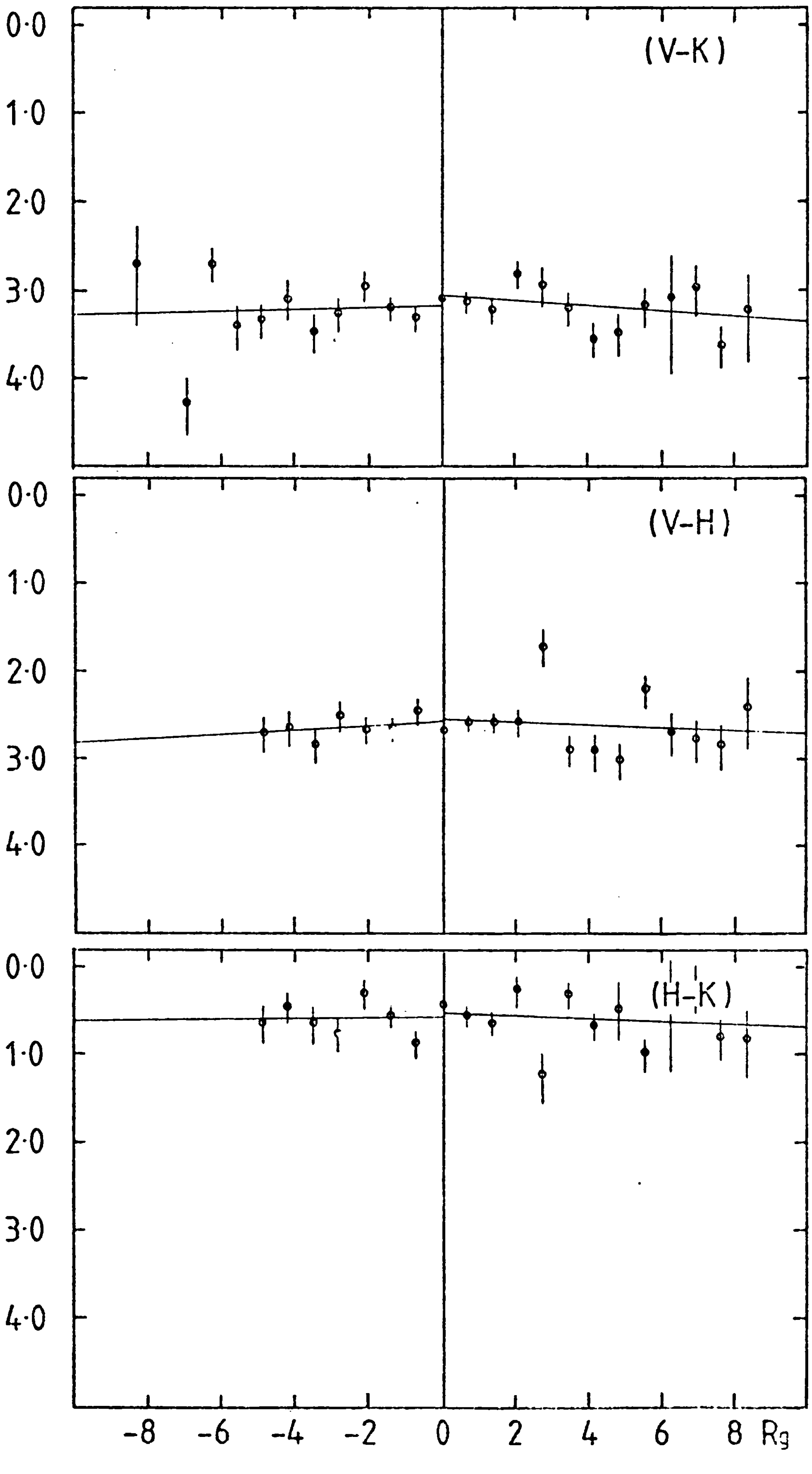

FIGURE 3.10

Radial colour index variation in NGC 5907.

Table 3.6

Linear Fits to Colour Index Across NGC 5907

Colour Index	Radial Range	$(CI=CI_0+BR_g)$	
		B	CI_0
(mag.)	(kpc.)	(mag/kpc)	(mag)
V - K	> 0.0	0.03±0.02	3.06±0.12
V - K	< 0.0	0.01±0.05	3.2 ±0.2
V - H	> 0.0	0.01±0.04	2.5 ±0.2
V - H	< 0.0	0.025±0.0026	2.6 ±0.7
H - K	> 0.0	0.015±0.03	0.5 ±0.16
H - K	< 0.0	0.004±0.04	0.56±0.13

caution, further quantitative discussion of this mean trend is not warranted by the data presently available, and we will be content to set limits: taking 0.03 mag.kpc^{-1} as an upper limit to the size of the V-K gradient, the corresponding metallicity gradient is less than 0.035 per kpc in log(Z), where we have used the strictly empirical calibration of V-K against metallicity given by Strom et al. (1976; see discussion in Chapter 1). The significance of this figure is seen by comparison with the Model 9 disk given by Larson (1973), which has a similar exponential scalelength (5-6 kpc.) and a metallicity gradient $d(\log Z)/dR_g = 0.024$ kpc^{-1} (Chapter 1).

The mean trend of the colour indices towards redder colour with increasing radius is, if real, in the opposite sense to that expected from Larson-type galaxy formation models, in which star formation rates, and hence mean metal content, are less in the relatively low-density regions far from the nucleus. One of the other mechanisms discussed in Chapter 1, namely population changes or thermal emission from H-II regions must therefore be dominant in this galaxy.

(iii) Detection out of the plane

As discussed in section 3.4(b), the scans of NGC 5907 were discovered, after binning, to have been too short to permit accurate determination of the background level at the scan-ends; although a problem for our present purpose, this implies that the galaxy is detectable in the IR at least 1 kpc. above the plane. Van der Kruit and Searle (1981) give z_0, the scaleheight of their best-fit model disk, as 0.83 kpc. (at 11 Mpc) in the optical. A programme of infrared photometry, aimed at determination of the detailed variation of the scale height with radius, is by no means impossible.

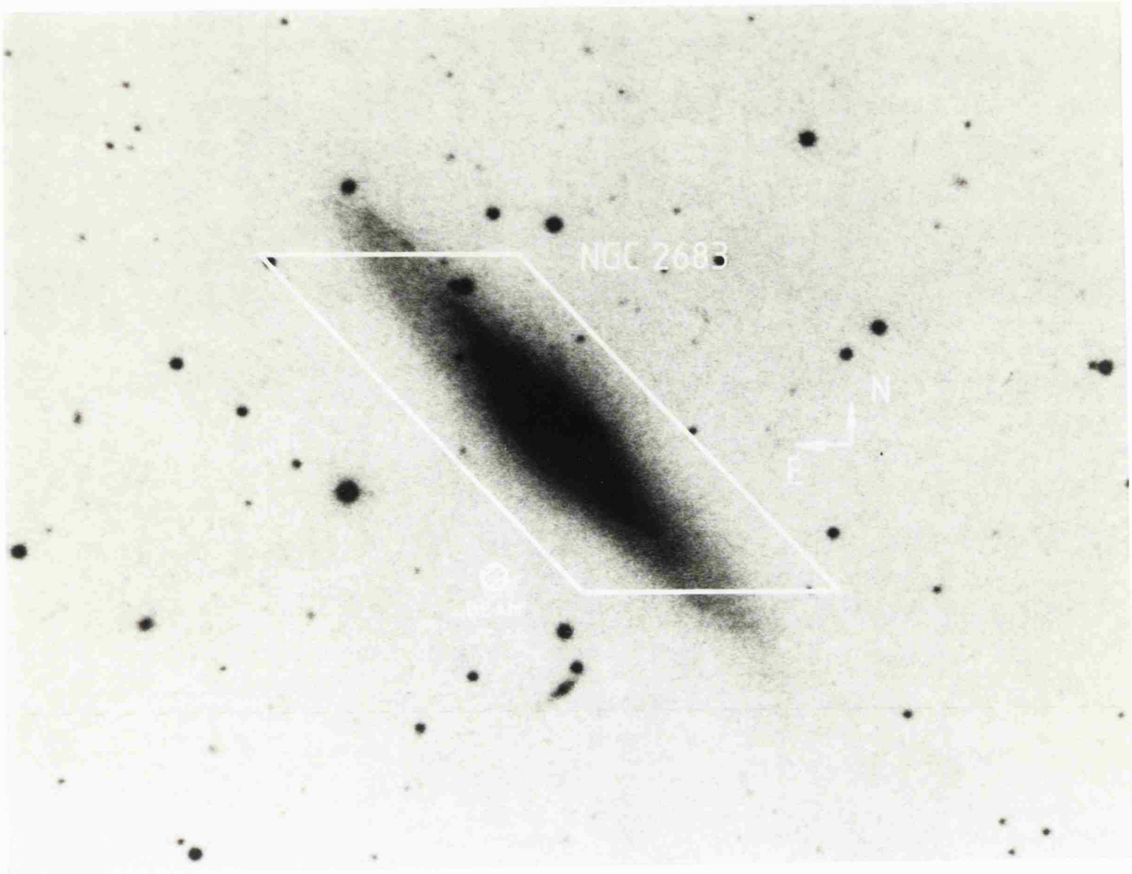

FIGURE 3.11

Palomar print of NGC 2683. The area covered by our observations is shown enclosed.

(c) NGC 2683

(i) Profiles and Preliminary Comparison with Previous Work

For the area indicated on the plate given in Figure 3.11, Figure 3.12 shows the radial surface brightness variation in the V, J and K bands, and fits to the disk distribution exterior to the central half-kiloparsec, which appear numerically in Table 3.7. With the exception of the 1.2 micron profiles, the north-south asymmetry was small. The 1.2 micron (mis)behaviour will be discussed in a later section.

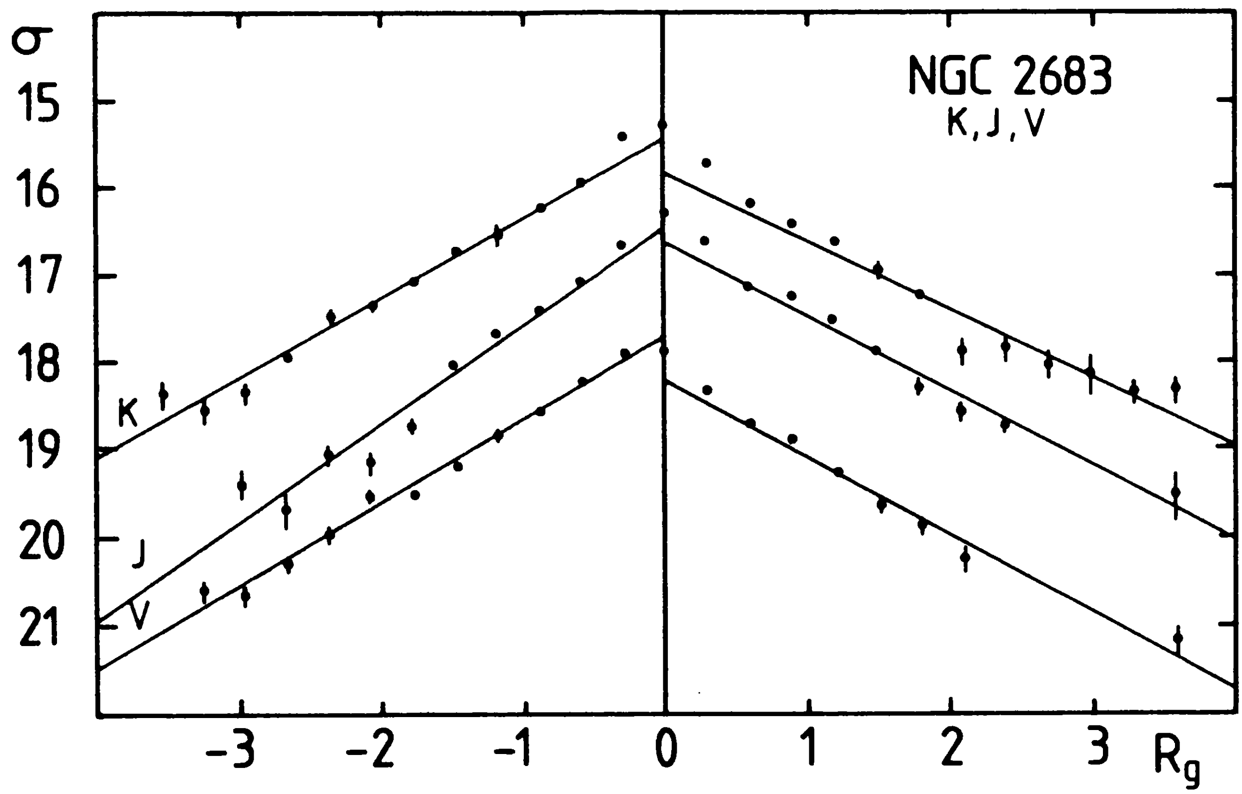

FIGURE 3.12

V, 1.2 and 2.2 micron surface brightness distribution in NGC 2683. The least-squares fits were made outside the central 1/2 kpc.

Table 3.7

NGC 2683 DISK PARAMETERS

(a) UNFOLDED

Johnson Band	Radial Range (kpc)	A (mag.arcsec^{-2}kpc^{-1})	SB_0 (mag.arcsec^{-2})	h (kpc)
		($SB = SB_0 + A\ R_g$)		($I=I_0e^{-R/h}$)
V	> 0.2	0.88 ± 0.05	18.19 ± 0.09	1.23(+0.08,-0.07)
V	<-0.2	0.94 ± 0.04	17.69 ± 0.08	-1.15(+0.04,-0.05)
J	> 0.5	0.85 ± 0.06	16.6 ± 0.1	1.28(+0.09,-0.07)
J	<-0.5	1.1 ± 0.1	16.5 ± 0.2	-0.98(+0.09,-0.10)
K	> 0.5	0.78 ± 0.06	15.8 ± 0.14	1.4(+0.1,-0.1)
K	<-0.5	0.90 ± 0.05	15.4 ± 0.1	-1.2(+0.06,-0.06)

(b) FOLDED

V	> 0.2	0.88 ± 0.06	17.95 ± 0.1	1.23(+0.09,-0.08)
K	> 0.5	0.84 ± 0.04	15.61 ± 0.1	1.29(+0.06,-0.06)

Few observations of NGC 2683 have been reported previous to this thesis; the decision taken in 1980 to incorporate an optical channel into the widethrow photometer has, in this respect, been borne out. Simkin (1967) made narrow beam (6") scans across the disk in a search for asymmetric dust absorption in front of and behind the nucleus. Her peak surface brightness, 18.8 mag.arcsec^{-2} in V, is fainter than our result by about one magnitude, in spite of the smaller aperture used. The discrepancy may be partly the result of dead-time calibration errors in our photometry, and partly because Simkin made no attempt to centre on the nucleus prior to performing her drift-scans. The former explaination is suggested as the most likely when the average value of V-K derived from our observations, $\langle V-K \rangle = 2.5$, is compared with the 3.5-3.6 quoted by Aaronson (1977); the uncertainties in our measurements of bright optical standards are thereby underlined.

Simkin (1975) repeated her observation of NGC 2683 in more detail, this time primarily in a search along the minor axis for an optical halo (a suggestion of one was found), but insufficient information was gathered to define an exponential disk, to which we will refer in the next section.

(ii) <u>Distribution of surface brightness</u>

The problem with the absolute level of the V profile in Figure 3.12 in no way affects our interpretation of the <u>scale</u> parameter of the disk. At all three wavelengths the scale length is very small in comparison with those of the other two objects described in this Chapter. The scale derived from the optical measurements (h_V = 1.1-1.2 kpc.) is smaller than the 1.5 kpc. obtained by Simkin (1975), even allowing for the slightly greater distance assumed by the latter author. It is possible that, with our limited radial coverage, the presence of a central component steeper than the exponential might be the culprit; however, inspection of Fig. 3.12 reveals that if this is the case, the ability of this component to mimic a classical disk is uncannily good. However, the furthest measured point on each profile in the Figure lies systematically above the best-fit disk; the possibility remains that the brightness distribution outside our radial range is substantially shallower than the behaviour at radii less than 4 kpc. would imply.

(iii) Colours of the disk

Figure 3.13 illustrates the radial variation of the colour indices; the least-squares treatment appears in Table 3.8. It can be seen in Fig. 3.12 that the measured 1.2-micron surface brightness south of the nucleus is discrepant in slope with all the other profiles. The 1.2 micron measurements north and south of the nucleus were performed on different nights; this, combined with the fact that both the V and K profiles south of the nucleus are significantly shallower than that at J, implies that this effect results from an infrared-instrumentation failure on one night only. The most plausible cause is a loss of synchronism between the rotating sector-wheel chopper and the mains frequency, which is known to cause beating in the output from the phase-sensitive detector. Serious discussion of the V-J and J-K colour indices south of the nucleus is, anyhow, precluded; the poor quality of these two indices is apparent in Figure 3.13. Note that the reasonable agreement between the V and K profiles south of the nucleus rules out atmospheric conditions as a possible cause of the 1.2 micron discrepancy.

North of the nucleus the colours are strictly constant to within 0.04 mag.kpc.^{-1} (Table 3.8) in all cases except the long-baseline V-K index, where a trend of 0.06 ± 0.04 towards redder colour with increasing radius may just have been detected. Note, however, that four of the large-radius points are missing due to star contamination of the V data north of the nucleus, effectively increasing the weight of the extreme

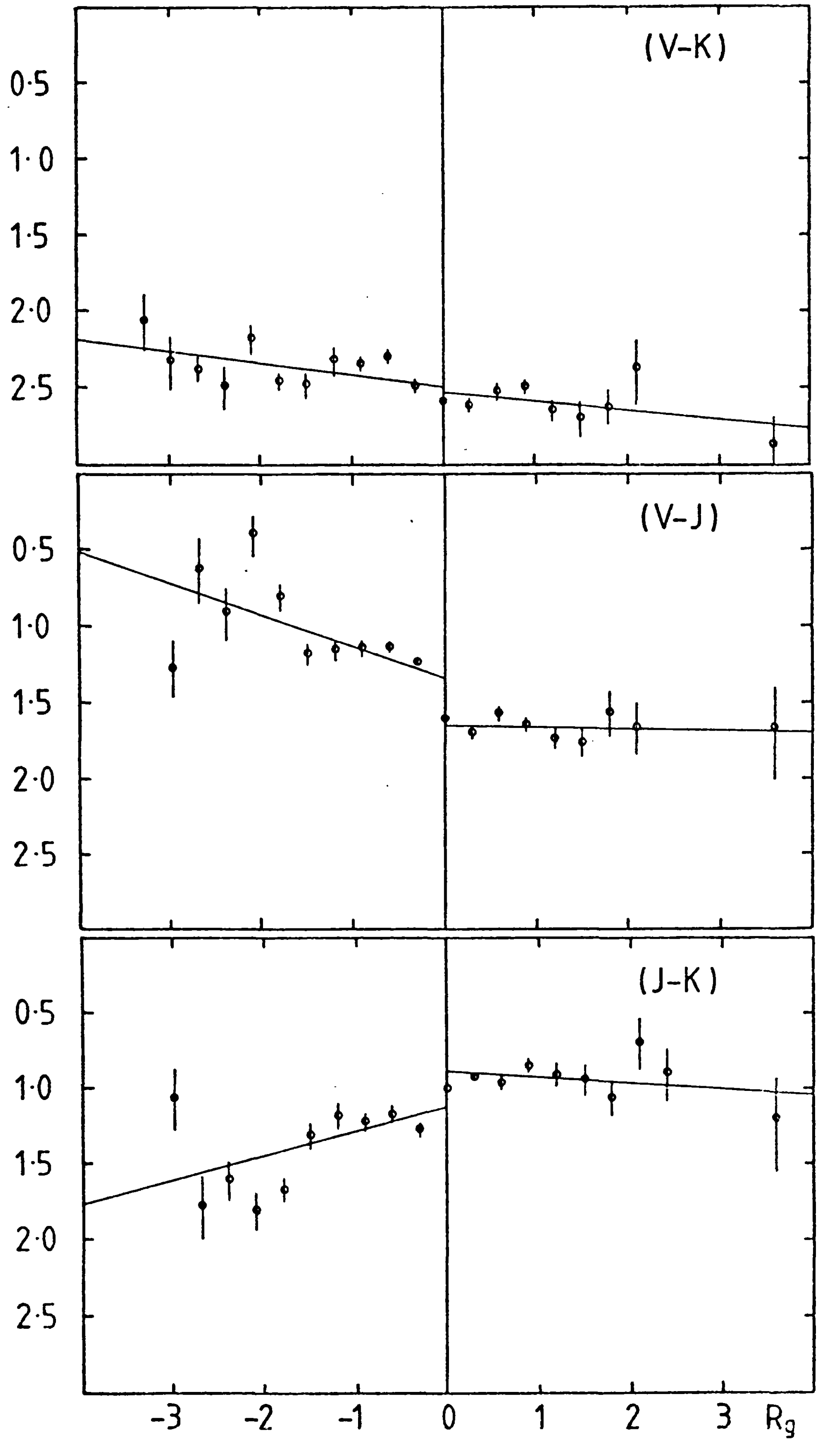

FIGURE 3.13

Colour index variations across the face of NGC 2683. The curious behaviour of the J measurements south of the nucleus is probably instrumental, and is discussed in the text.

Table 3.8

Linear Fits to Colour Index Across NGC 2683

Colour Index (mag.)	Radial Range (kpc.)	$(CI=CI_0+BR_g)$ B (mag/kpc)	CI_0 (mag)
V - K	> 0.0	0.06 ± 0.04	2.52 ± 0.07
V - K	< 0.0	-0.08 ± 0.04	2.49 ± 0.07
V - J	> 0.0	0.01 ± 0.02	1.64 ± 0.04
J - K	> 0.0	0.04 ± 0.04	0.88 ± 0.07

remaining measurement.

The only available colour index south of the nucleus, V-K, appears if anything to become bluer away from the centre. A detailed model is obviously not warranted by colour changes so marginally detected, but it is worthy of mention that V-K colour asymmetries might simplistically be expected in a view of a two-armed spiral pattern at large inclination (see,eg., Simkin 1967).

3.6 GENERAL REMARKS AND SUGGESTIONS

The feasibility of off-nucleus scanning to faint infrared light levels (SB_K around 19 mag.arcsec.$^{-2}$ per point) has been demonstrated. In the process we have been able to present useful limits on the size of (optical-infrared) colour gradients in the disks of two edge-on spirals, one of which, NGC 5907, appears to become redder with increasing radius in all three measured colour indices, suggesting that metallicity gradients inherent in gas-dynamical models of galaxy formation may prove difficult to detect in late-type spirals. We would suggest a thermal emission contribution to the IR fluxes as a likely cause of the behaviour of the colours; a halo of late-type dwarf stars seems less likely in view of the observation of the R-I colour in NGC 253 (Spinrad et al. 1978; described in Chapter 1), a similarly late-type spiral.

There are grounds for the exercise of caution in the interpretation of the least-squares treatments of, especially, the colour index data; the reader should take note of the fit ranges employed and realise that because the final slopes are generally at most only 1 sigma away from vanishing point, the range of radius chosen may considerably affect the results. We have been careful not to claim detection of colour variation except when repeated in all the indices, both north and south of the nucleus.

Values of the central surface brightness of the <u>disk</u> components have been derived as 16.2, 16.4 and 15.6 mag.arcsec.$^{-2}$, for NGC 4565, 5907 and 2683 respectively, where the K magnitude is quoted for its relative insensitivity to intrinsic interstellar reddening (but see Simkin 1975 for a brief discussion of the surprisingly small effect of inclination and reddening on the inferred V central brightness). For NGC 4565 and 5907, van der Kruit and Searle's (1982) tabulation of the disk scale height suggests that our 22 arcsecond aperture is approximately filled at the e-folding point, so that the brightness figures given above for these two objects are more or less distance-independent. Conversely, the geometric (cos i) factor in the surface brightness due to the inclination of the disk, whilst still present, will be approximately equal for objects so highly inclined that most of the z-extent of the disk is included in the aperture.

The light distribution inferred from any study of galactic systems is a summation along the line of sight: this becomes important for objects highly inclined to the plane of the sky. The model manipulation carried out by van der Kruit and Searle (1981) showed that the slope of the exponential part of the disk remained constant under observation as the disk was tilted from $i = 90^{\circ}$ to $i = 84^{\circ}$, suggesting that the scalelength inferred from observations is relatively insensitive to the inclination of the disk. This is borne out by preliminary results from a computer model implemented on the Leicester University Cyber 73 computer, in which a disk was modelled as a series of concentric ellipsoids; given a radial coverage of a number of scalelengths, the observed value was within 10% of the input scale.

For the future, we suggest:

(i) To observe NGC 5907 with higher resolution and to compare the optical and infrared scale heights (z-direction); observations clear of the disk will also be more sensitive to changes of stellar population.

(ii) To use the techniques developed here to observe the disk of an S0 system; metallicity driven colour changes will be more easily detected in the absence of intrinsic reddening and possible thermal emission from HII-regions.

Finally, for comparison with other observations to be found in this thesis, we present some statistics relevant to our observational efficiency (figures refer to the 2.2 micron scans of NGC 2683):

limiting brightness per point	19.2 mag.arcsec.$^{-2}$
area covered	260 x 200 arcsec.
beam size	22 arcsec.
time taken	240 minutes.

The time quoted for the observations is the time spent setting up and performing scans; omitted are object acquisition, standard measurements, dewar fills etc. Scanning times are effectively halved if the simultaneous optical data are taken into account. The results presented here would have been more quickly obtained at a telescope whose pointing axis could be scanned accurately along a specified position angle: even for NGC 2683, which represents the most efficient observing procedure we could achieve, 1/3 to 1/2 of the observing time was spent setting scans up, checking telescope drifts, and so on.

REFERENCES

Aaronson,M. 1977, Ph.D. Thesis, Harvard University.

Barford,N.C. 1967, Experimental Measurements: Precision, Error and Truth. Addison-Wesley Publ. Co. Inc.

de Vaucouleurs,G. 1958, Astrophys.J., 127,487.

de Vaucouleurs,G., de Vaucouleurs,A., & Corwin,H.G. Jr. 1975, Second Reference Catalog of Bright Galaxies, Austin, University of Texas Press.

Faber,S.M., & Gallagher,J.S. 1979, Ann.Rev.Astron.Astrophys., 17,135.

Frogel,J.A., Persson,S.E., Aaronson,M., Becklin,E.E., Matthews,K., & Neugebauer,G. 1975, Astrophys.J., 200,L123.

Heidmann,J., Heidmann,N., & de Vaucouleurs,G. 1971, Mem.Roy.astr.Soc. 75,121.

Hall,D.N.B., Aitkens,R.S., Joyce,R.R., Mc Curnin,T.W. 1975, Appl.Opt. 14,450.

Hegyi,D.J., & Gerber,G.L. 1977, Astrophys.J., 218,L7.

Hohlfeld,R.G., & Krumm,N. 1981, Astrophys.J., 244,476.

Johnson,H.L., Mitchell,R., Iriarte,B., & Wisniewski,W.Z. 1966, Ariz.Uni.Lunar.Planet.Lab.Comms, 4,99.

Kormendy,J., & Bruzual,G. 1978, Astrophys.J., 223,L63.

Sandage,A.R. 1961, The Hubble Atlas of Galaxies, Washington: Carnegie Institute of Washington.

Simkin,S.M. 1967, Astron.J., 72,1032.

Simkin,S.M. 1975, Astron.J., 80,415.

Spinrad,H., Ostriker,J.P., Stone,R.P.S., Chiu,L-T.G., & Bruzual,G. 1978, Astrophys.J., 225,56.

Strom,S.E., Strom,K.M., Goad,J.W., Vrba,F.J., & Rice,W. 1976, Astrophys.J., 204,684.

van der Kruit,P.C., & Searle,L. 1981, Astron.Astrophys., 95,105.

van der Kruit,P.C., & Searle,L. 1982, Astron.Astrophys., 110,61.

CHAPTER 4.

MEDIUM RESOLUTION MAPPING OF M 83 = NGC 5236.

CHAPTER 4.

MEDIUM RESOLUTION MAPPING OF M 83 = NGC 5236.

4.1 INTRODUCTION.

In this chapter we describe observations of M83 using the AAT IRPS in full DC-mapping mode. The objective was the acquisition of maps at J,H and K of a large part of the visible surface of this nearby face-on spiral galaxy. The observation was proposed for three reasons:

a) it permits a relatively reddening-free look at the so-called "exponential disk";

b) density wave theories of spiral structure require a varying surface density of the disk as defined by old stars; the near infrared passbands are insensitive to light from young tracers such as OB associations, allowing the amplitude of the underlying broad arms to be determined directly;

c) M83 is Freeman's prototype TypeII spiral (see Freeman 1970); we expected to be able to distinguish between models in which the Type II signature in the surface brightness profile is caused by interstellar reddening and those requiring a real deficit of material with a certain value of L_m , the angular momentum per unit mass.

The chapter is laid out as follows:

(i) Observational technique and parameters

(ii) Reduction of the data to maps and radial profiles

(iii) Summary description of the resulting diagrams

(iv) Discussion of the main features of the maps

(v) Discussion of the surface brightness profiles.

4.2 OBSERVATIONS

It was seen in Chapter 2 that DC observation of extended objects can be defeated by inadequate knowledge of the background level: the absolute flux levels for Cen A were saved by the availability of the difference count between the two beams. In order to keep a check on signal drifts and sensitivity at the telescope, it was necessary to map the object in single-beam mode, and a completely new scanning method was required. Each map therefore results from two different types of observation: (i) the telescope was scanned in a raster pattern over the area of interest (individual "legs" of the raster being in declination - Fig. 4.1), two rasters being made at each wavelength. The background light from the disk of this object is particularly intense, and the "sky" level was not reached even at the extremities of the area observed. Under the assumption that signal level drifts incurred during a single pass over the oject could be assumed to be linear, this problem was reduced to the need to determine the flux level at every point of the north and south ends of each raster "box". This was achieved through (ii) rapid point-by-point measurements along lines "A-A" and "B-B" in Fig.4.1 . These scans extended more than 700 arcsec. from the nucleus of the galaxy, and the sky background level was convincingly attained. Each raster covered an area of 350x350 arcsec. on the sky. The parameters were as follows:

Aperture diameter	: 14"
Separation of passes	: 7" in RA
No. of points per pass	: 51
Integration time per point	: 0.5 seconds
Separation of points	: 7" in Declination

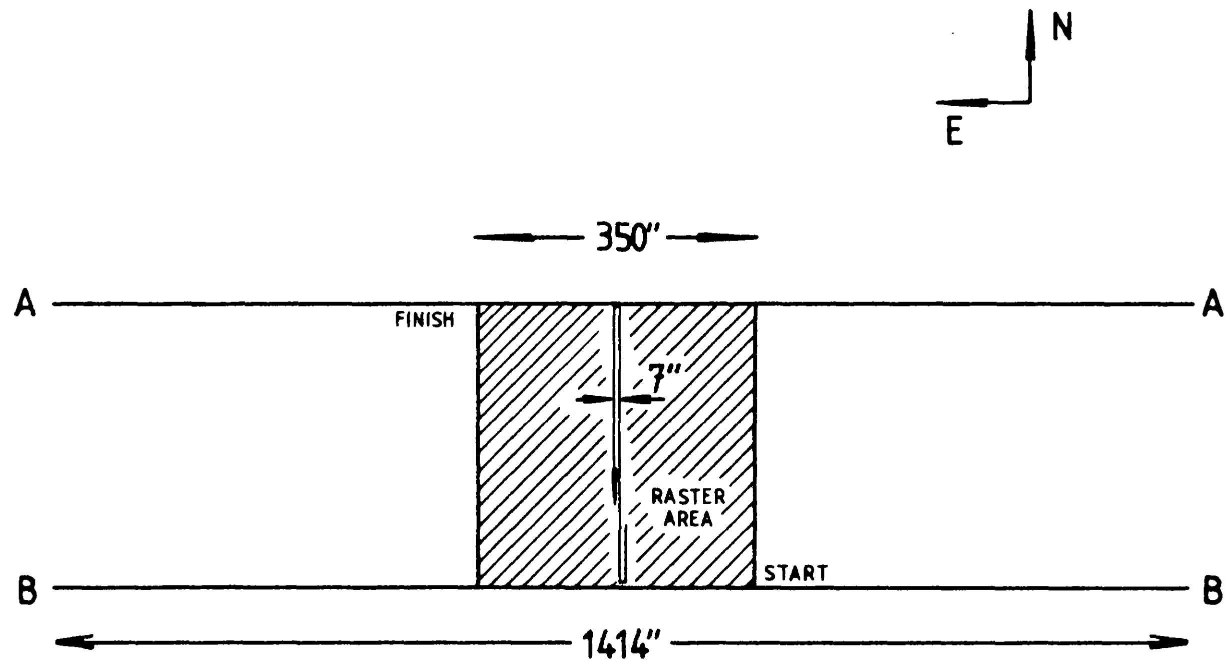

FIGURE 4.1

Layout of raster- and end- scans.

The worst signal drifts and individual "bad" passes were caused by the encroachment of the AAT windshield across the entrance aperture of the telescope; this sporadic hardware failure caused the loss of perhaps five passes over the object.

4.3 DATA REDUCTION

(i) Preliminaries

Previous experience with the standard AAO magnetic tape format suggested that some form of simplification whilst at the AAO base in Epping, NSW would pay dividends. The tape from the observatory was therefore read using a standard AAO program, and the photometry data were isolated and dumped in integer format onto a separate tape for transport back to the UK. The program failed to include any <carriage return/line feed> characters in the data stream. Back at Leicester, therefore, the raw raster scans were read from the second tape in the unfortunate form of a continuous series of integers, and required reduction to FORTRAN - readable records with the aid of a simple PASCAL program (Appendix B). Each run was split into individual passes over the object in the following manner:

a) the emission peak corresponding to the M83 nucleus was located;

b) the data were grouped into blocks of 51 integrations each such that the nuclear peak was the 26th bin of the 26th block. A few integrations were omitted from the beginning of each run, to allow for the delay between the photometry system's "start" pulse and the beginning of the telescope raster.

c) Alternate blocks (each now corresponding to an individual pass over the galaxy) were reversed, such that all blocks (hereafter referred to as "scans" or " passes") contained integrations made in order of increasing declination. The blocks for each raster were then stored on a computer file in order of increasing RA.

Figure 4.2 shows a complete raster run at 2.2 microns, at which wavelength thermal drifts were expected to be a major problem. A number of scans within each raster were found to contain unacceptably large signal drifts, due either to background level changes, or to the intervention of the AAO windshield system, mentioned earlier. However, as two rasters were performed at each wavelength, it was always possible to replace the offending scans with their positional duplicates. "Spikes" - individual high or low points, caused by spurious electronic or tape-reading problems - were removed by hand, simply replacing the affected integration with the average of adjacent bins. The "end-scans", performed to allow accurate determination of the flux levels at the ends of individual passes, were analysed as follows:

a) the location of the scan relative to the galaxy was found by matching star signals with star images on the Palomar plates;

b) drifts were removed by choosing background levels on either side of the galaxy and using a linear fit for the baseline;

c) the 51 relevant bins from the two end-scans at each extreme of the raster were averaged together (not at 1.2 microns);

d) a smooth curve was drawn through the result;

e) the count levels at each position were read off this curve.

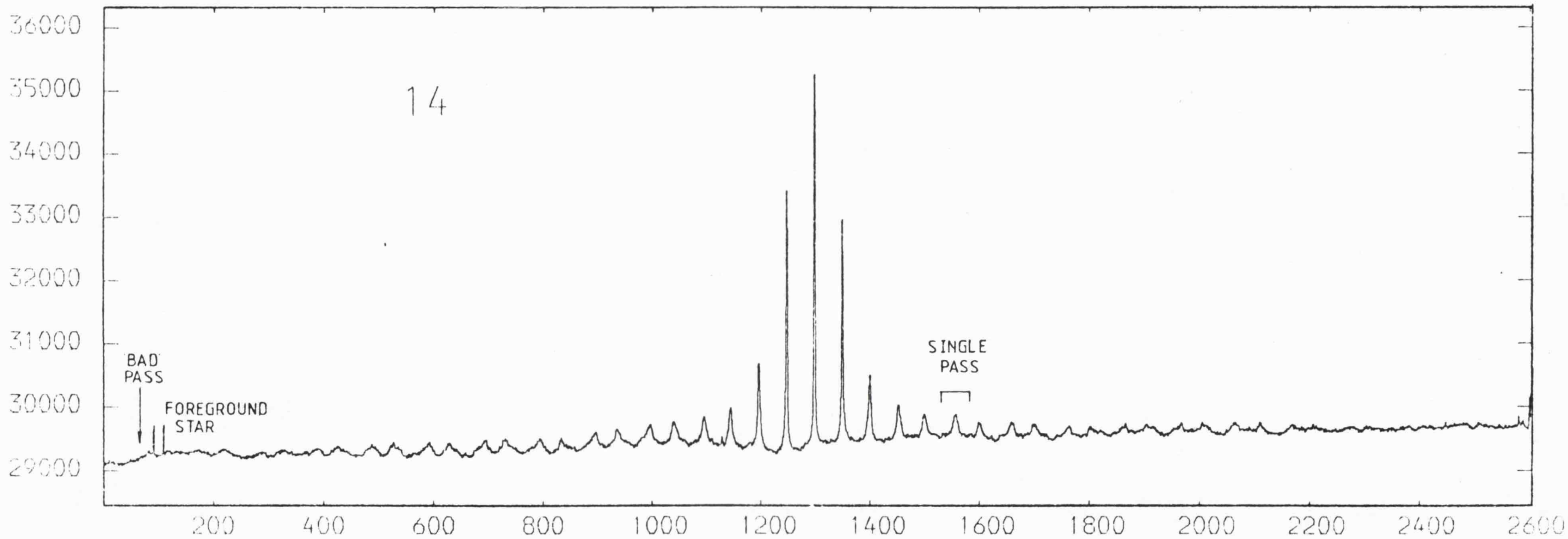

FIGURE 4.2

A complete 2.2 micron raster showing an individual pass over the object, a "bad" pass, and the effect of a foreground star.

Owing to a closing in of the weather, the signal-to-noise ratio of the south end-scans at 2.2 microns was particularly poor; we were therefore forced, in compiling the 2.2 micron map, to arbitrarily replace these measurements with those from the north side of the galaxy, in reversed RA order. The effect of poor signal-to-noise ratio on the end-scans is discussed more fully subsequently. Steps d) and e) above tend to smooth out star images in the end-scan integrations. This was intentional, since the inertia of the telescope results in overshoot and positional errors at the ends of each raster pass and consequently a certain smearing of the north and south map edges.

(ii) Maps

The anticipated problem with the DC measurement of faint surface brightness levels was that thermal (telescope) and sky background drifts would be too large and on too short a timescale to permit detection of the galaxy extremities. Fig.4.2 demonstrates that even at 2.2 microns the rasters were performed sufficiently rapidly that signal drifts on individual passes could be adequately compensated for using a linear fitting procedure between the ends of the pass. Reduction of the data to map form was accomplished by using this linear fitting procedure on the point-by-point average of the two arrays at each wavelength, adjusting the north and south ends of each averaged pass pair to the count levels determined from the endscans.

Counts were converted to surface brightness (mag.arcsec.$^{-2}$) via standard star measurements and the aperture diameter, determined by inspection of star profiles in the raster runs. Owing to an estimated $\pm$0.7 arcsec. uncertainty in the FWHM projected beam diameter, the surface brightness scale contains a possible systematic error of $\pm$ 0.1 mag.arcsec.$^{-2}$.

(iii) Radial Surface Brightness Profiles

Profiles were produced in an attempt to boost signal to noise in the faint areas at large galactocentric radii; it was hoped that this would permit discussion of the Freeman TypeI/TypeII problem and the detection of colour gradients across the disk. The method of reduction was as follows:

a) star images were located on the infrared maps and removed using linear interpolation between the galaxy fluxes in neighbouring pixels;

b) X-Y coordinates relative to the nucleus were determined for each pixel;

c) the coordinate system was rotated through 45° clockwise on the sky such that the rotated X-axis coincided with the major axis of the galaxy (Danver 1942, Talbot et al. 1979);

d) the Y-axis in the rotated frame was expanded by a factor of $(\cos i)^{-1}$, where i is the inclination of the galaxy to the sky, equal to 24° (see discussion in Talbot et al. 1979). The resulting X-Y coordinate system was in the plane of the galaxy.

e) Pixel fluxes were binned into circular annuli of 7" radial extent in the adjusted coordinate plane, and the average flux at each radius was converted to surface brightness via the standard star measurements.

4.4 SUMMARY OF NOISE AND SIGNAL DRIFTS

Besides detector and background noise, the accuracy with which surface brightnesses may be derived from our data is limited by signal drifts caused by slow variation of the background level. We now present the magnitude of the various effects and assess their importance.

(a) Noise

By this we refer to the fast variations responsible for the difference between adjacent integrations: this would be the limiting factor in the case of stellar photometry. We have estimated the RMS noise of selected sections of the endscans, clear of the galaxy light, where longer term variations (b) could be removed linearly. Table 4.1 gives the 1σ noise levels thus derived, in terms of magnitudes and fluxes per square arcsecond of a 14" aperture.

TABLE 4.1

Noise

Johnson Band	1σ Flux (F_ν) 1/2sec.	1 sec.	1σ mag.arcsec^{-2} 1/2 sec.	1 sec.	N
J	2.46	1.73	22.14	22.52	56
H	3.00	2.12	21.41	21.79	48
K	5.5	3.89	20.15	20.53	56

(fluxes in units of 10^{-32} W. m^{-2}. Hz^{-1}. arcsec^{-2})

N is the number of 1/2 second integrations used in the calculation.

(b) Short term drifts

Occuring on timescales of a few minutes, these are, through their effect on the endscans, the limiting factor in the determination of the colours of the disk (this will be discussed more fully in a subsequent section). Table 4.2 summarises the drift amplitudes incurred in making the endscans. For comparison with the signal drift amplitudes (subscripted "DR"), we have included in the Table the estimated galaxy surface brightness at the peak of the relevant endscan (these figures subscripted "G").

(c) Long term drifts

Drifts on longer timescales ($\sim {}^1/_2$ hr.), probably caused by the slowly varying airmass, were recorded during the raster scans. We have estimated their amplitude by reference to plots of the complete rasters, comparing the overall level at the end of the scan to that at the beginning. The results are summarised in Table 4.3. The characteristic timescale for these variations was so extended that their effect on individual raster legs was both systematic and about a factor of 5 smaller than the short term drifts mentioned before; they pose no great problems of data analysis, and are included here only for completeness.

These are the three fundamental limits on DC infrared photometry with a background-limited system. Which subset is important depends only on the type of observation: in our case, the short-term drifts and (to a lesser extent) the noise are dominant; in stellar photometry, normally involving beam-switching, noise alone is the overriding factor. An observational programme in which the long term drifts could play a part is hard to imagine.

TABLE 2

Short-term drifts and comparison with endscan galaxy detection.

ENDSCAN LABEL	JOHNSON BAND	SCAN LENGTH	SB_{DR}	SB_G	F_{DR}	F_G
9	H	203	19.0	18.7	2.76	3.64
10	H	102	20.0	18.4	1.10	4.80
11	H	102	18.4	18.8	4.80	3.32
12	H	102	19.0	19.0	2.76	2.76
15	K	102	----	18.1	----	3.63
16	K	102	17.6	18.4	5.74	2.75
17	K	102	18.7	19.1	2.09	1.44
18	K	102	----	19.9	----	6.91
21	J	102	20.2	19.6	1.47	2.56
22	J	102	20.8	19.8	0.85	2.13

(scan length in time seconds, SB in mag.arcsec.$^{-2}$, fluxes in 10^{-32} W. m^{-2}. Hz^{-1}. arcsec.$^{-2}$).

TABLE 3

Long-term drifts.

SCAN LABEL	JOHNSON BAND	TIME LENGTH	SB_{DR}
6	H	1300	17.10
8	H	1300	17.25
13	K	1300	-----
14	K	1300	16.35
19	J	1300	18.8

(length of scans in time seconds, SB in mag.arcsec.$^{-2}$).

4.5 PRESENTATION OF DATA.

The complete smoothed maps at J,H and K, and a reduction of the visible data given by Talbot et al. (1979) over the same region, are shown in Figures 4.3–4.6.

Figure 4.7 shows the 2.2 micron map superimposed upon an optical print of the galaxy.

The azimuthally - averaged radial surface brightness profiles are given in Figs. 4.8–4.10.

4.6 MAIN FEATURES OF THE INFRARED MAPS

(i) The Nucleus

The bright nucleus of M83 is prominent at all three IR wavelengths, the surface brightness (14" aperture) being:

(K) 13.66 ± 0.003 mag.arcsec.$^{-2}$ = 2.164×10^{-29} W.m^{-2}.Hz.arcsec.$^{-2}$

(H) 14.04 ± 0.001 mag.arcsec.$^{-2}$ = 2.660×10^{-29} W.m^{-2}.Hz.arcsec.$^{-2}$

(J) 14.79 ± 0.001 mag.arcsec.$^{-2}$ = 2.150×10^{-29} W.m^{-2}.Hz.arcsec.$^{-2}$,

where the quoted errors are exclusive of the uncertainties in the projected aperture, discussed previously.

These magnitudes are consistent with those of Glass(1973), who obtained

(K) 13.45 ± 0.1 mag.arcsec.$^{-2}$

(H) 13.62 ± 0.08 mag.arcsec.$^{-2}$

(J) 14.45 ± 0.1 mag.arcsec.$^{-2}$

in a 12 arcsecond aperture.

Note that the chopper throw employed by Glass was only 84 arcsec., north-south; the maps presented in this chapter demonstrate that this is not, in fact, clear of the detectable IR emission from the galactic disk, but the corrections are small enough ($\sim$0.02 mag in the 2.2 micron band) to be negligible, given the accuracy to which the latter author's results are quoted.

(ii) Spiral Structure

The most significant result of this work is the detection, for the first time at these wavelengths, of emission from the arms of a spiral galaxy. As pointed out in Chapter 1, observations at 1.2–2.2 microns are particularly sensitive to changes in the surface brightness of the "old disk" population in spirals: the spiral feature seen to the southeast of the nucleus therefore probably corresponds to an enhancement of the surface density of the old disk. The amplitude of this enhancement is of importance to theories of spiral structure which rely on density waves in the disk.

In the table below we have expressed this quantity as a percentage of the mean disk surface brightness at a radius of 105" using the definition of "contrast parameter" given in Equation I later in this section. Measured fluxes were binned over the two rectangular areas indicated in the 1.2 micron map, Fig. 4.3. Both are 120 arcseconds from the nucleus, assuming an inclination to the sky of 24°, but one lies on the southwestern spiral arm (A), and one in the interarm region (B). The contrast parameters are probably underestimates because of the degraded resolution resulting from the binning.

BAND	WAVE AMPLITUDE
1.2	$\pm$ 19.5%
1.6	$\pm$ 19.6%
2.2	$\pm$ 20.3%
V	$\pm$ 12 %

The "contrast" parameter in visible light was derived from those elements of the low resolution summary map given by Talbot et al.(their Appendix B, Table B2) which fell within the binning areas used in the infrared. The figure thus derived is probably affected by reddening and the binning, and would not, in any case, be representative of the

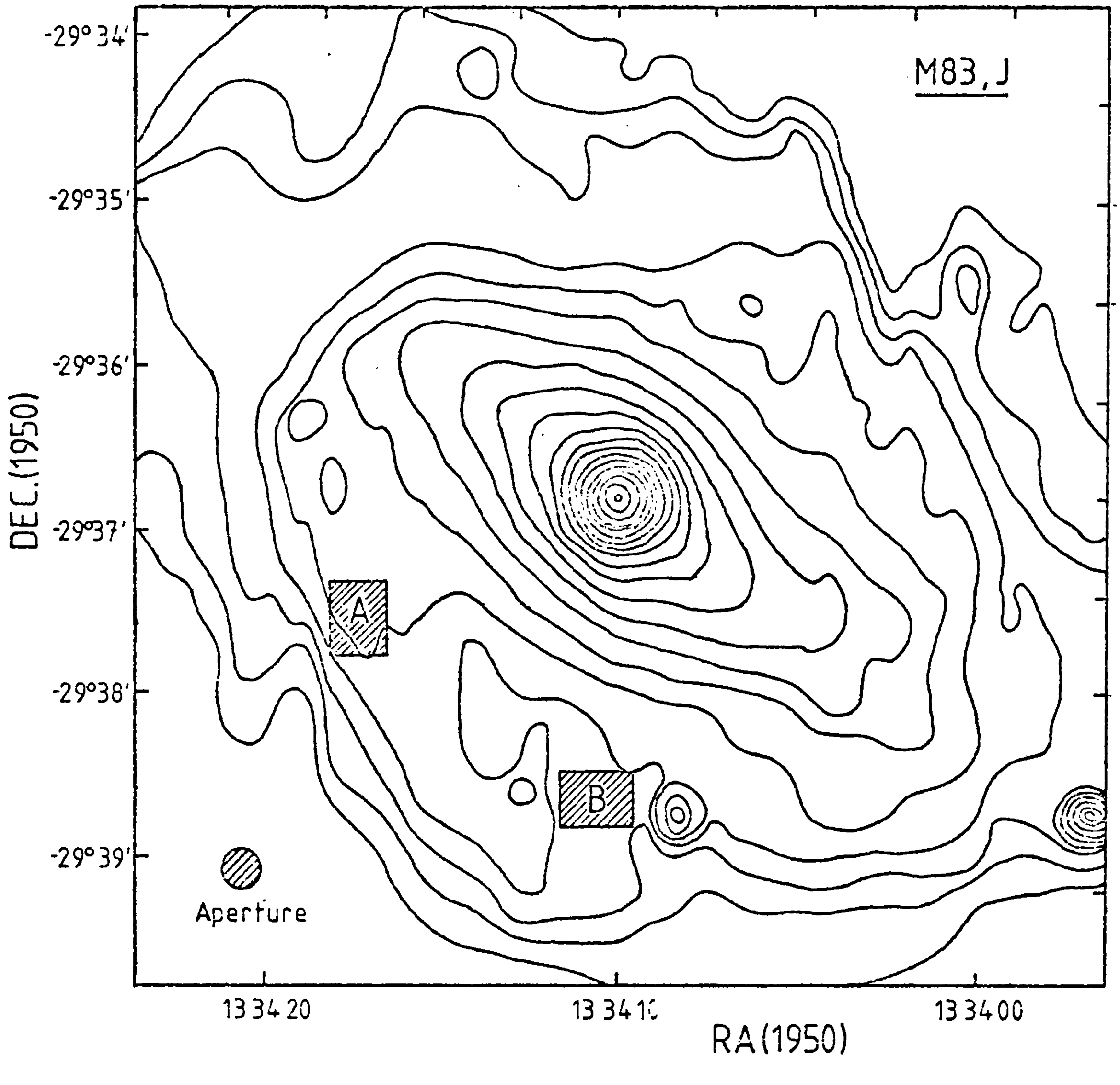

FIGURE 4.3

Smoothed 1.2 micron map of M83. Lowest contour: 20 mag.arcsec^{-2}.

Contour interval: -0.263 mag.

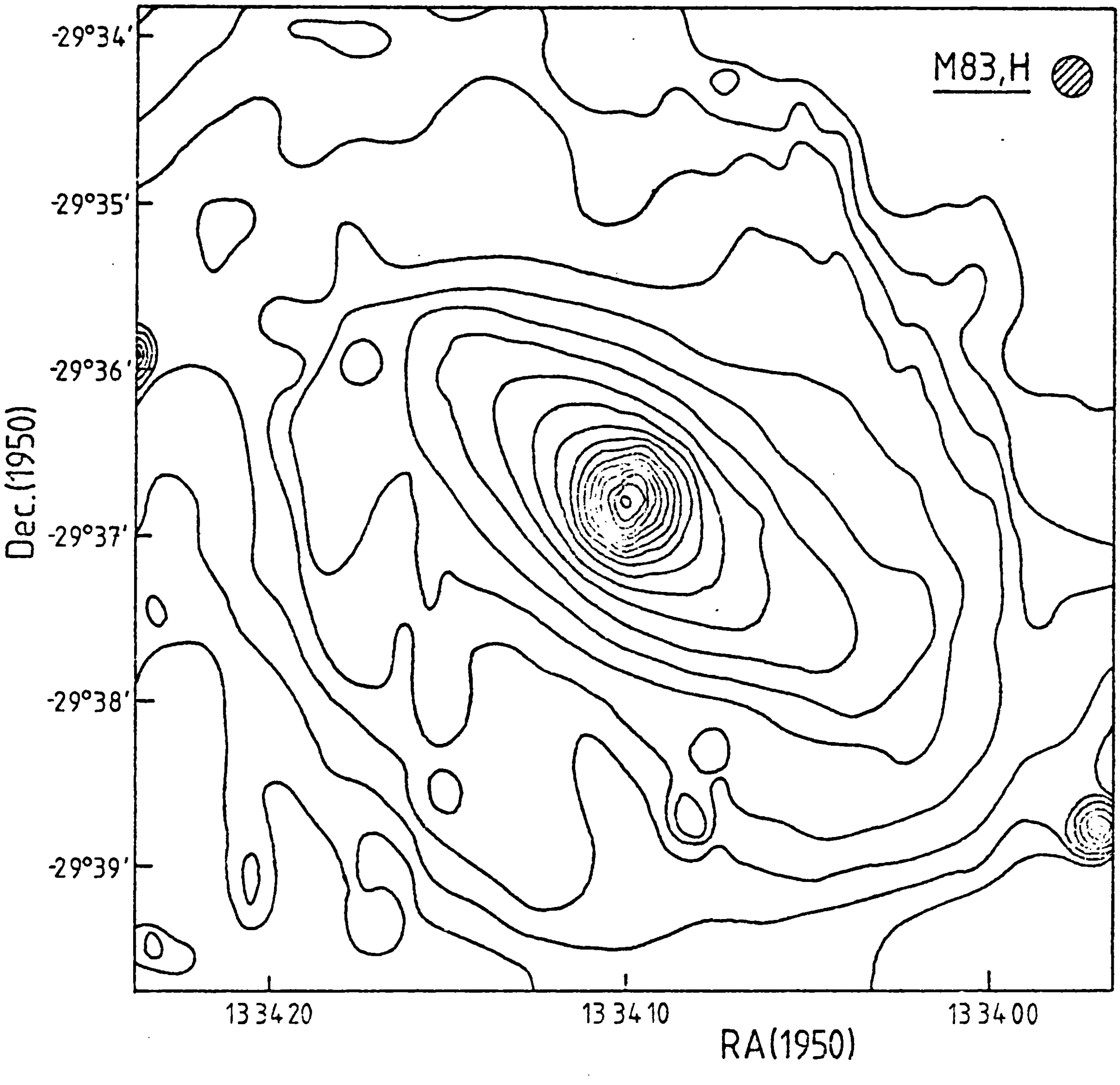

FIGURE 4.4

Smoothed 1.65 micron map of M83. Lowest contour: 19 mag.arcsec.$^{-2}$.

Contour interval: -0.263 mag.

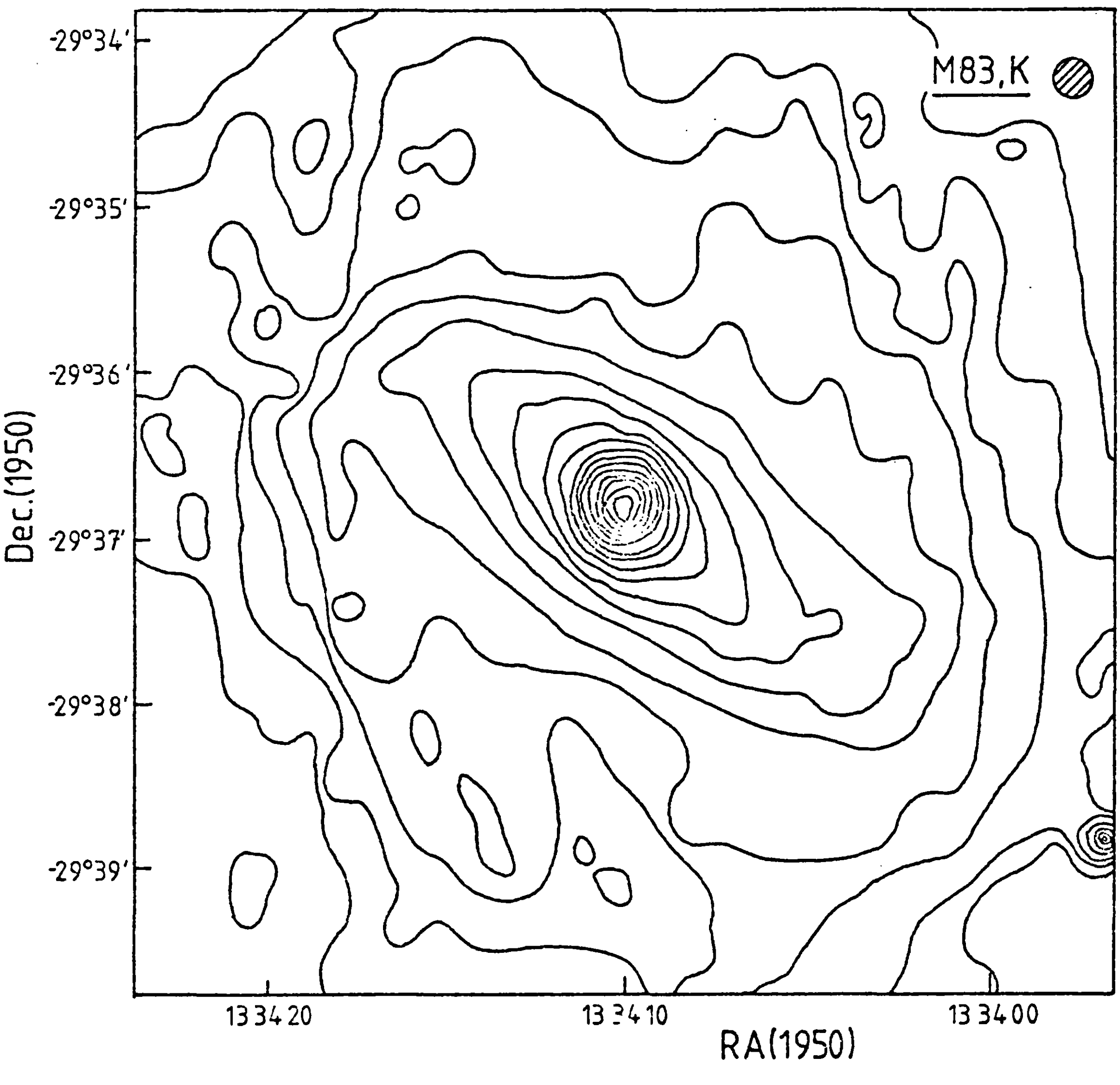

FIGURE 4.5

Smoothed 2.2 micron map of M83. Lowest contour: 18.5 mag.arcsec^{-2}.

Contour interval: -0.263 mag.

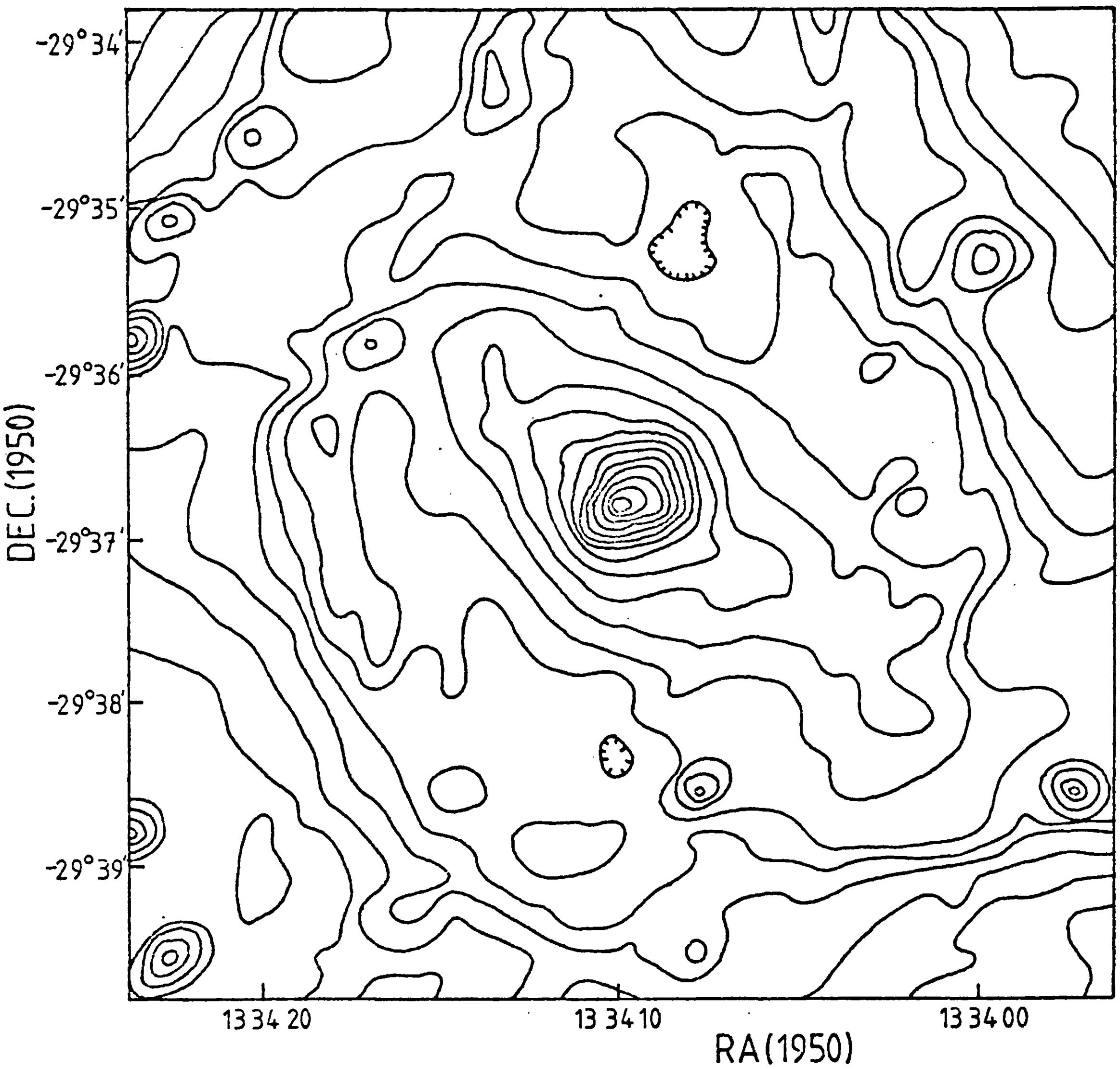

FIGURE 4.6

Hand-smoothed uncalibrated V map, from data by Talbot et al. (1979).

Contour interval is -0.255 mag.

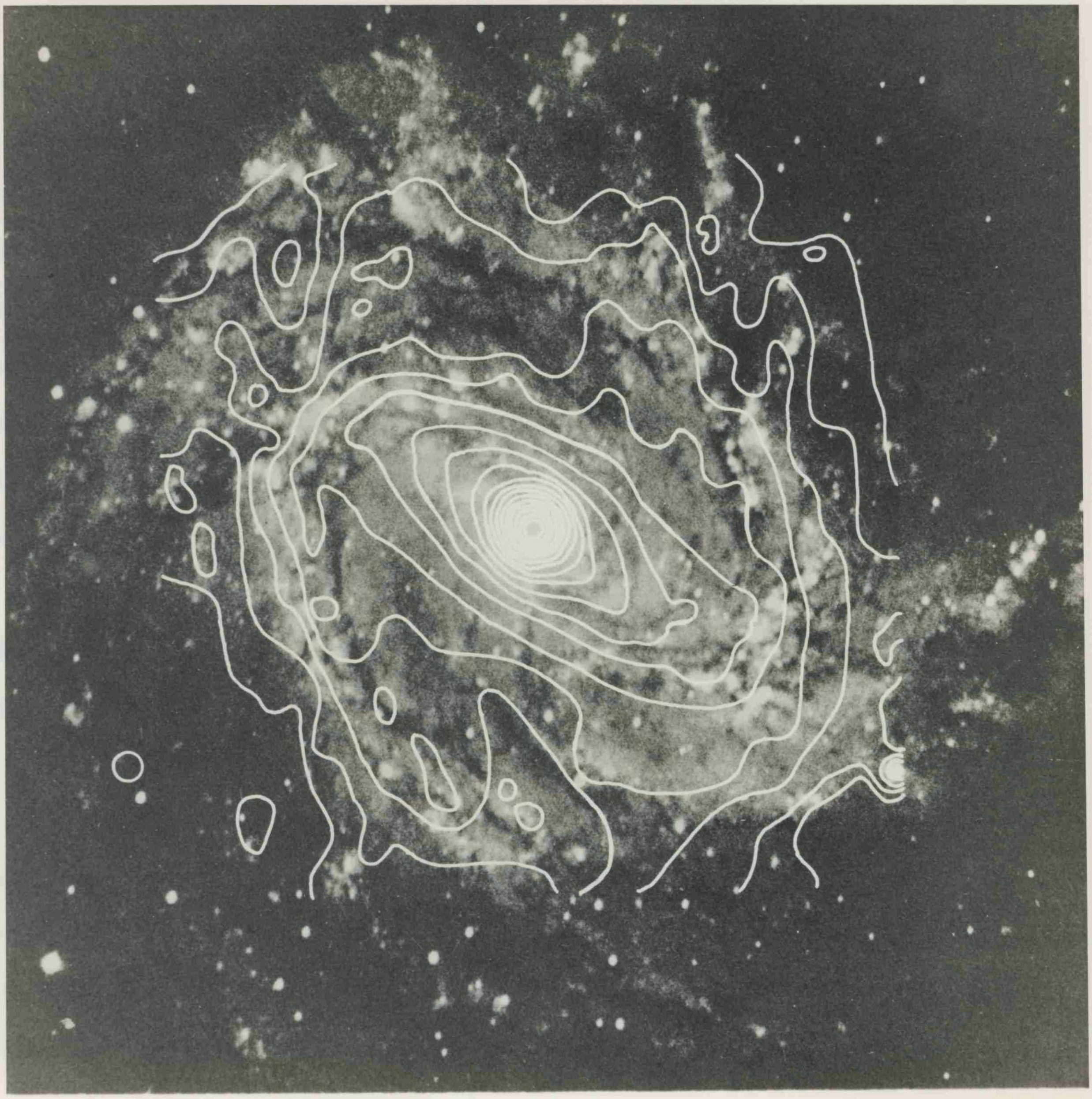

FIGURE 4.7

The 2.2 micron map superposed on the Hubble Atlas print of M83.

variation in the underlying disk. Schweizer's (1976) more careful treatment of fluxes in selected optical wavebands for a sample of classical northern galaxies led him to the discovery of broad spiral surface brightness features, arising wholly from the old disk, whose amplitude varied between ± 20% near the nucleus and ± 30% at large radii. The numerical coincidence between Schweizer's measurements and the contrast parameters derived roughly above increases our confidence in infrared mapping as a more direct method of determining old-disk wave amplitudes.

So far, we have assumed that the young population near the spiral arms is not bright enough to contribute significantly to the near infrared fluxes. This can be shown explicitly, as follows.

The contrast parameter at any wavelength, C_λ, is given by

$$C_\lambda = (F_{on}-F_{off})/(F_{on}+F_{off}) \text{ , x } 100 \% \qquad \text{(I)}$$

where F_{on} and F_{off} are the surface fluxes measured respectively on the spiral arm and in the interarm region. If we now decompose the fluxes at V and K into the contribution from young (OB) stars and from the "old disk", we have at V:

(on arm) $F_{OB}(V)$, $F_D'(V)$;

(off arm) $F_D(V)$, and at K:

(on arm) $F_{OB}(K)$, $F_D'(K)$;

(off arm) $F_D(K)$. Here the subscripts are self explanatory, and the primes denote the change in surface flux due to a wave in the old disk. The contrast parameters expressed as fractions are then,

$$C_V = (F_{OB}(V)+F_D'(V)-F_D(V))/(F_{OB}(V)+F_D'(V)+F_D(V)) \qquad \text{(II)}$$

$$C_K = (F_{OB}(K)+F_D'(K)-F_D(K))/(F_{OB}(K)+F_D'(K)+F_D(K)) \qquad \text{(III).}$$

Consider the visible contrast, and assume the disk flux at the spiral arm to be somewhat greater than in the interarm region:

$F_D'(V) = \beta F_D(V)$, $\beta > 1$. Then,

$C_V = (F_{OB}(V)+(\beta-1)F_D(V)) / (F_{OB}(V)+(\beta+1)F_D(V))$ and,

directly, $F_{OB}(V) = F_D(V) ((C_V(\beta+1)-(\beta-1)) / (1-C_V))$.

We saw above that C_V is about 10% , or 0.1 . In the extreme case in which the visible contrast is wholly accounted for by the presence of young stars at the arms (β =1),

$F_{OB}(V) = 0.22 F_D(V)$. The approximate colours of the two populations ($(V-K)_{OB} \sim -0.7$, $(V-K)_D \sim 3.0$; Johnson 1966) then lead to $\underline{F_{OB}(K) = 0.007 F_D(K)}$, a decreasing fraction as more of the visible contrast is provided by the old disk variation. The effect of F_{OB} on the 2.2 micron contrast (Equation III) is thus seen to be negligible.

(iii) The Bar.

M83 was classified by Sandage (1961) as an Sc/SBb spiral, the latter half of the classification deriving from the behaviour of the dust lanes close to the nucleus. The SB classification is supported by the infrared maps, which reveal an elongated luminous feature in p.a.48^o-49^o. The prominence of this feature in comparison with its appearance in the optical map probably results in part from extinction of the optical fluxes. If the K map adequately represents the underlying luminosity distribution, then the deviations apparent on the optical map from the regularity it implies suggest that the visible light is subject to patches of extinction up to A_V = 0.3-0.4 mag (about $1^1/_2$ contour intervals in Fig.4.5). This amount of obscuration would be effectively undetectable at 2.2 microns.

4.7 The Surface Brightness Profiles.

Our discussion of these profiles will necessarily be intertwined with consideration of the errors involved. We note at the start, therefore, that in Fig. 4.8 to 4.10, the error bars due to noise and beam size uncertainties are in all cases smaller than the symbols used in the plotting; the detailed morphology of the profiles is therefore correctly represented. The most important source of error is the effect of uncertainty in determination of the background level, which affects global properties of the profiles, such as the rate of fall of brightness with radius: these uncertainties will be discussed and quantified as the need arises. Three main components can be discerned in the profiles:

(i) The disk

Reasonably well defined for R_g > 150" (3kpc at 4 Mpc), the disk dominates the large-radius behaviour of the surface brightness. In the diagrams, the surface brightness in logarithmic units is plotted against a linear radial scale; with the possible exception of the 1.2 micron profile, the distributions are seen to be approximately linear with radius:

$$SB = kR_g + c \; ; \qquad \text{This may be written as}$$

$$SB = SB_0 + 1.0857 \; (R_g/h) \; ,$$

where SB_0 is the disk SB at $R_g = 0$, and h is the scalelength (see Chapter 1). Table 4.4 presents the measured near-infrared disk distributions, as derived from least-squares treatment of the data over the indicated ranges of galactocentric radius.

The profile at 1.2 microns is less well defined, possibly because of background level uncertainties or the effects of reddening and/or foreground stars. In particular, the rate of fall-off appears to increase substantially for R_g > 200 arcsec. These fainter points are prone to the first possible error just mentioned, and the figures given

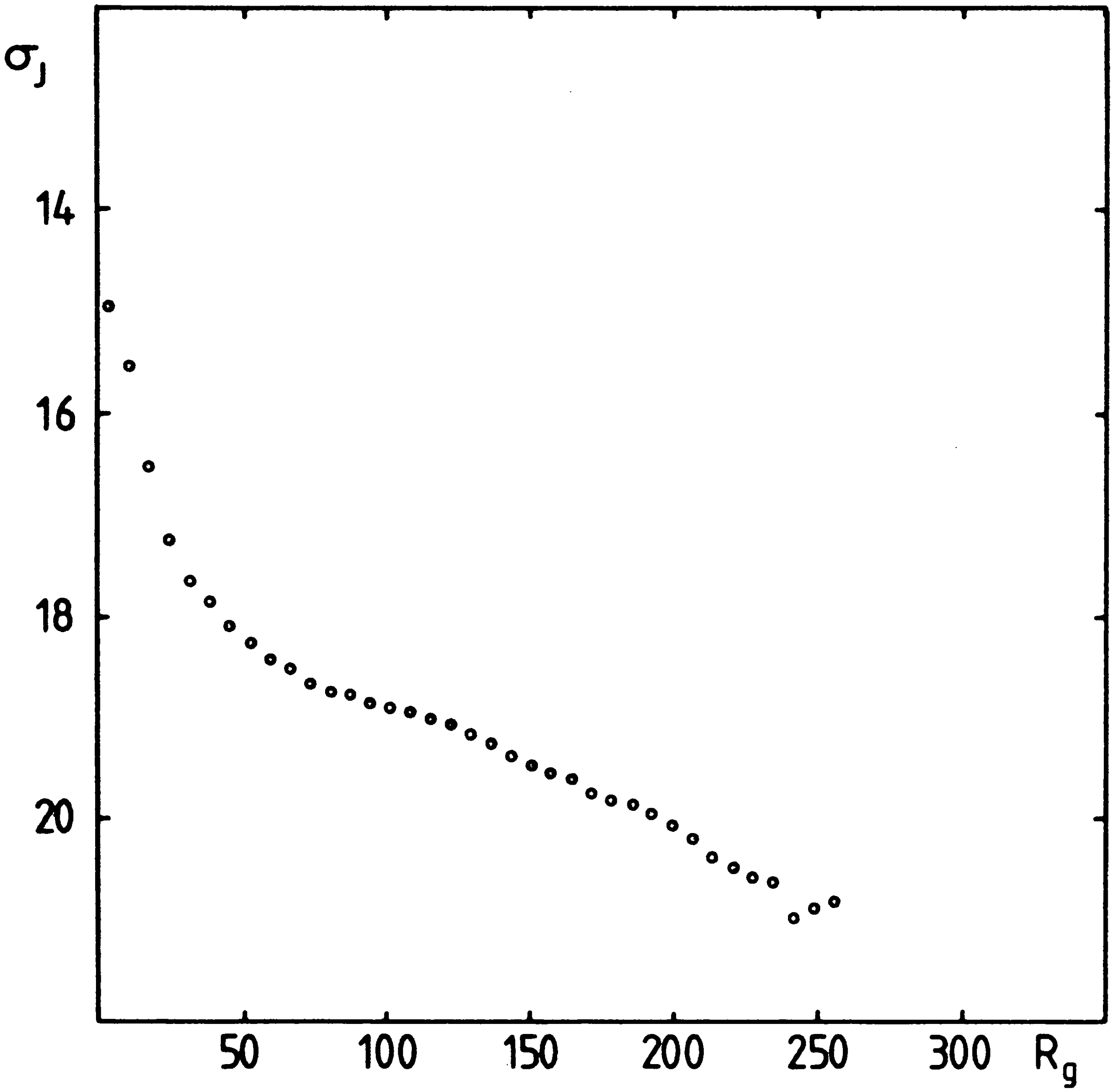

FIGURE 4.8

1.2 micron surface brightness as a function of mean annular radius in the plane of the disk, assuming an inclination of 24°.

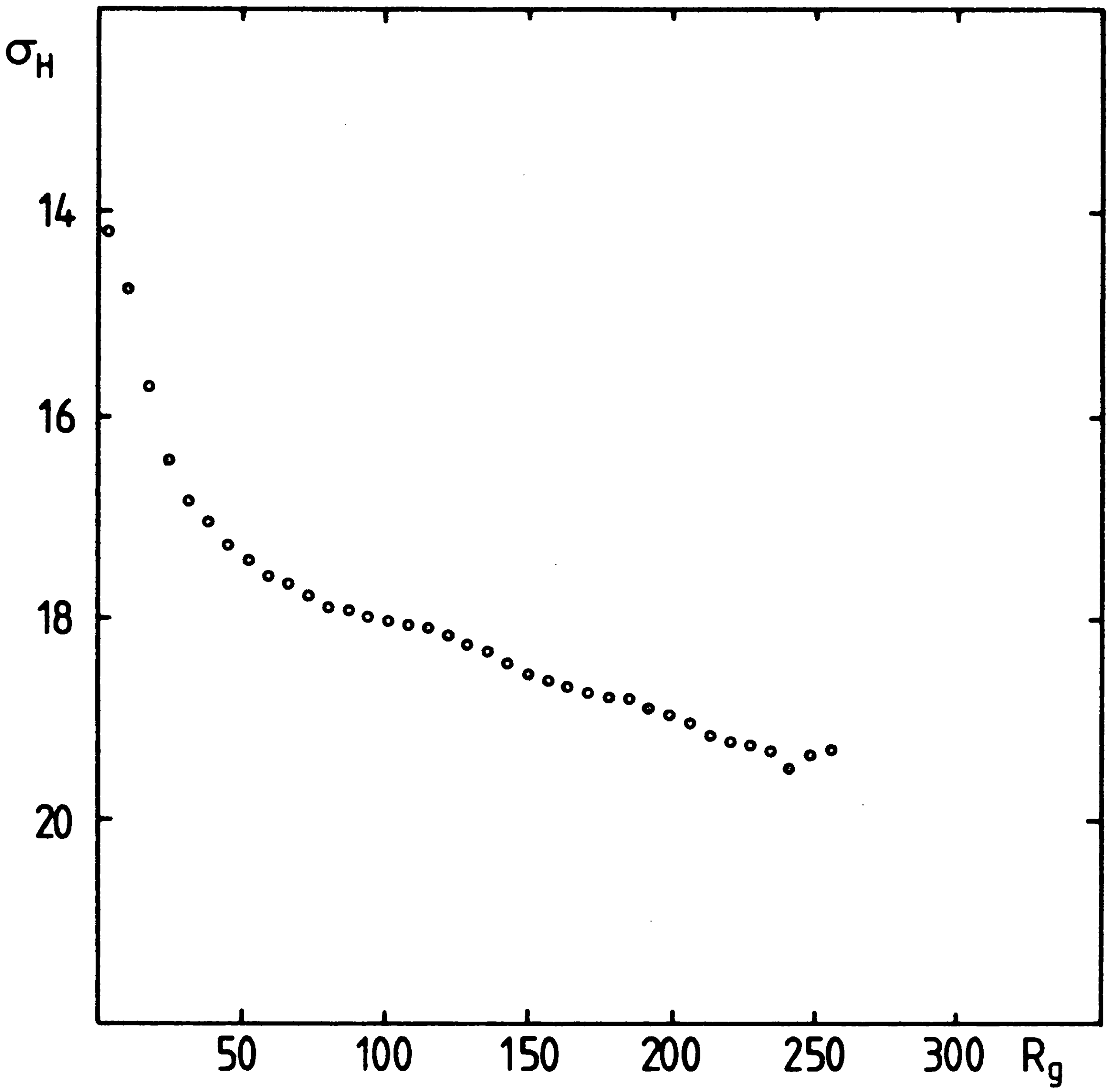

FIGURE 4.9

1.65 micron surface brightness (mag.arcsec^{-2}) as a function of mean annular radius in the plane of the disk, assuming an inclination of 24°.

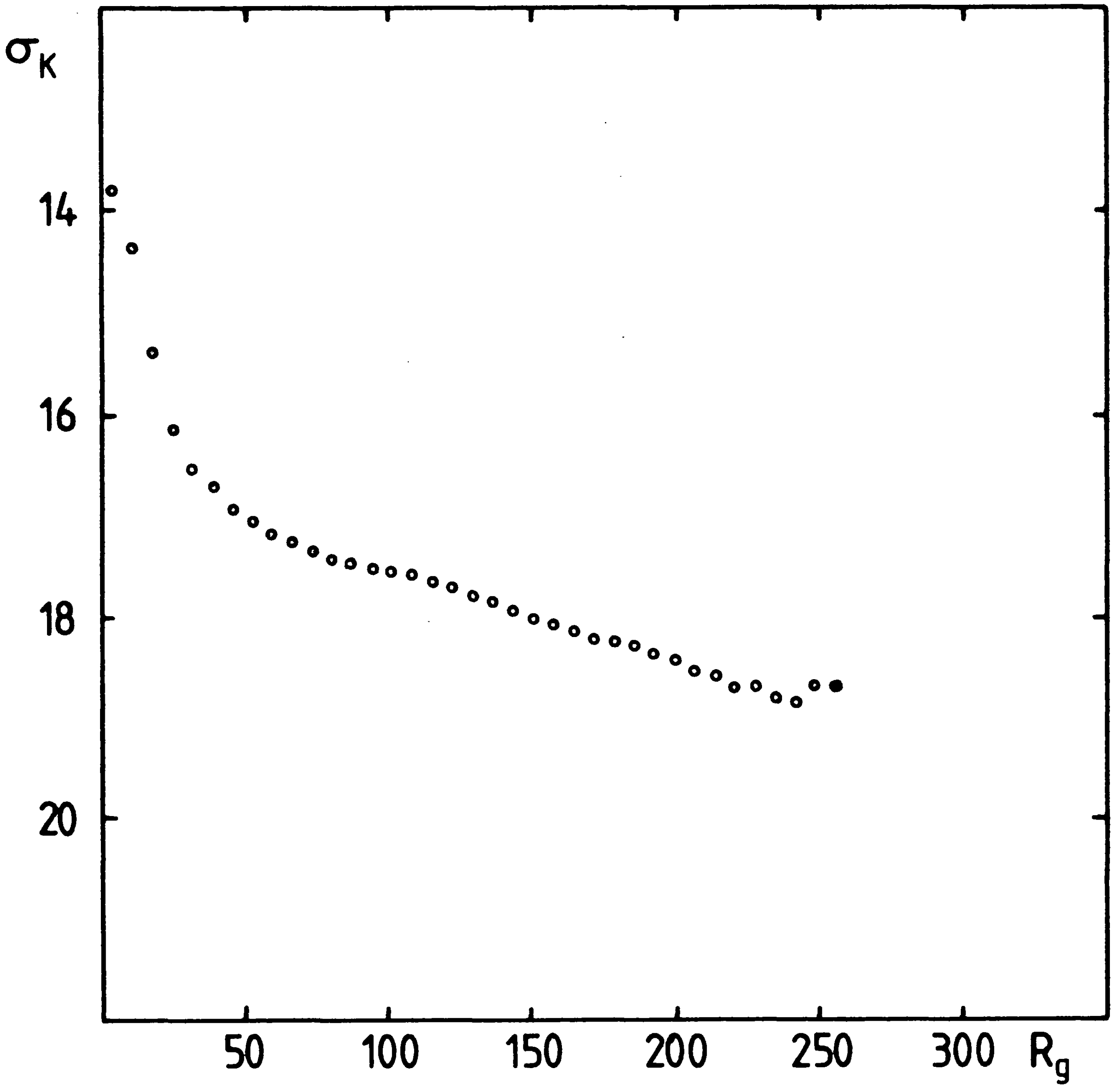

FIGURE 4.10

2.2 micron surface brightness as a function of mean annular radius in the plane of the disk, assuming an inclination of 24°.

for J in the Table below are a result of an eye-fit to the surface brightness from 70 to 80 and from 150 to 200 arcsec. (assuming the central bulge to be unimportant over the latter range; this approximation is shown to be reasonable later).

TABLE 4.4

Infrared Disk Parameters.

WAVEBAND	h (")	h (kpc)	FIT RANGE (")	($SB=SB_0+kR_g$) SB_0	k
J	98.7	1.9	70-80 , 150-200	17.86	0.011
H	125.0	2.4	> 150.0	17.2	0.0087
K	141.0	2.7	> 150.0	16.9	0.0077

The systematic increase of the scalelength with wavelength seems at first sight to imply that the galaxy becomes redder in the IR colours with distance. However, this first appraisal is to be treated with some caution, since the extreme faintness of the disk at large radii means that a small variation in the assumed background level can lead to a large change in the derived slope of the disk component, although the exponential character is retained.

We estimate that uncertainties in the endscan flux level caused by incomplete removal of the short term drifts discussed in a previous section amount to roughly 1 or 2 times the noise amplitude. The importance of such apparently small changes to the properties of the disk as derived by our procedure has been investigated by re-analysing the 2.2 micron data in exactly the way we have described, except that the mean endscan level was (i) raised; and (ii) lowered by 2 σ ,where σ is the noise level as given in Table 4.1. The result of this calculation, shown in Fig. 4.11, makes it clear that this uncertainty

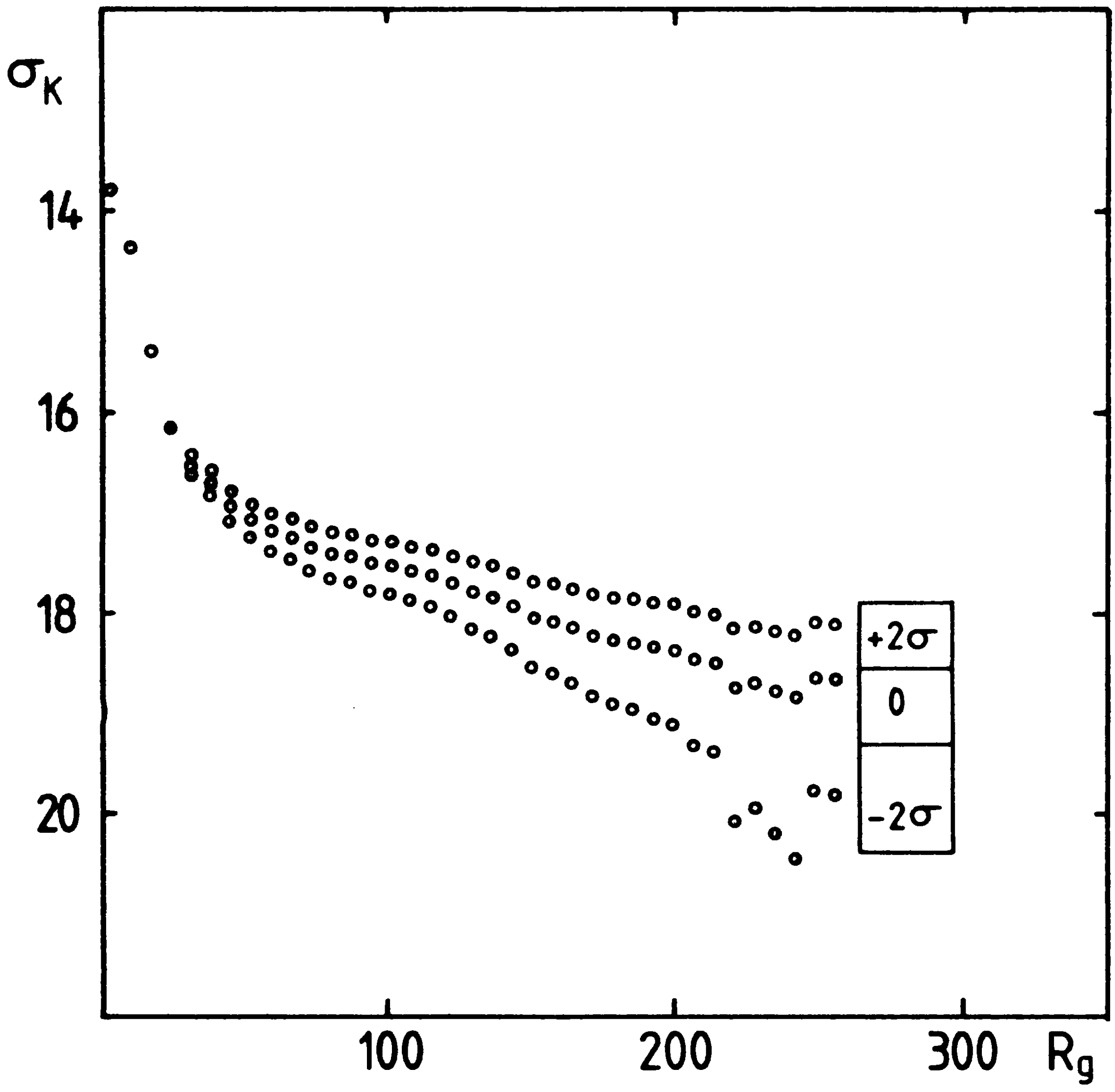

FIGURE 4.11

Effect on the 2.2 micron SB profile of (i) adding and (ii) subtracting twice the noise level from the endscan measurements.

reduces the significance of the colour gradients to which the unmodified surface brightness distributions seemed at first to point: although we expect the 2 σ level modification to be the most extreme possible case, its effect on the J-K colour index is enough to reverse the implied trend; even a 1 sigma level adjustment would reduce the trend to marginality.

In the absence of any corroboration, further discussion would seem unwarranted by the data presently available. The following two points may, however, provide some circumstantial evidence for the reality of the colour changes:

(a) A slow airmass-dominated change of sky transparency might have provided a plausible explaination if not for the fact that the observations were performed with H first, then K and finally J, as it was suspected that the 1.65 micron band would provide the optimal compromise between the source spectrum and uncertainties caused by sky and thermal drifts. Sky transparency variations therefore are probably not responsible for the colour trend observed, which would require a systematic deterioration in the order K,H,J.

b) A property of spiral galaxies well known to optical observers is their tendency to become bluer as the observing aperture is enlarged, as a result of the slow radial fall off of the blue light from the young arm population relative to that of the disk (Schweizer 1976). Proceeding to longer wavelengths, however, the situation could conceivably be reversed: the contribution from HII regions , also associated with the spiral structure, increases from 1.2 to 2.2 microns due to thermal dust and free-free emission (Wynn-Williams & Becklin 1974 ; Grasdalen & Joyce 1976) , and could be responsible for a colour change in the opposite sense to that observed optically.

For these reasons, one might cautiously suggest that the azimuthally-averaged J-K colour index increases by about $^1/_2$ mag.

between 3 and 5 kpc. in the disk of M83. Proof either way, however, awaits the improved determination of flux levels at the end points of our maps (via endscans performed faster than we attempted and repeated sufficiently to provide better signal-to-noise : an observing visit to the AAT is upcoming), and analysis of the data excluding areas possibly contaminated by thermal emission from HII regions.

(ii) The central bulge.

The central component dominates the SB profiles for values of R_g less than 60" (about 1.5 kpc). It is by now well established that the light in the bulges of most spiral galaxies is distributed according to the same law as governs the ellipticals throughout (see Chapter 1); we have tried therefore to test the infrared emission from the M83 bulge for adherence to this function. The bulge light was isolated from each azimuthally averaged bin by subtraction of the flux contributed by the exponential disk, calculated from the mean disk profiles derived earlier. The fluxes thus obtained were then converted back into magnitudes per square arcsecond. As seen in Chapter 1, de Vaucouleurs' law for elliptical galaxies requires that the surface brightness (in logarithmic units) be directly proportional to the fourth root of the galactocentric radius: our test of this relation for the bulge of M83 is presented graphically in Fig. 4. 12.

Apart from the points at smallest R_g, which are heavily affected by convolution through the beam, the profiles at all three wavelengths are remarkably close to the $R^{1/4}$ distribution, the mean residuals being 0.06, 0.07 and 0.08 mag. arcsec^{-2}. at J, H and K respectively. The 1.2 micron surface brightness at the extreme radial point is seen to be substantially below the best fit to the rest of the measurements, and was omitted from the linear regression. The flux from the bulge at this radius is at least an order of magnitude smaller than that originating in the disk, and the value inferred via the procedure above is probably affected by uncertainties in our eye-fit to the disk profile at this wavelength.

The bulge light is found to obey the following distributions:

$$SB_B(K) = (5.94\pm0.3) + (4.77\pm0.12)R_g^{1/4}$$
$$SB_B(H) = (6.1\pm0.2) + (4.84\pm0.09)R_g^{1/4}$$
$$SB_B(J) = (6.5\pm0.2) + (5.1\pm0.1)\ R_g^{1/4}$$

As the radial dependence of the H and K profiles is seen to be the same within the errors, the H-K colour is constant between 0 and 60 arcsec. in the M83 bulge. The J profile is marginally steeper, but once again this may result from uncertainties in the adopted disk contribution.

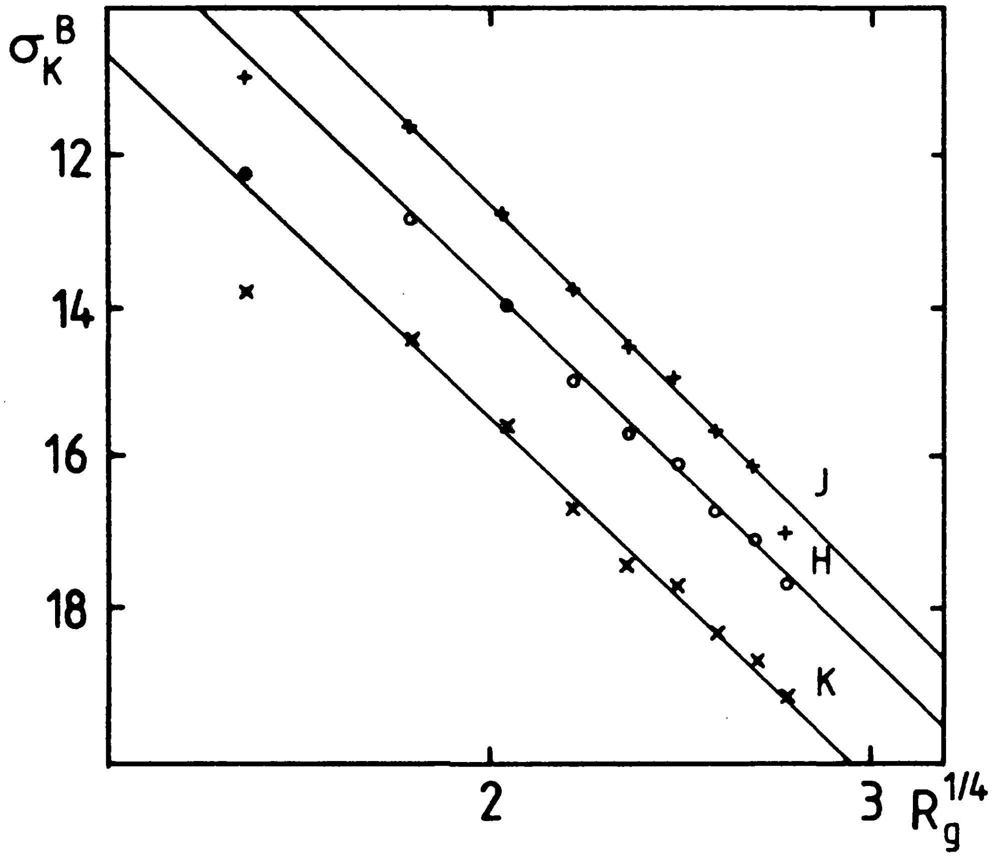

FIGURE 4.12

Infrared surface brightness profiles of the M83 nuclear bulge.

(iii) 2kpc<R_g<3kpc

The surface brightness in this radial range clearly deviates from the classical profile discussed in Chapter 1, the maximum discrepancy appearing at around 120". The scene is set for our discussion of this feature by the B and V observations presented by Talbot et al. (1979): their analysis, separating "young" (B-V < 0.4) and "old" (B-V > 0.65) pixels in their maps, shows that there is no obvious reddening of the disk component. The feature observed in the near infrared cannot, therefore, result from obscuration at 100 and 150 arcsec. R_g: from now on, we will interpret the feature as a "hump", in excess of the background disk light, which is also the impression gained from a first look at the profiles. In any case, uncertainties in the endscan level and the beam diameter at each wavelength prevent the formation of colour indices accurate enough to determine the near-infrared obscuration. The "Type II" profile proposed for this galaxy by Freeman (1970) is, however, ruled out from the start both by our observations and by the optical work of Talbot et al., because the feature responsible for the deviation from the classical profile is in excess of the exponential disk, extrapolated from larger R_g. Freeman(1976,1977) modified his original argument with the inclusion of a flat "lens" component in the density distribution. Such a component, presumably associated with Population II, could certainly give rise to the IR feature (although as we shall see, a toroidal distribution is probably closer to the truth); but whether a blue-light excess would then be expected is less than obvious.

Our observations, then, suggest that the surface brightness in this radial range is in excess of the light associated with the disk alone: Fig. 4.13. shows the excess fluxes around R_g = 120", after subtraction of a linear (in magnitudes; exponential in flux) interpolation between the measurements at 101.5 and 150.5 arcsec.

respectively. The peak contributions of the "hump" to the <u>total</u> emission from the disk are given in the Table below.

Table 4.5

Hump Fluxes.

Johnson Band	R_g	Peak Flux	% of Total
J	126	4.2	8.5
H	120	6.9	9.5
K	126	4.4	8.5

(fluxes in units of 10^{-32} $W.m.^{-2}Hz.^{-1}arcsec^{-2}$)

The hump is seen to contribute about one tenth of the total flux at each wavelength around 120 arcsec. from the nucleus: we must now attempt to account for its presence.

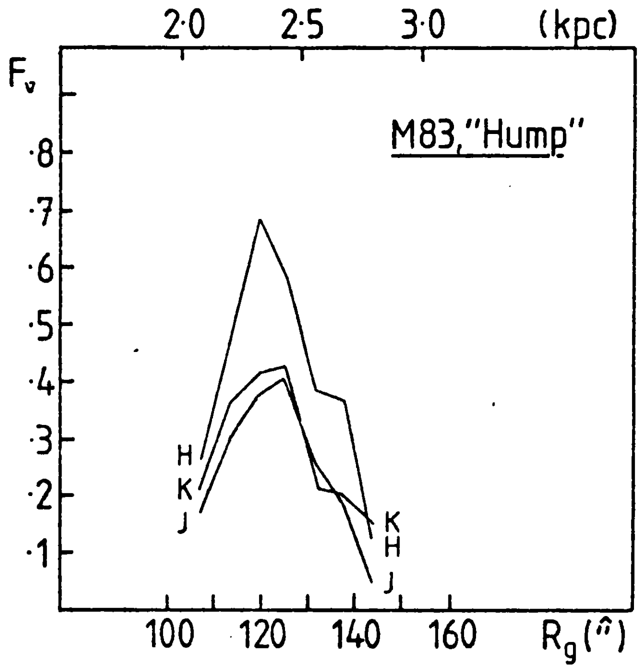

FIGURE 4.13

"Hump" fluxes.

Benedict (1976) surveyed the optical brightness distributions of a number of barred spirals, and found characteristic "shoulders" in the profiles, similar to the hump discussed here. His plots of the surface brightness along the bars of his galaxies demonstrated that the features in the averaged profiles could be more or less accounted for by excess fluxes originating in the brightest parts of the bar. Fig.4.14, a cut across M83 in p.a.48.5° (along the bar) shows conclusively that the azimuthally averaged hump in this object does not result from this type of effect.

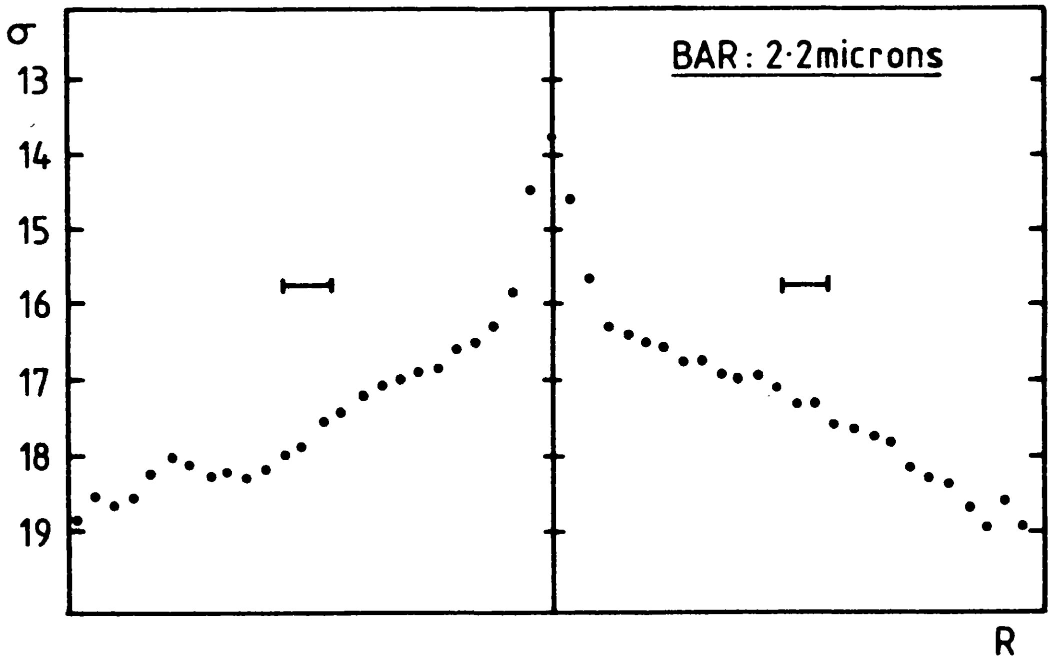

FIGURE 4.14

Surface brightness as a function of position along p.a.49°. Horizontal bars indicate the position of the hump in the azimuthally-averaged surface brightness profile.

If the excess flux were localised at the bar, it would subtend an angle of only about 20^{o} at the nucleus; in other words, it would fill only about $^{40}/_{360}$ths of the annuli over which the averaging was carried out. It has already been shown that the excess supplies 10% of the azimuthally averaged flux; the geometry then implies that one half of the light in the locality of the brightest part of the bar would be accounted for by the excess, and a hump of about 0.75 mag should be present in the profile of Figure 4.14. This is clearly not the case, as the figure demonstrates: the origin of the hump is probably in a region subtending a large angle, if not a full circle, at the nucleus.

The most likely source for the excess infrared flux lies in the spiral arms. The spiral structure seen south of the nucleus in the infrared maps crosses sky-projected galactocentric circles at a fairly oblique angle. This, in combination with the fact that (because of the galaxy's inclination to the sky) the spiral arms cannot be followed over the full range of radius presented in the surface brightness profile diagrams, could account for both the inner and outer edges of the hump. Without extended radial coverage, we cannot say that the outer cut-off of the hump is not caused by the loss to the annular averages of the spiral arm emission at the radius at which the arms cross the edge of our map. The physical origin of the excess fluxes is also as yet unclear, although a better determination of the endscan fluxes would, at a stroke, improve the situation in this respect. As it is, the lack of well-determined JHK magnitudes of the excess emission prevents us from discriminating between the old disk and young spiral tracers. We note that Talbot et al. attributed the hump seen in blue light entirely to the latter sources. However, the "old light" (B-V > 0.65) pixels in their Fig. 7b are still blue light intensities, and are therefore by no means as sensitive to properties of the old disk as the near-infrared fluxes. Furthermore, inspection of their diagram reveals that the number of old-light pixels is substantially reduced in regions where the hump is prominent. The overlaying of a young blue population on the old disk may be taking some of the "old" pixels over the colour threshold into the young category, thereby masking any excess in the old disk.

4.8 CONCLUSIONS

Observations at J,H and K of the bright southern galaxy, M83, reveal that:

I. Spiral structure is prominent at all three wavelengths: the 2.2 micron measurement is the first ever detection of spiral features at that wavelength.

II. The flux contrast between on-arm and interarm regions is the same at all three wavelengths (about $\pm$ 20% of the total disk emission), suggesting that emission from young OB-type stars is unimportant in the near-infrared: this was confirmed by a brief comparison with the contrast in optical light. The variation quoted above is therefore representative of the changing surface density of the "old disk" component of the galaxy, a result of significance to density wave theories of spiral structure.

III. Azimuthally-averaged radial profiles show a hump coincident with that observed by Talbot et al.(1979) in blue light. Our (correctable) inability to derive absolute infrared colours from our data leaves us unable to completely specify the nature of the sources responsible for the feature, but a stellar origin seems most likely.

IV. The radial brightness profiles show a change of the J-K colour index in the sense of redder colour with increasing distance from the nucleus. Inspection of the systematic errors introduced by the poorly determined background level diminishes the significance one can attach to this trend, but if real, the insensitivity of near-infrared colours to changes of (late) stellar type suggests that it might be due to a variation of the relative importance of thermal emission from HII regions across the disk.

REFERENCES

Benedict,G. 1976, Astron.J., 81,799.

Danver,C.-G. 1942, Ann.Obs.Lund., no. 110.

Freeman,K.C. 1970, Astrophys.J., 160,811.

Freeman,K.C. 1976, in "Galaxies", Sixth Advanced Course of the Swiss Society of Astronomy and Astrophysics, Ed. L.Martinet & M.Mayor.

Freeman,K.C. 1977, in Structure and Properties of Nearby Galaxies, IAU Symposium 77, D.Reidel 1978.

Glass,I.S. 1973, Mon.Not.R.astr.Soc., 164,155.

Grasdalen,G.L., & Joyce,R.R. 1976, Astron.Astrophys., 50,297.

Sandage,A.R. 1961, The Hubble Atlas of Galaxies, Washington: Carnegie Institute of Washington.

Schweizer,F. 1976, Astrophys.J.Suppl.Ser. 31,313.

Talbot,R.J., Jensen,E.B., & Dufour,R.J. 1979, Astrophys.J., 229,91.

Wynn-Williams,C.G., & Becklin,E.E. 1974, Publ.astr.Soc.Pacific, 86,5.

APPENDICES

APPENDIX A.

THE INTERSTELLAR REDDENING LAW.

Throughout this Thesis we have used the reddening curve due to van de Hulst (1949) and quoted by Johnson (1968). The various colour-excess ratios and ratios of total to selective extinction are given in the Table below.

TABLE A 1.

The van de Hulst reddening law.

$\frac{E_{B-V}}{E_{V-K}}$	$\frac{A_V}{E_{V-K}}$	$\frac{A_K}{A_V}$	$\frac{E_{B-V}}{E_{V-J}}$	$\frac{A_V}{E_{V-J}}$	$\frac{A_J}{A_V}$	$\frac{A_V}{E_{B-V}}$
0.36	1.10	0.09	0.43	1.33	0.245	3.05

The main import of these figures to our work lies in the ratio of the total extinction at 2.2 microns to the total visible extinction, A_K / A_V , seen in the table to be 0.09.

As an example, if the visible extinction to a source is such that only 1% of the V-band emission reaches the observer, fully 60% of the K flux is still available. The laws may be alternatively expressed in terms of optical depth, τ , to the source:

$$\tau_K = 0.09 \ \tau_V.$$

A path that is optically thick to optical light can still be well thin to near-infrared radiation. These facts are used to advantage in this thesis: the direct observation of the flat component in Cen A is impossible in the optical; the IR measurements of the disk scalelengths in highly-inclined systems, presented in Chapter 3 are more accurate in the relative absence of reddening; and finally the discussion of the Freeman TypeII profile in M83 (Chapter 4) was more direct than optical observations permit.

REFERENCES

Johnson, H.L. 1968, in "Nebulae and Interstellar Matter", Stars and Stellar Systems, Vol.7, ed. B.M.Middlehurst (Chicago: University of Chicago Press), page 167.

van de Hulst, H.C. 1949, Rech.Astr.Obs.Utrecht, 11, part 1, 1.

APPENDIX B. "HOLPASC".

```
PROGRAM CONVERT ( INPUT , OUTPUT )
 VAR I : INTEGER;
   CHR :     CHAR;
   BEGIN
     LINELIMIT ( OUTPUT , -1 ) ;
     I := 0
     WHILE NOT EOF ( INPUT ) DO
     BEGIN
       READ  ( CHR ) ;
       WRITE ( CHR ) ;
       IF ( EOLN ( INPUT ) ) THEN BEGIN
                                    READLN  ;
                                    WRITELN ;
                                    I := 0  ;
                                    END     ;
       I := I+1 ;
       IF I = 80 THEN BEGIN
                        I := 0  ;
                        WRITELN ;
                      END       ;
     END ;
   END.
```

This program, supplied by Chris Holland (research student), was used to convert the continuous string of ASCII characters and ASCII-coded AAT photometry data on M83 into FORTRAN-readable 80-column records.

APPENDIX C

Archived data files on the Leicester University CDC Cyber-73.

Quoted below are all the major data files employed in compiling this Thesis, and some others containing useful information but of which time has not permitted analysis. Where possible, the files contain raw data, complete with informative scan headers. Retrieval of a given file is achieved by the following "archive package" command:

ARCGET,<file name>,UN=DJA/CY=<cycle number>,PW=*.

A more complete set of files is also available: to list the file directory,

ARCLIST,ID=ADA,UN=DJA,LO=F/PW=*.

The subset of files described below is in approximate order of date of observation.

FILE NAME	CYCLE NUMBER	CONTENTS
	AAT, April 1980	
ADACETT	1	NGC 5128 raw data. RA position offset given in polar angle for each scan, measurements within a scan in order of increasing declination.
ADACENM	1	NGC 5128 final array: value at each point is mag.arcsec.$^{-2}$ x 100. Positional information is given in the header. Separation of measurements in dec.:2 arcseconds.

TENERIFE, Jan. 1981. Night 1 was 23-24 Jan.

ADADAY8	1	NGC 4565 K data, raw. 2 mm. aperture (22 arcseconds). Night 8.
ADATD5	1	Scans of NGC 2683 with 4.5 mm. aperture (halo observation), K and J. Night 5.
ADATD5	2	As cycle 1, but with more calibration information. Night 5.
ADATD9	1	NGC 4565 K halo scans. Raw. Night 9.
ADATD3	1	NGC 4565 4.5 mm. and 2 mm. scans, night 3.
ADATD62	1	NGC 4565 2mm. 1.2 micron scans. The main 1.2 micron run.

TENERIFE, July 1981. Night 1 was 22-23 July.

ADATJU6	1	NGC 5907 main 2.2-micron run, 22 arcsecond aperture. Raw data.
ADATJ62	1	NGC 7814 2.2-micron scans. Raw.
ADATJU7	1	NGC 5907 1.65-micron main run, 22 arcsecond aperture.

TENERIFE, Feb. 1982. Night 1 was 17/18 Feb.

ADATF51	1	Night 5 raw data on NGC 2683 halo. 4.5mm. aperture.
ADATF3	1	Night 3 NGC 2683 2.2-micron disk observations and some long 4.5mm. scans across NGC 5194. No headers.

ADATF7	1	Night 7: NGC 2683 J disk measurements, and NGC 5194 small-scale mapping.
ADATF6	1	Night 6: NGC 2683 1.2 micron halo scans with 4.5mm. aperture, also star scans.
ADATF4	2	Night 4 NGC 2683 K and V disk measurements around $\pm$ 77 arcseconds declination offset from the nucleus.
ADATF9	1	NGC 4594 data and large-beam scans of Orion Nebula. Raw data.
ADATF8	1	NGC 5194 data and a brief observation of a cataclysmic variable for I. McHardy, X-Ray Astronomy Group.

AAT, March 1982.

ADA83KF	1	Final processed M83 K data in count form: scans in order of decreasing RA. Measurements in scans in order of increasing declination. Scan separation 7", integration separation 7".
ADA83HF	1	Final processed M83 H count array. Filed as before.
ADA83JF	1	Final processed M83 J count array. Filed as for H and K data.
ADA83KB	1	M83 final array in calibrated K surface brightness form (mag.arcsec.$^{-2}$). Ordered as the count arrays.
ADA83HB	1	M83 final H surface brightness array.
ADA83JB	1	M83 final J surface brightness array.

ADAENDS	1	M83 endscan counts, raw. Measurements in order of increasing RA, separation of points is 7".
ADAENKS	1	M83 final processed (drift removed, etc.) form of K endscans: 51 points in order of increasing RA at N and S ends of the box raster. Also contains the measured south end K counts (see text).
ADAENHS	1	H, as above. North and south-end measured values only.
ADAENJS	1	J, as above. North and south-end measured values only.
ADA83BS	1	M83 surface brightness profiles resulting from annular averaging performed on individual rasters.

TENERIFE SCANNING DATA: FINAL SURFACE BRIGHTNESS PROFILES.

ADALOD	1	A directory of these files.
ADALO17	1	NGC 4565, 2.2 microns. Radii in kpc., measurements in Mag.arcsec.$^{-2}$. Also gives 1-sigma upper and lower limits.
ADALO18	1	NGC 4565 final 1.2 micron profile.
ADALOC7	1	NGC 5907 final 2.2 micron profile.
ADALOC6	1	NGC 5907 final 1.65 micron profile.

APPENDIX D.

Published Paper:

Adams et al. 1983, Mon.Not.Roy.astr.Soc., 202,241

Mon. Not. R. astr. Soc. (1983) **202**, 241–248

A 2.2-μm map of NGC 5128

D. J. Adams, A. J. Adamson and A. B. Giles*
Astronomy Department, University of Leicester, University Road, Leicester LE1 7RH

Received 1982 April 26; in original form 1981 October 30

Summary. A 2.2-μm map of the peculiar radio galaxy NGC 5128 (Centaurus A) is presented. The elliptical component of the galaxy has a surface brightness which varies with radius in accordance with de Vaucouleurs' law and a $V-K$ colour which becomes bluer with increasing radius. The 'dust lane' of the galaxy contains an emission feature at 2.2 μm, and the observations are consistent with there being a stellar disc of projected radius 80 arcsec and projected thickness 15 arcsec, centred on the nucleus of the galaxy and aligned with the dust lane. The 2.2–10 μm colour of a conspicuous part of the disc is discussed.

1 Introduction

NGC 5128 is the nearest of the radio galaxies and possesses a compact nucleus which can be observed at radio, infrared and X-ray wavelengths. Optically, the galaxy to which the compact nucleus belongs is of 'peculiar' morphology. It appears to be an elliptical galaxy whose image is bisected by a prominent dust lane. The dust lane is generally envisaged as encircling the elliptical component and lying in a plane oriented close to the line-of-sight.

NGC 5128 has recently been the subject of detailed study by observers working at visible wavelengths from large telescopes in the southern hemisphere. From studies of photometric colour indices across the face of the galaxy, van den Bergh (1976) and Dufour *et al.* (1979) obtained extensive evidence for the presence of blue stars and H II regions within, and close to the dust lane. These young objects indicate that star formation has taken place within the dust lane as recently as 25 million years ago. Measurements of radial surface brightness profiles and stellar bands have shown the main, unobscured part of the galaxy to be similar to normal ellipticals, although it is slightly bluer in colour. Graham's (1979) spectroscopic observations of H II regions in the dust lane, and of stars in the elliptical component, showed that the dust lane is rotating rapidly in its plane, whereas the elliptical component is only slowly rotating.

It is at present unclear how the slowly rotating elliptical component acquired the rapidly rotating dust lane, although it has been suggested that the dust lane is the remnant of a spiral

*Present address: Physics Department, University of Tasmania, Hobart, Tasmania 7001, Australia.

galaxy which collided with the elliptical. It is also unclear why NGC 5128 should have developed an active nucleus and radio lobes, although the origin of the galaxy's activity could well have been related to the onset of star formation in the dust lane some 25 million years ago. The answer to these questions in NGC 5128 should shed light on the evolution of more distant double-lobe radio galaxies, which are also centred on apparent elliptical galaxies.

Previous infrared observations of NGC 5128 by Becklin *et al.* (1971), Kleinmann & Wright (1974) and Grasdalen & Joyce (1976) have concentrated on the heavily obscured nuclear region, which contains a single peak of emission. Telesco (1978) observed strong 10-μm emission from various regions in the dust lane. 10-μm fluxes are normally dominated by the emission of warm (100 K) dust in H II regions. It is to be expected that these H II regions occupy a volume of space shared by normal stars, which should be detectable at wavelengths around 2.2 μm. An unpublished 2.2 μm map of the galaxy made with a 22 arcsec beam at the South African Astronomical Observatory by Adams & Giles in 1978 suggested that an emission feature coincides with the dust lane, although the morphology is confused by the presence of field stars which are visible on underexposed photographs of the galaxy, and are apparent in the higher-resolution infrared work presented here. Maps at J and K presented by Harding, Jones & Rodgers (1981) showed no small-scale structure, largely because of the 30 arcsec aperture used.

Dust extinction at 2.2 μm is less than 10 per cent of the associated visible extinction: van de Hulst's curve no. 15 (see Johnson 1968) gives $A_K = 0.09 A_V$, whilst the work of Jones & Hyland (1980) on heavily reddened stars implies $A_K = 0.07A_V$ when extrapolated to optical wavelengths. The former value is assumed throughout this paper, but it is clear that mapping of dusty galaxies at near-infrared wavelengths can provide useful information on the underlying stellar structure: this is the objective of the present paper on NGC 5128.

2 Observations

The observations were made in 1980 April with the 3.8-m Anglo-Australian telescope at Siding Spring, NSW, Australia. The AAO infrared photometer was used with its standard K (2.0–2.4 μm) filter and a 7 arcsec photometric aperture. A series of declination scans were made across the galaxy, separated by 4 arcsec of right ascension (3 arcsec on the sky) to ensure that each scan overlapped its neighbours. Guidance errors, checked by peaking up the infrared signal on the bright nucleus of NGC 5128, were less than 2 arcsec.

The AAO infrared photometer is conventional in that it uses an Indium Antimonide detector and a focal-plane vibrating mirror chopper. The detector amplification system is unconventional (Barton & Allen 1980) and has good DC stability. Independent measurements may therefore be made of the flux levels in each of the sky-chop channels. The present observations were made with the chopper throwing 12 arcsec east–west on the sky. Each declination scan was analysed to give two galaxy profiles, separated by the chopper throw in right ascension. Comparison of these profiles with others along the same track gave confidence in the DC stability of the system. A map was built up from these single beam scans, and the cumulative errors encountered when working with differences between two chopper channels were avoided. Difference readings between the two channels were used to establish the flux levels at the extremities of the declination scans.

The surface-brightness response of the system was calibrated by measurements of a series of standard stars and by scanning a star through the beam to determine the aperture size. Uncertainties in the determination of this aperture size result in a possible systematic error of 10 per cent or 0.1 mag per square arcsec in the surface brightness scale.

The map constructed from the declination scans is presented in Fig. 1. The contour levels

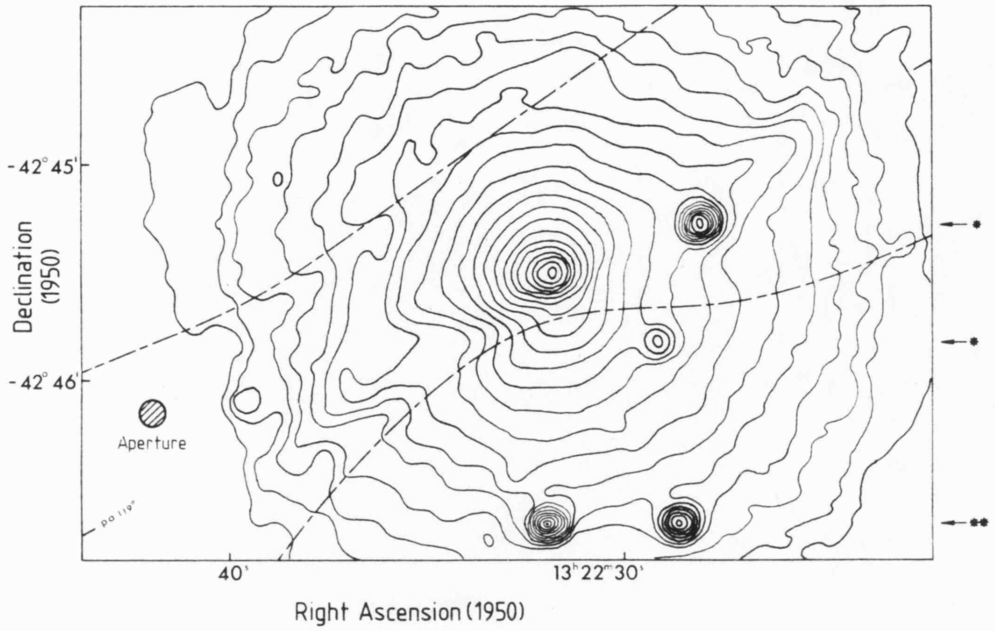

Figure 1. Smoothed 2.2-μm contour map of NGC 5128. Outermost contour is at 17.5 mag arcsec^{-2}; contour interval is -0.25 mag arcsec^{-2}. The dashed lines indicate the north and south edges of the dark lane; the aperture size is shown by the hatched circle. Four foreground field stars are also indicated.

are spaced logarithmically with surface brightness increments of a factor 1.259 or 0.25 mag, the lowest level being 17.5 mag per square arcsec. The total dynamic range from lowest to highest contour level amounts to a factor of 100. The accuracy of the outermost contour line is limited by uncertainties in the background sky-level determination rather than by detector noise. The maximum possible error amounts to 30 per cent of the lowest contour level.

3 Discussion

The map of Fig. 1 should be compared with a visible wavelength photograph of NGC 5128, such as that in the *Hubble Atlas of Galaxies* (Sandage 1961). The plate published by Grindlay *et al.* (1975) is conveniently marked with right ascension and declination scales. The nucleus of the galaxy, which is completely inaccessible to visible observations, appears prominently on the infrared map. The elliptical component, which is obvious optically only beyond the edges of the obscuring lane, can be traced in to the nucleus in Fig. 1. Absorption features are seen at the edges of the dust lane (marked by dashed lines). The deepest of these is in the region around $\Delta\alpha = +30''$, $\Delta\delta = -25''$ from the nucleus, being about 0.7 mag deep at 2.2 μm (in the absence of any underlying emission regions).

The bright nucleus of the galaxy yielded a signal of $K = 8.3 \pm 0.1$ mag in our 7 arcsec aperture. This is consistent with the observations by Grasdalen & Joyce (1976) who obtained $K = 8.59 \pm 0.03$ and $K = 7.92 \pm 0.03$ in 5.2 and 12.2 arcsec apertures respectively. The aperture used for the present observations was too large to place limits on the variability of the $K = 9.2$ mag point source discussed by Grasdalen & Joyce.

The flux from the E component of NGC 5128 has been shown to follow de Vaucouleurs' (1959) law for elliptical galaxies:

$$\log(B/B_e) = -3.33[(R/R_e)^{1/4} - 1]$$

(where R_e is the 'effective radius', containing one half of the total light and B_e is the surface flux at R_e), in the V and B band observations of van den Bergh (1976) and Dufour *et al.* (1979). It is reasonable to expect that the near-infrared surface brightness, also primarily due to stellar continuum emission, should follow the same law, although $V-K$ gradients could alter the derived constants.

The variation of 2.2-μm surface brightness with galactocentric radius R was evaluated as follows: for values of R spaced at 4 arcsec, the measured fluxes were averaged over a 90° annular segment of 4 arcsec radial extent whose centre lay on a line perpendicular to the dust lane, in PA 209°. The south-western sector was chosen because the nucleus is asymmetrically placed in the dust lane (see Fig. 1), permitting the unobscured E component to be measured at small radii. Points within the dust lane were excluded from the averages, as were three of the four bright foreground stars seen in Fig. 1. The result was an excellent linear least-squares fit of surface brightness, σ_K, to $R^{1/4}$:

$$\sigma_K = (2.54 \pm 0.02)\, R^{1/4} + (9.33 \pm 0.06).$$

Rewriting this as:

$$\sigma_K = 8.325 \;\{[R/(116 \pm 5)]^{1/4} - 1\} \; + (17.65 \pm 0.06),$$

we see that the data are described by de Vaucouleurs' law with effective radius

$$R_e = 116 \pm 5 \text{ arcsec.}$$

In Fig. 2 we plot the surface brightness, σ_K, as a function of $R^{1/4}$ for one quarter of the measurements used to produce the map of Fig. 1. A comparison of Fig. 2 with the similar diagram given for visible wavelengths by van den Bergh (1976) shows that extinction effects are indeed much smaller than in the visible. If infrared points at the largest radii (where background-level corrections are important) are ignored, the maximum downward deviation from the best-fitting straight line is only 0.6 mag, as compared with 3.5 mag for the visible data. We have found that, for the southern sector of NGC 5128, a constant correction of 0.48 mag is sufficient to bring reddened measurements within the dust lane into agreement with the best fit to de Vaucouleurs' law calculated using the unreddened points only. This corresponds to a visible extinction of 5.3 mag (van de Hulst, curve 15).

The linear least-squares fit to the annular integration data (shown as a solid line in Fig. 2) indicates a value for the de Vaucouleurs' effective radius of 116 ± 5 arcsec. This value is substantially smaller than those measured in blue and visible light by Dufour *et al.* (1979) and van den Bergh (1976), who both obtained values greater than 300 arcsec. This finding is qualitatively in agreement with the results of Frogel *et al.* (1978) and Strom *et al.* (1976), who showed that the $V-K$ colours in the outer regions of elliptical galaxies are bluer than those near the nuclei. At distances from 50 to 100 arcsec from the nucleus we obtain an observed $(V-K)$ colour index of 2.8 ± 0.3 by comparison with the data of van den Bergh, or an intrinsic value of $(V-K) = 2.5 \pm 0.3$ after correction for a foreground visible extinction of $A_V = 0.3$.

Inspection of the isophotes approximately 60 arcsec north-west of the nucleus in PA 299° shows that the flux from this region, in spite of the dust extinction, is in excess of the elliptical component flux measured at the same radius outside the dust lane. This emission,

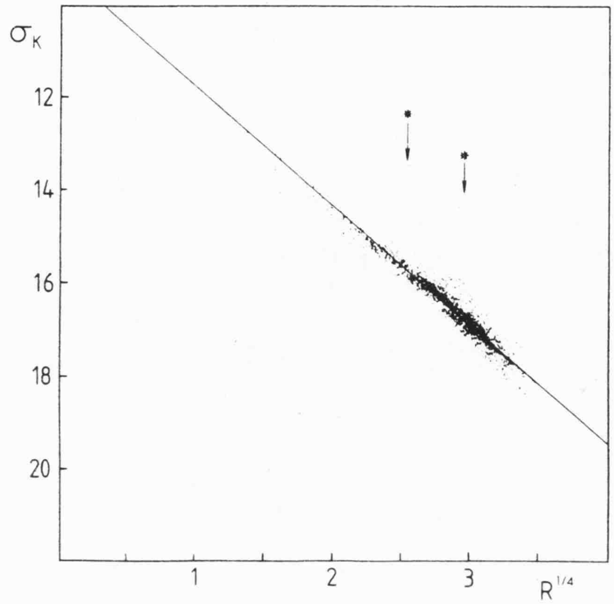

Figure 2. 2.2-μm surface brightnesses of NGC 5128 (in mag arcsec^{-2}) plotted as a function of $R^{1/4}$. The straight line represents the least squares fit to the south-west sector annular averages described in the text. Points affected by field stars are indicated.

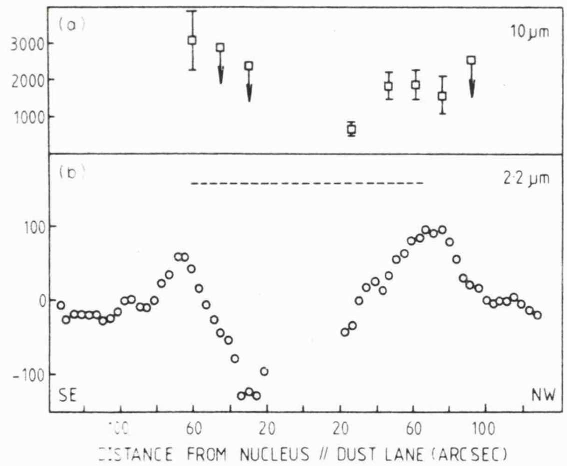

Figure 3. (a) 2.2-μm fluxes in the dust lane after subtraction of the measured elliptical component, plotted as a function of position along a line in PA 119°. The dashed line shows the flux level assumed in calculation of the total excess (see text). (b) Telesco (1978) 10 μm data for a 14-arcsec beam. Fluxes in both plots are in units of 10^{-32} W m^{-2} Hz^{-1} arcsec^{-2}.

which is also seen on the opposite side of the nucleus, is resolved in declination by individual scans, having a full width across the dust lane of 15 arcsec, considerably less than the 60 arcsec total width of the lane itself. The excess emission can be traced to within 50 arcsec of the infrared nucleus.

Fig. 3 shows the excess dust lane fluxes measured in an 18 arcsec width strip along PA 119°. Measurements were averaged over annular segments of 4 arcsec radial extent within the strip. The elliptical component of the galaxy was then subtracted using averaged points from the south-west sector discussed previously. Points within 20 arcsec of the nucleus were not treated in this way because of uncertainties caused by the steepness of the E component at small galactocentric radii. The figure shows two peaks of 2.2-μm emission, equally spaced at about 65 arcsec or 1.625 $(D/5)$ kpc (where D is the distance of NGC 5128 in Mpc) on either side of the nucleus. The north-western peak is approximately 1.5 times brighter than that in the south-east, probably because of the difference in character between the dust extinctions of these two regions.

It is interesting to compare the observed surface brightnesses of the dust lane excess with the 10-μm values measured by Telesco (1978). Telesco's data have been included in Fig. 3, and a degree of correlation with the 2.2-μm excess is apparent. Averaged over the 18 arcsec wide strip, the peak 2.2-μm surface brightness is 9.7×10^{-31} W m^{-2} Hz^{-1} arcsec^{-2} 65 arcsec north-west of the nucleus. Interpolating between sources 7 and 8 of Telesco to locate the same position in the dust lane, the 10-μm surface brightness is 1.7×10^{-29} W m^{-2} Hz^{-1} arcsec^{-2} through a 14 arcsec aperture. The ratio of flux densities observed at this position is therefore of order 20, and will not change by more than a factor of 2 from this value if averaged over a larger region in the dust lane.* In Table 1 we list 10 μm/2.2 μm ratio for the dust lane excess of NGC 5128 alongside estimates of the same ratio for galactic H II regions, normal stars, and the centre of M 82 (a well-studied region of star formation). It appears that the emission from the dust lane of NGC 5128 has a 2.2–10 μm colour which is consistent with the source region being composed of an admixture of normal stars and H II regions. The colour is similar to that observed in the much brighter area of star formation in the centre of M 82. We conclude that it is most likely that we are indeed looking at a region of recent star formation, as discussed for the dust lane by Rodgers (1978).

In order to discuss the structure of the region yielding the excess 2.2 μm emission, it is necessary to consider the possible effects of extinction. The following analysis assumes that the emission regions lie largely behind dust clouds which contribute the bulk of the reddening; the reader should note that the effects of obscuration would be altered if the true geometry involved mixing of the emitting and absorbing material. The effects of reddening on the ordinate of Fig. 3 are greatest close to the nucleus of the galaxy, where the difference between unreddened and dust lane reddened elliptical stellar component dominates any contribution from sources associated with the dust lane. To investigate the plausibility of the simple disc-like structure assumed by Telesco (1978), we will postulate the unobscured appearance of the dust lane excess to be one of constant surface brightness from $R = -65$

Table 1. 10 μm/2 μm flux ratios.

Object	10 μm/2 μm flux ratio	Reference
H II region	300	Wynn-Williams & Becklin (1974)
Cen A dust lane	20	This paper.
M 82: 5.8″ beam	20	Rieke *et al.* (1980) Abolins *et al.* (1979)
M 82: 35″ beam	10	Kleinmann & Low (1970)
M0V star	0.05	Bopp *et al.* (1974)

*The region discussed here was measured at 3.5 μm in 1980 June by AJA and Ian Gatley of the UK Infrared telescope (UKIRT), Hawaii. A 3 σ upper limit of 3.83×10^{-30} W m^{-2} Hz^{-1} arcsec^{-2} was recorded in a 10.8 arcsec aperture. Chopping was 15 arcsec north–south and comparison of alternate beam-switch pairs indicated that contamination caused by the gradient of the E component of NGC 5128 was negligible.

to +65 arcsec. We also suppose that the surface brightness should be the peak measured value in Fig. 3, corrected for 0.56 mag of extinction [from van den Bergh 1976, $E(B-V)$ = 1.85]. We then calculate the differential 2.2-μm extinction between the dust lane and the elliptical component necessary to produce the observed differences in Fig. 3. The resulting values of extinction range from 0.22 to 0.36 between 20 and 70 arcsec north-west of the nucleus, and from 0.38 to 0.68 between 20 and 70 arcsec south-east of the nucleus. These values imply visible extinctions up to 7 mag; such have been inferred in visible studies by van den Bergh (1976). It is clear from inspection of photographs that the exinction is higher in the south-east. We conclude from this that the excess dust-lane emission we observe is consistent with there being stars formed into a disc-shaped feature centred on the nucleus of NGC 5128. We have insufficient information to assert whether the disc surface brightness shows a maximum or a minimum at the centre of the galaxy; either situation could be fitted with realistic extinction values. The infrared map of Fig. 1 shows that at radial distances greater than 70 arcsec from the nucleus, the excess emission stands out clearly against the elliptical background. Hence, the decrease in surface brightness with increasing radius seen in Fig. 3 is likely to be an intrinsic property of the disc, rather than an artefact of extinction. We conclude that a disc structure, of radius 80 arcsec or $2.0(D/5)$ kpc is consistent with our observations. It may be noted that the 'ring' of H II regions discussed by Graham (1979) lies at a radius of $4.1(D/5)$ kpc, well outside the 2.2-μm disc.

The total (unobscured) 2.2-μm flux from the dust-lane feature can be estimated on the basis of the disc structure postulated above. The excess flux from the 18-arcsec strip, from $R = -80$ to +80 arcsec along position angle 119° is 4.5×10^{-27} W m^{-2} Hz^{-1}, corresponding to an integrated apparent magnitude of 7.8. The corresponding 2.2-μm magnitude of the spheroid component is 3.75, obtained by integration of de Vaucouleurs' law (see. e.g., van den Bergh 1976) using the constants determined earlier. It appears therefore that the feature we observe in the dust lane would contribute about 2 per cent of the unobscured 2.2-μm luminosity of NGC 5128.

Acknowledgments

We acknowledge advice and assistance from Dr David Allen and other staff of the Anglo-Australian Observatory in the conduct of the observations, and useful discussions with Dr J. A. Abolins. The 3.5-μm datum was obtained while one of us (AJA) was a guest observer of Ian Gatley of the UK Infrared Telescope Unit, Hawaii. The work was supported by SERC of the UK.

References

Abolins, J. A., Adams, D. J., Jameson, R. F., Hough, J. H. & Axon, D. J., 1979. *Mon. Not. R. astr. Soc.*, **186,** 23P.

Barton, J. R. & Allen, D. A., 1980. *Anglo-Australian Observatory Preprint.*

Becklin, E. E., Frogel, J. A., Kleinmann, D. E., Neugebauer, G., Ney, E. P. & Strecker, D. W., 1971. *Astrophys. J.*, **170,** L15.

Bopp, B. W., Gehrz, R. D. & Hackwell, J. A. 1974. *Publ. astr. Soc. Pacific* **86,** 989.

de Vaucouleurs, G., 1959. *Handbuch der Physik,* **53,** 311.

Dufour, R. J., van den Bergh, S., Harvel, C. A., Martins, D. H., Schiffer, F. H., Talbot, R. J., Talent, D. L. & Wells, D. C., 1979. *Astr. J.*, **84,** 284.

Frogel, J. A., Persson, S. E., Aaronson, M. & Matthews, K., 1978. *Astrophys. J.*, **220,** 75.

Graham, J. A., 1979. *Astrophys. J.*, 232, 60.

Grasdalen, G. L. & Joyce, R. R., 1976. *Astrophys. J.*, **208,** 317.

Grindlay, J. E., Schnopper, H., Schreier, E. J., Gursky, H. & Parsignault, D. R., 1975. *Astrophys. J.*, **201,** L133.

Harding, P., Jones, T. J., & Rodgers, A. W., 1981. *Astrophys. J.*, **251**, 530.
Johnson, H. L., 1968. In *Nebulae and Interstellar Matter*, p. 167. eds Middlehurst, B. M. & Aller, L. H.
Jones, T. J. & Hyland, A. R., 1980. *Mon. Not. R. astr. Soc.*, **192**, 359.
Kleinmann, D. E. & Low, F. J., 1970. *Astrophys. J.*, **161**, L203.
Kleinmann, D. E. & Wright, E. L., 1974. *Astrophys. J.*, **191**, L19.
Rieke, G. H., Lebofsky, M. J., Thompson, R. I., Low, F. J. & Tokunaga, A. T., 1980. *Astrophys. J.*, **238**, 24.
Rodgers, A. W., 1978. *Astrophys. J.*, **219**, L7.
Sandage, A. R., 1961. *The Hubble Atlas of Galaxies*, Carnegie Institute of Washington, Washington.
Strom, S. E., Strom, K. M., Goad, J. W., Vrba, F. J. & Rice, W., 1976. *Astrophys. J.*, **204**, 684.
Telesco, C. M., 1978. *Astrophys. J.*, **226**, L125.
van den Bergh, S., 1976. *Astrophys. J.*, **208**, 673.
Wynn-Williams, C. G. & Becklin, E. E., 1974. *Publ. astr. Soc. Pacific*, **86**, 5.

ACKNOWLEDGEMENTS

A large number of people have heroically put up with my company for some or all of the last three years: for that, and for the individual reasons I shall detail, they are worthy of more thanks than can ever be conveyed by mere wordprocessor on paper.

Firstly, Dave Adams, my supervisor, for his continual interest, enthusiasm, and ideas; Vince Brooksbank and Chas Maddock for many and varied jobs on the widethrow photometer, and Vince again for building the optical channel; John Fernley, Robert McCheyne, Mandy Sherrington, and Simon Green for being the (unwilling) butt of some pretty awful jokes; Nick Eaton, Chris Holland, Jeremy Bailey and Jim Hough for help at the Tenerife flux-collector, and Jeremy again for assistance at the AAT; Rosana Hernandez for speeding crates of equipment through customs at Tenerife; Jack Abolins for useful advice early in the campaign, and Ian Gatley for his generous invitation to UKIRT and for advice at the telescope.

Last and most, thanks to Janice Cooper for two years of understanding and help, which were far more valuable than I can remember admitting.

INFRARED SURFACE BRIGHTNESS DISTRIBUTIONS OF GALAXIES

A.J.ADAMSON Ph.D. 1983

ABSTRACT

Near-infrared (1.2-2.2 micron) and optical (V) surface brightness measurements across the faces of a sample of nearby galaxies have been obtained using a number of instrumental techniques.

NGC 2683, 4565, and 5907, seen approximately edge-on, were observed with a widethrow-chopping infrared photometer designed by Dr. D.J.Adams; simultaneous optical data were obtained for two of these. Chapter 3 details the results of these observations, the near-infrared measurements providing obscuration-free estimates of the scale sizes of the edge-on disks, and the optical-infrared colours being used to place constraints on possible mechanisms for the production of spatial colour-index gradients.

The remaining two observational chapters deal with infrared measurements of NGC 5128 (Cen A) and NGC 5236 (M 83), made with the Anglo-Australian Telescope infrared photometer. These chapters are a chronological record of the move towards DC-mapping techniques, which were tried tentatively for Cen A, and then used exclusively in observing M 83. The optically-dark lane of NGC 5128 is seen to contain an emission feature at 2.2 microns, and this is interpreted as a region of active star-formation. M 83 is a face-on spiral; maps at 1.2, 1.65 and 2.2 microns are presented, all showing well-defined spiral structure (never before detected at 2.2 microns), identified as a "density wave" in the stars of the old disk, which may drive the star-formation responsible for the optical spiral pattern.

Chapter 1 gives a brief review of some of the outstanding problems of extragalactic astronomy, and details the uses of infrared observations such as appear in the subsequent chapters.